Trinity College Dublin
Coláiste na Tríonóide, Baile Átha Cliath
The University of Dublin

School of Mathematics

On the Symanzik improvement of gradient flow observables

Argia Rubeo

14328566

supervised by

Stefan Sint

June, 2019

A Project submitted to The University of Dublin for the degree of Doctor in Philosophy

Declaration

I hereby declare that this project is entirely my own work and that it has not been submitted as an exercise for a degree at this or any other university.

I have read and I understand the plagiarism provisions in the General Regulations of the University Calendar for the current year, found at `http://www.tcd.ie/calendar`.

I have also completed the Online Tutorial on avoiding plagiarism 'Ready Steady Write', located at `http://tcd-ie.libguides.com/plagiarism/ready-steady-write`.

Signed: _____ Date: _____

To my mother,
to the memory of Judit,
to all strong and compassionate human beings in my life

Summary

On the Symanzik improvement of gradient flow observables

Argia Rubeo

The Standard Model of particle physics is the most precise description of phenomena governed by the strong, weak, and electromagnetic interactions. However, it is not a complete theory and in the quest for new physics the precision tests of such a model require better control of QCD effects. The gradient flow provides a new class of renormalised observables which can be measured with high precision in lattice simulations. This is relevant for many interesting applications. However, such applications are made difficult by the large discretisation effects observed in many gradient flow observables. We refer to the pure gauge theory at $O(g_0^2)$ in perturbation theory, where the structure of the Symanzik effective theory and all counterterms are known. At this order in perturbation theory, the theoretical expectation is that $O(a^2)$ Symanzik improvement is achieved when the action, the observable and the flow are $O(a^2)$ improved. We compute numerically the simplest observable, i.e. the action density, both with SF and SF-open boundary conditions. The first outcome of our computation confirms the theoretical expectation about the $O(a^2)$ improvement. Then we analyse a set-up with unimproved action. In finite volume, we study if it is possible to improve the observables by tuning the coefficient in the initial condition for the flow. Our analysis shows that very different values of c_b are needed depending on the specific observable we want to improve. We show that the hypothesis that there is a hierarchy of cutoff effects between flow and non-flow observables is not valid, therefore it is not possible to find a universal value for the coefficient related to the only counterterm needed with respect to the 4 dimensional theory.

Acknowledgements

Firstly, I would like to thank Prof. Stefan Sint for the supervision during the course of this project, for teaching me what doing research is about. I hope I will always keep in mind his approach to analyse and study a scientific problem. Also, without his comments this thesis would have never been completed.
I would also like to especially thank my collaborators, Marina Marinkovic in particular for giving me advice, and much more than I could have ever expected. Thanks to Alberto Ramos for advice, cross-checks, and useful discussions. Thanks to all the people at Trinity I shared my path with, to all the lattice group.
I also thank the people in the school of maths. Chris tak for your friendship, hope we will manage to keep meeting each other during our lives.
I am grateful for all the prompt support from the HPC team.
Special thanks to my parents, my brothers and Daniele for always being next to me. To the Roman friends, in some way you all helped me to be where I am: Angela, Carlo, Massimo, Nicola, Kristian, Raffo, Mimmo, Monica... well, the whole list would be so long! And many thanks to my friend Daniel for his help and to Sam for his patience. Thanks to Massimo Testa, it is a privilege to have such a master, every time I manage to do something good, I know I am just imitating your style. Thanks to Silvano Petrarca for his support, and to Dario Francia for always being present.
Thanks to the lattice guys who have thought me so much when I had a chance to talk to them, Michele Della Morte, Agostino Patella, Francesca Cuteri and Martin Hansen in particular. Thanks to my dear friend Simone, always next to me since childhood.
I would like to thank the school of maths for providing the funding which allowed this work to be finished. In particular, I thank the Trinity's alumni who allowed me to benefit from the Hamilton Scholarship.
Finally, thanks to my current collaborators Antonio Rago and Vincent Drach for their support and I would also like to especially thank David Wilson and Prof. Chris Allton for the critical reading of a previous version.

Contents

List of Figures

List of Tables

1 Introduction

The Standard Model (SM) of particle physics gives a unified theoretical description of phenomena governed by the strong, weak, and electromagnetic interactions. The SM has been incredibly predictive in a wide range of experiments. Yet, despite its success it is an effective field theory because it does not explain the complete picture. For instance, it does not include gravity, it does not explain dark matter or the observed matter-antimatter asymmetry, it has a number of other open questions concerning the nature of the Higgs particle and it does not explain the hierarchy problem or the origin of flavour. It is not clear at what energy the SM will require new laws of physics, but at some scale a more general theory with new fundamental degrees of freedom will manifest itself. Both theorists and experimentalists have been looking for evidence of new physics, beyond the SM.

Quantum Chromodynamics (QCD) is the theory which describes the strong interaction whose fundamental degrees of freedom are the fields associated to quarks and gluons. The lattice QCD approach we use in this work, is a powerful tool to identify signals of physics beyond the SM. There are two ways of researching the possible extensions of the SM on the lattice. First, it is possible to research extensions of the SM on the lattice in a direct way: one can perform simulations with either different gauge groups or different representations for the matter fields, as those models can provide viable extensions of the SM. Second, one can make precision measurements at low energies in order to recognise small effects of any new physics. Experimentally, one can explore the physics at higher and higher energy scales in order to see if new degrees of freedom manifest in the dynamics, but this, of course, is difficult, and requires larger and more powerful colliders. By assuming the existence of new physics, its effects can manifest themselves at low energies as virtual particles. As these effects are very small, it is crucial to have higher precision on the theoretical prediction on one side, and in experimental measurements on the other side. Any detected discrepancy would indicate the presence of new physics. For instance, a very precise determination of the parameters which control the flavour mixing would make it possible to find small contributions to decay amplitudes coming from

new particles. These contributions depend upon the hadronic matrix elements which are non-perturbative quantities and cannot be computed in perturbation theory [9–11].

From a mathematical point of view, QCD is a Yang-Mills theory, described by a lagrangian based on a local non-abelian symmetry group, $SU(3)_C$, where C refers to the colour charge. It contains a few parameters, namely the gauge *bare* coupling g_0 and the quark *bare* masses m_0^f (where f labels the flavour). The physical quantity which accounts for its dependence on the energy scale μ is the *renormalised* coupling g ($\alpha_s = \frac{g^2}{4\pi}$). Its expression [12] shows the important property of asymptotic freedom, discovered by Gross, Wilczek and Politzer [13, 14] in 1973, and for which they were awarded with the Nobel prize for physics. In Fig. 1.1 we show how the coupling behaves as a function of the energy scale.

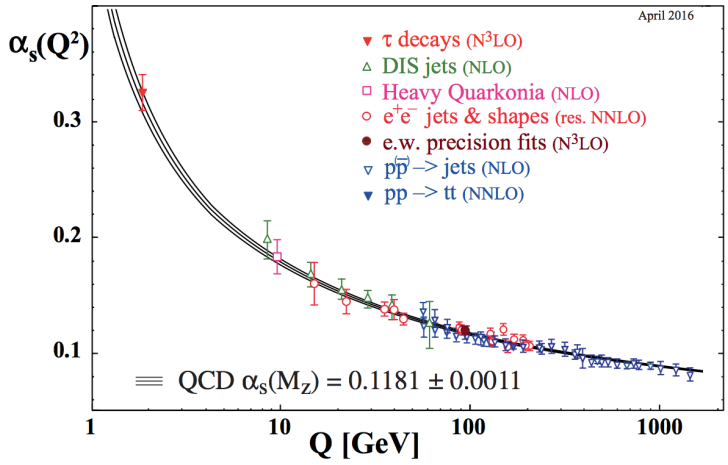

Figure 1.1: Experimental data showing the qualitative behaviour of the QCD running coupling which exhibits the asymptotic freedom in the ultraviolet regime [1]. In the infrared regime, it has such a large value that the perturbative expansion is not reliable and lattice numerical simulations must be used as a tool for computation.

In the context of the SM, one of the difficulties to overcome is that it involves QCD at different regimes: at high energies (at the mass of the W-boson $M_W \sim O(100\,GeV)$) asymptotic freedom makes it possible to perform a perturbative expansion, while at the hadronic scale, $\sim O(1\,GeV)$, the coupling constant becomes increasingly strong and we need to use a non-perturbative approach. One year after the discovery of asymptotic freedom, Wilson proposed what is nowadays known as lattice QCD [15], which is the only known way of studying QCD at all energy scales, starting from first principles (in particular, in lattice QCD the so-called Schrödinger Functional allows one to perform both perturbative and non-perturbative computations [16–22], for a review see [12]). This formulation is defined by replacing the continuum euclidean spacetime by a discrete grid, in such a way that the path integral is mathematically well-defined, as the discretisation

naturally imposes a cutoff which is the inverse of the lattice spacing a. In this formulation the system is formally identical to a statistical physics model and the equivalence allows us to use Monte Carlo techniques for the numerical computation [23]. Eventually, in order to recover the original theory of QCD, the *continuum limit* (lattice spacing going to zero) as well as the thermodynamic limit should be taken. Once the coupling can be computed at low energies, by means of the non-perturbative formulation, another difficult problem arises, which is to bridge the large scale difference. An elegant way to solve this is to use a finite size-scaling, which makes the connection between low and high energies possible. In fact, by identifying the renormalisation scale with the box size it is possible to define a discrete version of the beta function (which measures the variation of the coupling within the energy scale), known as the step scaling function [24]. In this way we can study how the coupling depends on the energy scale by changing the lattice size and we can connect perturbative and non-perturbative regimes [25].

In this work lattice QCD is used to study the Gradient Flow (GF), a recent development which allows the definition of observables (represented by composite operators) with simple renormalisation properties and very useful applications[26] [4]. In general, composite operators in quantum field theory require a *renormalisation* procedure. In the case of GF observables it has been shown, at all orders in perturbation theory, that when the observables are defined in terms of flowed gauge fields they do not require additional renormalisation[27] (to the standard renormalisation of QCD). At positive flow time, just after the standard renormalisation of QCD parameters and fields, the so-called energy density, which is the simplest composite operator we can consider, is finite and it can be measured on the lattice with high statistical precision. This allows for many interesting applications, for example the use of the GF on the lattice, in both setting the scale and using step-scaling techniques, leading to unprecedented precision [6, 7, 28, 29]. This is the motivation of our work, the GF is a powerful tool which offers the possibility of reaching the precision that, together with experimental precision measurements can lead to the indirect observation of new physics through the detection of some inconsistency. Working on such a tool to understand how to make use of it is then crucial.

The flip side of the GF observables is that they have quite large discretisation effects. In Fig. 1.2 we show an exploratory example of how large such effects are, which hold true for the whole class of such observables [30]. The lattice discretisation unavoidably introduces artifacts which are not physical. Not only is their nature of theoretical interest, but also at a practical level it is of essential importance to understand how to minimise them using the *universality of the continuum limit*. This ensures the best use of the computational resources used to obtain reliable extrapolations to the continuum limit. A

systematic way to either remove or minimise the leading cutoff effects is the Symanzik improvement programme [31]. These effects are introduced by the discretisation of three elements: the action, the flow equation and the observable we choose. We analyse each source of cutoff effects, and we study how such effects vary for different choices of these three elements. However, there is an additional issue: on one hand we have the Symanzik effective theory which works for a local theory, and on the other hand by introducing the flow time, we perform a smearing operation which renders the theory non local. In order for the improvement programme to be applied, we need to reformulate the theory in $4+1$ dimensions. For an arbitrary $SU(N)$ gauge theory, the leading contribution to the cutoff effects is $O(a^2)$[1]. Once the theory is formulated in five dimensions, where the additional dimension is the flow time t, in addition to the three aforementioned sources, there is only one couterterm we need to include to realize the $O(a^2)$ Symanzik improvement programme [3]. This counterterm belongs to the boundary of the theory, $t = 0$, and corresponds to a modification in the initial condition of the flow. By tuning a coefficient in such a modified initial condition, one is able to fully realize the improvement programme.

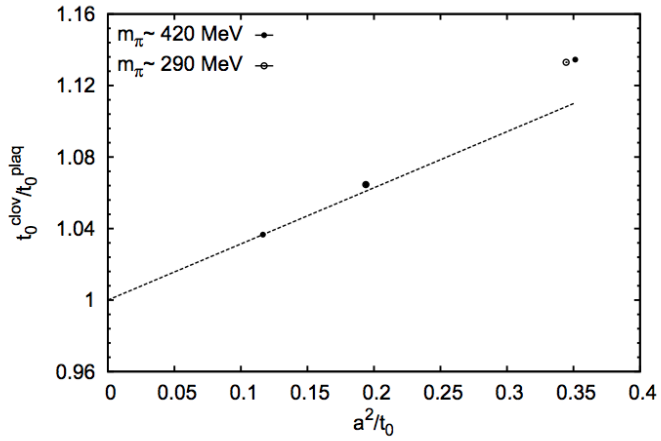

Figure 1.2: Example which shows the presence of large discretisation effects in gradient flow observables [2]. The quantity t_0 is computed using two different discretisations, clover and plaquette, which implies that their ratio must go toward one in the continuum. Looking at how this quantity scales in a^2, the slope indicates that the effects are strong.

The purpose of this work is to numerically test various aspects in this regard. First of all, we consider the lowest non-trivial order of the perturbative expansion of the energy density and we study different discretisations of the components of such observable. We study the effect of using the Wilson (W) gauge action compared to the Lüscher-Weisz (LW) action, which is tree-level improved [32]. We test the efficacy of the so-called Zeuthen (Z) flow by comparing it with the Wilson flow. The Z flow is defined by using

[1]By including fermions in the theory we obtain $O(a)$ leading contribution for the discretisation effects.

the LW action in the flow equation and defining the improved second derivative on the lattice [3]. Also, we verify the expectation obtained in [3] at the lowest non-trivial order in perturbation theory for the coefficient to be tuned in the modified initial condition for the flow. We check that the improvement is fully realized using Symanzik improved quantities: the action, the flow equation and the observable, with the value of the coefficient being zero as expected from the perturbative computation. In the case in which there is no complete basis of counterterms to realize the improvement, we compute numerically the value of the coefficient in the initial condition. In this particular situation the coefficient is not universal, in the sense that if we select a set of observables we can only compute it for one of them. Understanding if it is possible to find a universal condition for the coefficient in the initial condition of the flow equation is at the core of this work. Finally, we check the equivalence of tuning the aforementioned coefficient with the phenomenological improvement introduced in [33].

1.1 Outline

This thesis is organised as follows.

In Chap. 2, we briefly review the QCD theory in the continuum and then the path integral formulation which is used to formulate the theory on the lattice.

In Chap. 3, the GF is defined, and the local formulation of the theory (in $4+1$ dimensions) is discussed.

In infinite volume, we introduce the simplest local gauge-invariant expression defined in terms of the flowed fields, the action density (also called energy density). By considering its perturbative expansion we show that a well-defined finite quantity is obtained up to next-to-next-to-leading order. It has also been shown by Lüscher and Weisz that is a finite quantity at all orders in perturbation theory. The property of being finite after the renormalisation of the coupling is what allows for interesting uses of the flow. We list the succesful applications, such as the scale setting and the so-called GF coupling and the other possible applications which motivate our work of studying the improvement of the GF observables. In fact, on one hand the renormalisation properties are the advantage of such an approach, on the other hand large cutoff effects are observed (as shown for example in Fig. 1.2).

In finite volume, we can introduce more observables to probe the theory. This is the playground in which we make numerical tests. We impose Schrödinger Functional

boundary conditions and show they can be obtained from an orbifolding construction. We use such a prescription to write the gluon propagator for the flowed fields, which appears in the perturbative expansion of the observable. This leads us to split the observable into colour magnetic (spatial) and electric (mixed) components. We report the expressions for the two components and their derivatives in euclidean time, which we will use later on to probe the theory at length scales given by the smearing radius induced by the flow.

In Chap. 4, we review the Symanzik improvement programme, the classical expansion which leads to the Zeuthen flow, and the improved expression for the observables.

In Chap. 5, we analyse the results of the numerical computation of the observable at non-trivial leading order in perturbation theory ($O(g_0^2)$). Part of our work is to write the code that we use to study the effects of different choices of discretising the action, the flow equation and the observables, which are the magnetic and electric components of the energy density.

After checking the expectations coming from perturbation theory, we introduce the dependence upon the coefficient in the initial condition for the flow equation to make other tests in the case where we do not have a complete basis of counterterms to realize the improvement. This is a way to look for a "phenomenological" improvement and it serves as a guide to go beyond perturbation theory. If the improvement would work in PT then would be interesting to see if the result is kept non-perturbatively. This is not the case as we discuss.

2 Quantum Chromodynamics

2.1 QCD in the continuum

QCD is the local quantum field theory which describes the strong nuclear interaction. The gauge symmetry $SU(3)_C$ determines the form of the lagrangian expressed in terms of the fundamental degrees of freedom: the gluonic field A_μ and the matter and anti-matter fields, ψ and $\bar{\psi}$ respectively. The latter have N_f components, the are six flavours, u, d, s, c, b, t. The action of the full theory, in an Euclidean spacetime, is given by a gluonic and a fermionic term:

$$S[A, \psi, \bar{\psi}] = S_G[A] + S_F[A, \psi, \bar{\psi}]. \tag{2.1}$$

The gluonic part, which describes the pure gauge sector, is given by:

$$S_G[A] = -\frac{1}{2g_0^2} \int d^4x \, \mathrm{Tr}\left(F_{\mu\nu} F_{\mu\nu}\right), \tag{2.2}$$

where the parameter g_0 is the gauge bare coupling of the theory and the field strength tensor is defined by:

$$F_{\mu\nu}(x) = \partial_\mu A_\nu(x) - \partial_\nu A_\mu(x) + [A_\mu, A_\nu]. \tag{2.3}$$

The fermionic part has the form:

$$S_F[A, \psi, \bar{\psi}] = \int d^4x \, \bar{\psi}(x)(\not{D} + M_0)\psi(x), \tag{2.4}$$

where the Dirac operator $\not{D} = \gamma_\mu D_\mu = \gamma_\mu(\partial_\mu + A_\mu)$ is the covariant derivative contracted with the gamma matrices and the matrix M_0 contains the other parameters of the theory, which are the bare quark masses m_0^f, one for each flavour.

2.1.1 Path integral formulation

Given the action of the theory $S[A, \psi, \bar{\psi}]$, we consider a Euclidean spacetime where the path integral is defined by:

$$\mathcal{Z} = \int \mathcal{D}[A]\mathcal{D}[\psi]\mathcal{D}[\bar{\psi}]e^{-S[A,\psi,\bar{\psi}]}, \tag{2.5}$$

where the measure of the integral is formally written as the following products:

$$\mathcal{D}[A] = \Pi_{x,\mu,a} dA^a_\mu(x), \quad \mathcal{D}[\psi] = \Pi_f \Pi_{x,I,a} d\psi^f_{I,a}(x), \quad \mathcal{D}[\bar{\psi}] = \Pi_f \Pi_{x,I,a} d\bar{\psi}^f_{I,a}(x), \tag{2.6}$$

in the first equation x is the the four-dimensional spacetime coordinate, $\mu = 0, ..., 3$ is the Lorentz index, $a = 1, ..., 8$ is a vector-index in the adjoint representation; in the second and third we have the flavour index f, the Dirac index $I = 1, ..., 4$ and the colour index $a = 1, ..., N$ which labels the fermion field in the fundamental representation. The expectation value of an operator $O[A, \psi, \bar{\psi}]$ is given by:

$$\langle O \rangle = \frac{1}{\mathcal{Z}} \int \mathcal{D}[A]\mathcal{D}[\psi]\mathcal{D}[\bar{\psi}] O[A, \psi, \bar{\psi}] e^{-S[A,\psi,\bar{\psi}]}. \tag{2.7}$$

In order for this expression to make sense we need to gauge-fix, then regularise and renormalise the theory. In fact, the integration measure is extended over all gauge configurations, even those related by a gauge transformation. This means that we are counting infinite field configurations which are physically equivalent (they lie in the so-called gauge orbits), instead we want to select only one field configuration per orbit (no Gribov ambiguities are present). The problem is solved using the Faddeev-Popov procedure [34] (not true in the case of incomplete gauge-fixing). In addition, as we will see, for the path integral to make sense we need to apply a *regularisation* and *renormalisation* procedure. The regularisation consists of imposing a momentum cutoff Λ, in order to make finite the ultraviolet divergences generated in the perturbative expansion of the Green's functions. There are many ways to apply a regularisation, one of them is given by the lattice introduced in Sect. 2.2, where the cutoff is given by the inverse of the lattice spacing. The renormalisation step is done by imposing a number of conditions equal to the number of parameters and fields which enter the *bare* action (eq. (2.2) and eq. (2.4)). By computing physical quantities in the regularised theory and fixing them to experimental values one takes the limit $\Lambda \to \infty$ in order to remove the cutoff. When the theory is renormalizable the observables stay finite after this limit. The choice of the renormalisation conditions and the energy scale μ at which we impose them, is arbitrary and defines the renormalisation scheme. The relation among the physical quantities do not depend upon

the particular choice of the renormalisation scheme. The dynamics of QCD is described by the action which has a compact form, still there are non-trivial mechanisms to be analysed in order to explain all the experimental phenomena observed in nature, e.g. the mass spectrum of QCD, the running of coupling and so on. An extremely important step in the understanding of the theory was taken by Gross, Wilczek and Politzer, in 1973, with the discovery of asymptotic freedom: according to this property at high energies (at the mass of the W-boson $M_W \sim O(100\,GeV)$) the (renormalised) QCD coupling becomes smaller. This anti-screening property is peculiar of non-abelian gauge theories like QCD; for an abelian theory such as QED we observe the opposite behaviour, the running of the coupling is such that at low energies the fine structure constant becomes smaller. This property implies that at high energies α_S is small enough to enable the validity of a perturbative expansion; on the other hand, at the hadronic scale, $\sim O(1\,GeV)$, the perturbative approach is no longer valid, and we need to use a non-perturbative formulation.

2.2 Lattice QCD

Lattice QCD was formulated in 1974 by Wilson, and it provides the only known way to treat QCD non-perturbatively starting from first principles [35]. It is defined through the discretisation of the path integral (2.10), where the continuum spacetime is replaced by a lattice, in such a way that the minimal distance between two points is the lattice spacing a. It provides a regularisation of the theory, which is something needed in quantum field theory because, when we consider the product of operators at the same point, we obtain divergences which have no physical meaning and in order to remove them we need to first regularise the theory, and then perform the so-called renormalisation procedure. The first step, i.e. the regularization, can be done in different ways; the purpose of it is to render all the quantities finite.

The lattice formulation is defined by replacing the continuum spacetime $\mathbb{R}^4$ with a discrete set $\mathbb{Z}^4$ of points (see for example the following textbooks [36–38]):

$$\Lambda = \{x : x_\mu = a n_\mu\}, \qquad n_\mu \ \text{integer} \tag{2.8}$$

where a is the lattice spacing and the 4-vector $n_\mu = (n_0, n_1, n_2, n_3)$ labels the 4 directions in the spacetime. If we consider a lattice with finite volume $L^3 T$, then the temporal direction is labeled by $n_0 = 0, 1, ..., \frac{T}{a} - 1$ and $n_i = 0, 1, ..., \frac{L}{a} - 1$, with $i = 1, 2, 3$ indicating the spatial directions. In this formulation, the fundamental variables are the group-valued link variables $U_\mu(n)$ which are integrated over in the path integral. In the continuum,

the gauge fields $A_\mu(x)$ take values in the Lie algebra. For a compact group there is no need to gauge fix as the Haar invariant measure over the group is finite. A *gauge field configuration* is a set of values for all link variables on the lattice:

$$U = \{U_\mu(x), \text{ for } x \in \Lambda\}. \tag{2.9}$$

2.2.1 Gluonic action

For a pure gauge theory, in a Euclidean spacetime[1], the path integral is defined by:

$$\mathcal{Z} = \int \mathcal{D}[U] e^{-S[U]}, \tag{2.10}$$

where the integration measure for the link variables is formally written as:

$$\mathcal{D}[U] = \Pi_n \Pi_\mu dU_\mu(x). \tag{2.11}$$

The gauge action on the lattice is not unique, different discretisations may be defined to have the same continuum limit. The easiest pure gauge action on the lattice is the so-called W plaquette (or gauge) action:

$$S_{WG}[U] = \frac{\beta}{N} \sum_x \sum_{\mu<\nu} \mathrm{ReTr}[1 - P_{\mu\nu}(x)], \tag{2.12}$$

where $\beta = \frac{2N}{g_0^2}$ is the inverse coupling, N is the number of colours, and the trace is taken over the colour components. The action is defined in terms of the gauge invariant variables plaquette $P_{\mu\nu}(x)$, which is the smallest closed loop that one can define on the lattice, see Fig. 2.1, and is defined by the product of the four link variables:

$$P_{\mu\nu}(x) = U_\mu(x) U_\nu(x + a\hat{\mu}) U_\mu(x + a\hat{\nu})^\dagger U_\nu(x)^\dagger, \tag{2.13}$$

where $\hat{\mu}$ and $\hat{\nu}$ denote the unit vectors in directions μ and ν, see Fig. 2.1. The constraints that the action must satisfy are the gauge invariance and the right continuum limit: for $a \to 0$ eq. (2.12) must reproduce the action in the continuum, eq. (2.2). Other regularisations have been formulated to achieve a faster convergence to the continuum limit, which means a convergence with a higher power p of the lattice spacing a. The on-shell $\mathcal{O}(a^2)$ improved at tree-level gauge action, in 4 dimensions, on the lattice, can

[1]We assume to be in a Euclidean space-time everywhere in this work.

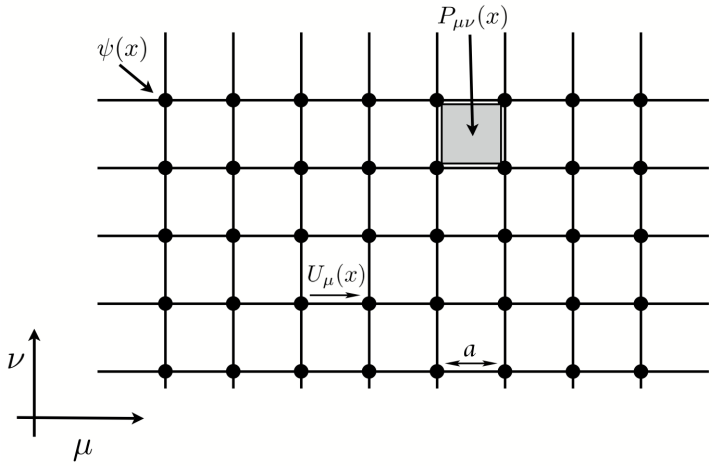

Figure 2.1: Representative illustration of a lattice in two dimensions. The minimal distance between two points is the lattice spacing a. The fermion field $\psi(x)$ lives on the lattice site x, while the gauge field, the link variable $U_\mu(x)$ is the connection of two neighboring lattice points. The plaquette $P_{\mu\nu}(x)$ is the smallest holonomy on the lattice, defined by the product of four link variables, eq. (2.13). The two directions on the lattice are labeled by μ and ν.

be parametrised as [32]:

$$S_G[U, c_i] = \frac{1}{g_0^2} \sum_{i=0}^{3} c_i \sum_{\mathcal{W} \in \mathcal{S}_i} \mathrm{tr}(1 - U(\mathcal{C})), \tag{2.14}$$

where

- c_i are the coefficients that normalise the action by requiring $c_0 + 8c_1 + 16c_2 + 8c_3 = 1$;
- the second sum extends over all oriented Wilson loops which are: the usual plaquette $\mathcal{S}_0$, the 2 x 1 planar loop or "rectangle" $\mathcal{S}_1$, the bent rectangle or "chair" $\mathcal{S}_2$, and the "parallelogram" $\mathcal{S}_3$;
- $U(\mathcal{C})$ is the ordered product of the link variables $U_\mu(n)$ along $\mathcal{C}$.

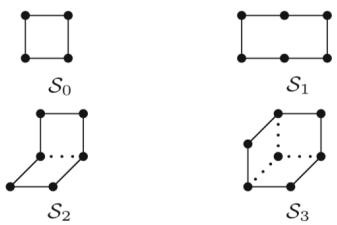

Figure 2.2: Wilson loops made by 4 and 6 link variables [3].

The two choices we consider in this work are: the W plaquette action ($c_0 = 1$, $c_{1,2,3} = 0$) and the tree-level improved LW action ($c_0 = \frac{5}{3}, c_1 = -\frac{1}{12}, c_{2,3} = 0$). There is

also the Iwasaki action which is a pure gauge action, similar to the LW action but with different coefficients for the plaquette and rectangle terms [39].

2.2.2 Gluon propagator

By expressing the plaquette variables in terms of the links (2.13), the quadratic part of the Wilson action can be written as:

$$S_G^0[U] = \frac{-a^4}{2g_0^2} \sum_x \sum_{\mu\nu} A_\mu(x) \left[(-\sum_\sigma \partial_\sigma^* \partial_\sigma)\delta_{\mu\nu} + \partial_\mu \partial_\nu^* \right] A_\nu(x), \tag{2.15}$$

where the lattice derivatives are defined in (A1.21) and (A1.22). This is similar to what one does in the continuum case (see for example [40]), with the difference implied by the regularization, such as doing an integration by parts on the lattice:

$$\sum_x (\partial_\mu f(x)) g(x) = -\sum_x f(x) \partial_\mu^* g(x). \tag{2.16}$$

In order for the kernel of $S_G^0[U]$ to be invertible we need to add a generic gauge fixing term:

$$S_{GF} = \frac{1}{2\lambda} \sum_x \sum_\mu (\partial_\mu^* A_\mu(x))^2 = -\frac{1}{2\lambda} \sum_x \sum_\mu (A_\mu(x) \partial_\mu \partial_\nu^* A_\nu(x)), \tag{2.17}$$

in such a way that we obtain the expression

$$S_G^0 + S_{GF} = \frac{1}{2} \sum_x \sum_{\mu\nu} A_\mu^a(x) \left[-\delta_{\mu\nu} \Box + \left(1 - \frac{1}{\lambda}\right) \partial_\mu \partial_\nu^* \right] A_\nu^b(x). \tag{2.18}$$

where $\Box = \partial_\rho^* \partial_\rho$. Fourier transforming, we rewrite the action in terms of the kernel $K_{\mu\nu}^{ab}(p, \lambda)$

$$S^0 = S_G^0 + S_{GF} = \frac{1}{2} \sum_{\mu\nu} \int_{\mathcal{B}} \tilde{A}_\mu^a(-p)\, K_{\mu\nu}^{ab}(p, \lambda)\, \tilde{A}_\nu^b(p) \tag{2.19}$$

defined by

$$K_{\mu\nu}^{ab}(p, \lambda) = \delta^{ab} \left[\delta_{\mu\nu} \hat{p}^2 - \left(1 - \frac{1}{\lambda}\right) \hat{p}_\mu \hat{p}_\nu \right]. \tag{2.20}$$

The lattice momenta $\hat{p}$ are defined in (A1.7). The kernel for the W action is:

$$K_{\mu\nu}^{W}(p, \lambda) = \left[\delta_{\mu\nu} \hat{p}^2 - \left(1 - \frac{1}{\lambda}\right) \hat{p}_\mu \hat{p}_\nu \right]. \tag{2.21}$$

Similarly to the continuum [40], the inverse kernel is:

$$K^{W}_{\sigma\mu}(p,\lambda)^{-1} = \frac{1}{\hat{p}^2}\left[\delta_{\sigma\mu} - (1-\lambda)\frac{\hat{p}_\sigma \hat{p}_\mu}{\hat{p}^2}\right], \tag{2.22}$$

where we obtain exactly the same expression we have in the continuum, with the difference that the momentum p is replaced by $\hat{p}$, defined on the lattice. The expression for the kernel from the LW action[2],

$$K^{\mathrm{LW}}_{\mu\nu}(p,\lambda) = \hat{p}^2\delta_{\mu\nu} + (\lambda-1)\hat{p}_\mu\hat{p}_\nu + \tfrac{a^2}{12}\left[(\hat{p}^4 + \hat{p}^2\hat{p}^2_\mu)\delta_{\mu\nu} - \hat{p}_\mu\hat{p}_\nu(\hat{p}^2_\mu + \hat{p}^2_\nu)\right]; \tag{2.23}$$

The gauge field propagator is given by:

$$\langle \tilde{A}^a_\mu(p)\tilde{A}^b_\nu(q)\rangle = (2\pi)^4\ \delta^{(4)}_P(p+q)\ \delta^{ab}\ K_{\mu\nu}(p,\lambda)^{-1}, \tag{2.24}$$

where $\delta^{(4)}_P$ incates the periodic Dirac δ-function, with period $\frac{2\pi}{a}$ and we consider $K_{\mu\nu}(p,\lambda)^{-1}$ to be either W or LW. It is useful to introduce the time-momentum representation of the propagator on a infinite lattice:

$$D_{\mu\nu}(x_0, y_0, \mathbf{p}) = \int_{-\frac{\pi}{a}}^{\frac{\pi}{a}} e^{ip_0(x_0-y_0)}\ K_{\mu\nu}(p,\lambda)^{-1} dp_0. \tag{2.25}$$

This will be useful because we will extensively use the so-called Schrödinger Functional (SF) boundary conditions, originally introduced in [41], which treat space and time coordinates differently.

2.2.3 Fermionic action

The full QCD action contains fermions and also in this case there is no unique way to define the action on the lattice. Different discretisations of the fermionic action correspond to different expressions for the Dirac operator. The easiest way to discretise the fermionic action (so-called naïve action) is to start from the continuum expression (2.4) and replace the derivative with the operator defined by:

$$D = \sum_\mu \frac{1}{2}\gamma_\mu[\Delta^*_\mu + \Delta_\mu], \tag{2.26}$$

[2]Note that by $\hat{p}^2$ we mean $(p_0^2 + p_1^2 + p_2^2 + p_3^2)$ and by $\hat{p}^2_{mu}$ we are just squaring one component.

where the covariant derivatives on the lattice are

$$\Delta_\mu \psi(x) = \tfrac{1}{a}[U_\mu(x)\psi(x+a\mu) - \psi(x)] \tag{2.27}$$

$$\Delta^*_\mu \psi(x) = \tfrac{1}{a}[\psi(x) - U_\mu(x-a\mu)^\dagger \psi(x-a\mu)]. \tag{2.28}$$

The problem with this choice is that it gives rise to unphysical poles which correspond to the so-called *doublers*. There is the Nielsen-Ninomiya no-go theorem (see for example [42]) which states that a discretisation of the Dirac operator, hermitian and such that it defines a local and translationally invariant action implies that we have to renounce either to the absence of the doublers or to the chiral invariance (for the chiral symmetry on the lattice see [43]). If we add to (2.26) the Wilson term:

$$D_W = \sum_\mu \left[\frac{1}{2} \left(\gamma_\mu [\Delta^*_\mu + \Delta_\mu] - a \Delta^*_\mu \Delta_\mu \right) \right], \tag{2.29}$$

we remove the doublers but we also break chiral symmetry. We have cutoff effects which are of $O(a^2)$ for the gauge action but for the fermionic part they are $O(a)$, then it is most likely required an improvement which can be realised by applying the Symanzik programme [44]. In this particular case, the classification of the counterterms, once we remove the redundant ones, is reduced to a single one which is the Sheikholeslami-Wohlert term [45]. The operator D_W satisfies γ_5-hermiticity

$$D_W^\dagger = \gamma_5 D_W \gamma_5 \tag{2.30}$$

which implies that the determinant of D_W is real and this is relevant for lattice simulations. There are other ways to discretise the fermion on the lattice, among the most popular the staggered fermions [46], and the domain-wall fermions [47].

The significant advantage of the lattice formulation is that it allows one to evaluate the expectation value of a generic operator (2.7) using Monte Carlo methods that we define in the next section.

2.3 Monte Carlo methods

In quantum field theory the physical information is contained in the correlation functions which, in the path integral formulation, are written as (2.7). On the lattice, for a pure

gauge theory, the integral in terms of the link variables reads:

$$\langle O \rangle = \frac{1}{\mathcal{Z}} \int \mathcal{D}[U]\; O[U]\, e^{-S[U]}. \tag{2.31}$$

The expectation value (2.31) of an operator O, defined in terms of a normalised probability density:

$$p(U) = \frac{1}{\mathcal{Z}} e^{-S[U]}, \tag{2.32}$$

is formally identical to the average of a classical statistical system, where the partition function given by:

$$\mathcal{Z} = \int [\mathcal{D}U]\, e^{-S[U]}. \tag{2.33}$$

The average is done with respect to the Boltzmann weight factor $e^{-S[U]}$. The analogy with a classical statistical system implies that the expectation value can be estimated summing over a discrete ensemble of representative gauge field configurations, $\{U\}_i$, generated according to the aforementioned probability density $p(U)$. Given N field configurations $\{U\}_i$, the general strategy to evaluate the expectation value is to take the average:

$$\langle O \rangle \approx \frac{1}{N} \sum_{i=1}^{N} O(\{U\}_i). \tag{2.34}$$

The value obtained is correct up to correction of $O(\frac{1}{\sqrt{N}})$, this is asymptotically ($N \to \infty$) ensured by the central limit theorem. Using the Monte Carlo importance sampling it is possible to approximate the integral (2.31) with the sum by sampling a small number of Boltzmann distributed field configurations. The larger the number of gauge field configurations the smaller the statistical error, but of course to generate a large number of configurations is also computationally demanding. One can start from setting all link variables to the unit matrix (cold start) or to some random values (hot start). The random updates U_i form the so-called Markov chain and we say that the system is thermalised when it reaches the equilibrium distribution, that is the one to which the Markov chain converges. One can check the behaviour of a set of observables, i.e. how they change with the number of updates (Monte Carlo histories) and when the values of the observables stabilise around a mean value then one can consider the configurations thermalised. In the evaluation of the statistical error the autocorrelation time plays an important role. The importance sampling methods are employed in such a way that the number of configurations required to have a good estimation of the expectation value is

not too large.

Due to the large number of variables it is difficult to evaluate it, lattice QCD makes use of Monte Carlo techniques to compute this integral numerically (see for example the following textbooks [36–38] and [48–51]). There is a number of algorithms one can use. In the case of a pure gauge theory, the heat bath algorithm is more efficient that other used for dynamical fermions. The heat bath algorithm was firstly proposed in 1980 by Creutz for a SU(2) gauge theory [23] and it has been extended by Cabibbo et al. to a generic gauge group SU(N) [52] and finally improved [53–56].

The process of thermalising the link with the next-neighbor is the reason for which is called heat bath, and it is originally used in statistical mechanics. The overrelaxation update step allows to make faster the decorrelation between subsequent configurations. This step is performed without changing the action and this makes it non-ergodic, therefore it has to combined it with another algorithm, such as the heat bath. The transition probability for going from the configuration i to the subsequent i' by using such algorithm does not depend on previous and it is proportional to the Boltzmann factor:

$$\mathcal{P}(i \to i') \propto e^{-S(i')}. \tag{2.35}$$

Ideally, the configurations are not correlated, but in practice one observes that they are. It is possible to study the correlation between configurations which appears in the measured quantities, there are many binning techniques one can employ, such as jackknife or bootstrap, where one naively computes the averages of the bin in which the data are divided, assuming that they are uncorrelated. A more refined strategy is defined in [57] in order to determine autocorrelation functions and times, which allows one to better estimate the statistical error, in comparison to the popular binning techniques aforementioned. In fact, the autocorrelation function Γ_A is defined such that it only depends on the difference $i - j$ and not on the starting point:

$$\Gamma_{\mathcal{A}}(i-j) = \langle (a_i - \mathcal{A})(a_j - \mathcal{A}) \rangle \tag{2.36}$$

where a_i is the measurement on the i-th configuration of the primary observable $\mathcal{A}$ (also derived quantities are defined in the reference). Increasing the separation between i and j the autocorrelation function exponentially decreases $\Gamma_{\mathcal{A}} \sim e^{-\frac{t}{\tau}}$. The integrated autocorrelation time is defined by:

$$\tau_{int} = \frac{1}{2} \sum_{t=-\infty}^{t=+\infty} \frac{\Gamma_{\mathcal{A}}(t)}{\Gamma_{\mathcal{A}}(0)} \tag{2.37}$$

where $\Gamma_{\mathcal{A}}(0)$ is the variance of the observable $\mathcal{A}$. Increasing the statistics, for $N >> \tau$ the integrated autocorrelation time can be approximated by

$$2N\tau_{int} = N \sum_{t=-\infty}^{t=+\infty} \frac{\Gamma_{\mathcal{A}}(t)}{\Gamma_{\mathcal{A}}(0)} \simeq \sum_{i=1}^{N} \sum_{j=1}^{N} \frac{\Gamma_{\mathcal{A}}(i-j)}{\Gamma_{\mathcal{A}}(0)} \tag{2.38}$$

where $\Gamma_{\mathcal{A}}(t)$ is estimated by

$$\Gamma_{\mathcal{A}}(t) \simeq \frac{1}{N-t} \sum_{i=1}^{N-t} \left(a_i - \frac{1}{N} \sum_{j=1}^{N} a_j \right) \left(a_{i+t} - \frac{1}{N} \sum_{k=1}^{N} a_k \right) \tag{2.39}$$

which also has an error. In order to have a good estimation of $\Gamma_{\mathcal{A}}(t)$ it is useful to check it graphically. All the details of the analysis are explained in [57] where the author gives an implementation in MATLAB. There are also equivalent implementations to compute the statistical error, the hadron library in R (`https://github.com/HISKP-LQCD/hadron/blob/master/R/UWerr.R`) and a code in python (`https://github.com/argiarubeo/py-uwerr`). The error is given by:

$$\sigma^2(N, \mathcal{A}) = \frac{\mathrm{var}(\mathcal{A})}{\frac{N}{2\tau_{int}}}, \tag{2.40}$$

where $\mathrm{var}(\mathcal{A})$ is the variance. The smaller the integrated autocorrelation time τ_{int} the better performing the algorithm.

One of the main problems in lattice QCD simulations is that it is difficult to estimate the relevant time-scale of the algorithm used and then to verify the correctness of the analysis of a particular observable. One has to test it empirically within the statistical errors. The critical slowing down is the phenomenon for which an increase in computational effort is required when approaching critical points of a theory [58]. When one takes the continuum limit is approaching a continuum phase transition and a critical slowing down is expected. This means that the auto-correlation times of the observables increase. Auto-correlation times are not universal quantities, in fact they depend on the algorithm, the correlation lengths and on the discretisation of the theory. In order to ensure that the simulation is ergodic enough, one has to measure such times and make sure that they are much shorter than the total run. An observable that has been studied over the years and exhibits long auto-correlation times for either pure Yang-Mills theory or QCD is the topological charge Q. On the lattice the variable Q, defined as:

$$Q(t) = \frac{1}{16\pi^2} \sum_{x} G_{\mu\nu}(x,t) \tilde{G}_{\mu\nu}(x,t), \tag{2.41}$$

where $F_{\mu\nu}$ is defined in eq. 2.3. While in the continuum the topological sectors are separated, on the lattice one observes that the simulations tend to get trapped in the topological charge sectors of field space [59]. The consequent problem with this issue is that the transition from one sector to another is suppressed in such a way that this might cause bad sampling because of the very long autocorrelation times. Different boundary conditions have been studied to overcome this problem [59]. By studying the autocorrelation of topological charge Q, as it is notoriously long, one can set the requirements for the simulation time in such a way that the observables are not correlated [58].

In summary, in this chapter we have reviewed how the theory of QCD is defined in the continuum spacetime, and then how it can be discretised on the lattice. The simplest action on the lattice is the Wilson plaquette action, which represents the pure gluonic action. It is possible to write an improved version, which we use later in this work, the so-called Lüscher-Weisz action.

We have also mentioned the main ways of discretising the fermionic part on the lattice and the problems that unavoidably emerge depending on which discretisation we choose.

Finally, we briefly define Monte Carlo methods which are used in non-perturbative lattice simulations, and the analysis which is needed in order to evaluate the statistical error.

3 Gradient flow equation in the continuum: definition and perturbative expansion of the observable in the Schrödinger Functional

We follow [4] to introduce the GF, which is a very useful tool in lattice gauge theories as it provides a class of observables with simple renormalisation properties. In general, in quantum field theory there are problems due to both infrared and ultraviolet divergences. In QCD the behaviour of the coupling makes the ultraviolet regime perturbative. In this regime it is possible to apply the renormalisation procedure while it is much harder to show that Yang-Mills (YM) theories have a mass gap. The advantage of the GF is that it allows one to define composite operators which are finite at positive flow time. As the ultraviolet divergences are smeared out one can use the flow as a tool for interesting applications. We report the explicit example of the perturbative value first computed by Lüscher of the so-called action density to show that it is finite after the renormalisation of the coupling. Then we list some applications and finally we move to the finite volume.

Most of this chapter is a review of the literature, our own contribution is to perform the computation of the continuum values of the energy density, at leading order in perturbation theory, with SF-open boundary conditions.

3.1 Definition of the gradient flow

The GF is a mapping:

$$A_\mu(x) \to B_\mu(t,x), \tag{3.1}$$

which introduces the dependence of the gauge field on an additional parameter $t \geq 0$, the flow time. For the sake of clarity, we remind the reader that the argument of the gauge field, x, is a four-vector including the three spatial coordinates and the euclidean time, not to be confused with the flow time, which has the dimension of length squared, $[t] = L^2$. The dependence of the gauge field on the flow time is dictated by the differential equation:

$$\begin{cases} \frac{\partial}{\partial t} B_\mu(t,x) = D_\nu G_{\nu\mu}(t,x) \\ B_\mu(t,x)|_{t=0} = A_\mu(x). \end{cases} \tag{3.2}$$

In the first equation, the derivative is taken with respect to flow time, and both the covariant derivative and the field strength tensor are similar to those in four dimensions, but here they are defined in terms of the $B_\mu(t,x)$ field, which also depends on the flow time:

$$\begin{aligned} D_\mu &= \partial_\mu + [B_\mu, \cdot] \\ G_{\mu\nu}(t,x) &= \partial_\mu B_\nu(t,x) - \partial_\nu B_\mu(t,x) + [B_\mu(t,x), B_\nu(t,x)]; \end{aligned} \tag{3.3}$$

the second equation in (3.2) is the initial condition; it states that at flow time $t = 0$ the new gauge field $B(t,x)$ is the original gauge field $A_\mu(x)$ in four dimensions. The evolution in flow time given by the equation (3.2) is gauge-covariant, for a gauge transformation:

$$B_\mu \to \Omega(x) B_\mu(x) \Omega^\dagger(x) + \Omega(x) \partial_\mu(x) \Omega^\dagger(x). \tag{3.4}$$

It is useful to extend the gauge symmetry to the flow time coordinate $x_4 = t$, [26], so that the transformation on $B_4(\tilde{x})$ is:

$$B_4(\tilde{x}) \to \Lambda(\tilde{x}) B_4(\tilde{x}) \Lambda(\tilde{x})^\dagger + \Lambda(\tilde{x}) \partial_4 \Lambda(\tilde{x})^\dagger \tag{3.5}$$

where $\tilde{x} = (x_4, x)$ and $x = (x_0, x_1, x_2, x_3)$ is the four-dimensional spacetime coordinate. The flow time derivative is replaced by the covariant derivative

$$\partial_t \to \partial_4 + [B_4, \cdot] \tag{3.6}$$

and

$$\partial_t B_\mu(t, x) \to G_{4\mu}(x_4, x), \tag{3.7}$$

so that replacing the flow time derivative with the covariant derivative the flow equation F_μ transforms as

$$F_\mu \to \Lambda F_\mu \Lambda^\dagger, \tag{3.8}$$

where:

$$F_\mu(t, x) = \partial_t B_\mu - D_\nu G_{\nu\mu}. \tag{3.9}$$

The flow equation can be extended to the fermion fields [28]:

$$\begin{cases} \partial_t \chi = \Delta \chi \\ \chi|_{t=0} = \psi, \end{cases} \tag{3.10}$$

$$\begin{cases} \partial_t \bar{\chi} = \bar{\chi} \overleftarrow{\Delta} \\ \bar{\chi}|_{t=0} = \bar{\psi}, \end{cases} \tag{3.11}$$

where $\Delta = D_\mu D_\mu$. [1]

3.1.1 Smearing procedure: solution of the gradient flow equation at leading order in perturbation theory

The r.h.s. of the flow equation (3.2), is proportional to the gradient of the YM action:

$$\frac{\partial}{\partial t} B_\mu(t, x) = -\frac{\delta S_{YM}}{\delta B_\mu}, \tag{3.12}$$

[1] One could also choose $\not{D}\not{D}$.

hence it is called the gradient flow. From this equation it is clear that we are pushing the field configuration towards the stationary points of the action S_{YM}, which is a smoothing operation. Rescaling the field by the bare coupling and performing a perturbative expansion[2] of the gauge field, we have:

$$B_\mu(x,t) = \sum_n B_{\mu,n}(x,t) g_0^n. \tag{3.13}$$

The flow equation with a gauge fixing parameter, α, for a choice of Λ (see [60]), is:

$$\frac{dB_\mu}{dt} = D_\nu G_{\nu\mu} + \alpha D_\mu \partial_\nu B_\nu. \tag{3.14}$$

For $\alpha = 0$ the flow equation at leading order reads:

$$\frac{\partial B_\mu}{\partial t} = \partial^2 B_{\mu,1} - \sum_\nu \partial_\mu \partial_\nu B_{\nu,1}, \tag{3.15}$$

which is nothing but the heat equation and a gauge-fixing term. In momentum space the gauge field is:

$$B_{\mu,1}(x,t) = \int_p e^{ipx} \tilde{B}_{\mu,1}(p,t), \tag{3.16}$$

where we use the shorthand $\int_p = \int \frac{d^4p}{(2\pi)^4}$. The l.h.s. is:

$$\frac{dB_{\mu,1}(x,t)}{dt} = \int_p \frac{d\tilde{B}_{\mu,1}(p,t)}{dt} e^{ipx} \tag{3.17}$$

and the r.h.s.:

$$\partial^2 B_{\mu,1} - \sum_\nu \partial_\mu \partial_\nu B_{\nu,1} = -\int_p p^2 \tilde{B}_{\mu,1}(p,t) e^{ipx} + \sum_\nu \int_p p_\mu p_\nu \tilde{B}_{\nu,1}(p,t) e^{ipx}. \tag{3.18}$$

Then the flow equation for $\alpha = 0$ in momentum space is written as:

$$\frac{dB_{\mu,1}(p,t)}{dt} = -\sum_\nu (p^2 \delta_{\mu\nu} - p_\mu p_\nu) \tilde{B}_{\nu,1}(p,t); \quad \tilde{B}_{\mu,1}(p,0) = \tilde{A}_\mu(p). \tag{3.19}$$

We can choose any value of α to fix the gauge, and the choice cannot change the value of any observable which is gauge independent as it must be. For $\alpha = 1$ the solution can

[2] In general by taking a few terms one can have a good idea of the perturbative behaviour, and one can also check how much the result change by adding the next term.

be written as:

$$B_\mu(x,t) = \int d^D y\, A_\mu(y)\, K_t(x-y), \tag{3.20}$$

the convolution of the gauge field with the heat kernel, which is:

$$K_t(x) = \frac{e^{-\frac{|x|^2}{4t}}}{(4\pi t)^{\frac{D}{2}}}, \tag{3.21}$$

with smearing radius $\sqrt{2Dt}$ (see Fig. 3.1).

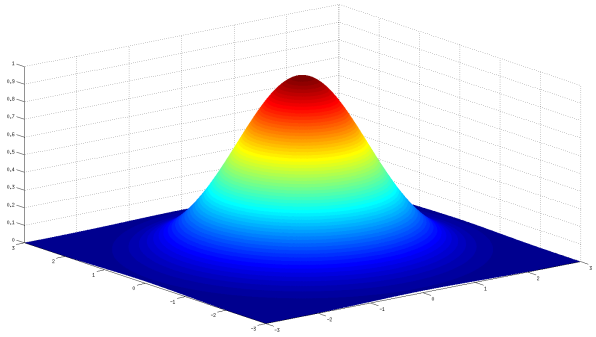

Figure 3.1: The gauge field is smeared over a region (a gaussian bell) of radius which is $\sqrt{8t}$ in $D = 4$ dimensions.

The lowest order and the next-to-leading order terms in the perturbative solution of the flow equation do not contain loops in the bulk. From here, we obtain the intuitive picture of the smoothing process: the gauge field is spread over a spherical region, where the radius, in dimension $D = 4$, is $\sqrt{8t}$. This is just a geometrical trick to remove the ultra-violet divergences and it has no physical meaning. We want to use the advantage of this property in the context of renormalisation of composite operators.

We want to mention that the idea of the smearing procedure is not completely new, in fact it was introduced in a different context for other motivations. The first smearing was proposed by the APE collaboration [61] and other variants were used in quenched studies. Later, the stout-link smearing [62] was introduced by Morningstar and Peardon, and used in dynamical simulations. Other examples of smearing are the Hyper-cubic (HYP) blocking [63] or cooling [64]. The cooling method is performed by making discrete steps, while the GF ensures the smoothing process is imposed through the differential eq. (3.2).

3.2 Local field theory in $D+1$ dimensions

The theory with the flowed field $B_\mu(x,t)$ is non-local and in order to study the renormalisation properties of the theory we need to have a local formulation. In particular, in order to apply the Symanzik improvement programme, which is designed to systematically reduce the cutoff effects by adding local counterterms to the action and the observables, we need to have a local formulation. It is possible to formulate the theory equivalently in a local and renormalisable fashion, such that the non-local operators in the 4-dimensional theory are mapped to local operators in the 5-dimensional theory. In this formulation the flow time t is the extra-coordinate. It has been shown, for a Langevin equation, that

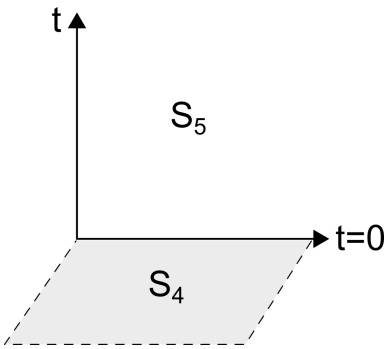

Figure 3.2: Extra-dimensional theory: S_5 is the 5-dimensional action defined in the half-space $t \geq 0$, while S_4 lives at the 4-dimensional boundary $t = 0$.

the correlation function of the flowed field in D dimensions coincides with the correlation function in a local $D+1$-dimensional field theory (Zinn-Justin and Zwanziger [65, 66]). The GF equation is a particular case of the Langevin equation [27], where the noise term is taken to zero. Given the action in D dimensions it is possible to formulate the theory in a local form, including a Lagrange multiplier field $L_\mu(t,x) = L^a_\mu(t,x)T^a$, which has colour and Lorentz degrees of freedom and which allows one to include the flow equation (eq. (3.2)) as a constraint. In dimension $D = 4$, we have that S_4 is the 4-dimensional YM action:

$$S_4 = -\frac{1}{2g_0^2}\int d^4x \ \mathrm{Tr}\left\{F_{\mu\nu}F_{\mu\nu}\right\} \tag{3.22}$$

and we use the equivalence with the extra-dimensional theory, see Fig. 3.2, in order to rewrite the path integral as:

$$\int \mathcal{D}[A]\ O[\bar{B}]\ e^{-S_4} = \int \mathcal{D}[B]\mathcal{D}[L]\ O[B]\ e^{-S_4-S_5}, \tag{3.23}$$

where $\bar{B}$ is the solution of the GF equation and S_5 reads:

$$S_5 = i \int \mathrm{Tr}\left(L_\mu \left\{\partial_t B_\mu - D_\rho G_{\rho\mu}\right\}\right) d^4x\, dt, \tag{3.24}$$

where L_μ has real components. By integrating over L_μ we obtain a delta functional

$$\int \mathcal{D}L_\mu\, e^{-S_5} = \int \mathcal{D}L_\mu\, e^{i2a^4 \int_0^\infty dt \sum_{x,\mu} \mathrm{Tr} L_\mu(t,x) F_\mu(t,x)} = \delta(F_\mu), \tag{3.25}$$

which imposes the flow equation, and where F_μ is defined in eq. (3.9) in order to write the lattice gradient flow equation as $F_\mu(t,x) = 0$ [3]. We defined the flow equation and now we look at the simplest gauge invariant object we can consider in the continuum, the action density. Its perturbative expansion is finite at positive flow time, unlike the same observable at $t = 0$ which diverges. It has been shown that this is true at all orders in perturbation theory [27]. Next, we see that the action density has been computed explicitly to next-to-next-to-leading order. We also see that the property of being finite allow for useful application concerning the coupling constant and the scale setting.

3.3 Perturbative expansion of the observable $\langle E(t)\rangle$ in infinite volume

The simplest object, satisfying gauge invariance, that we can define is the action density:

$$E(t,x) = -\frac{1}{2}\sum_{\mu,\nu} \mathrm{Tr}\{G_{\mu\nu}(t,x) G_{\mu\nu}(t,x)\}. \tag{3.26}$$

The perturbative expansion of $\langle E(t)\rangle$ has been computed [4], in infinite volume with dimensional regularisation. In perturbation theory the gauge potential is scaled by the bare coupling:

$$A_\mu \to g_0 A_\mu, \tag{3.27}$$

and consequently the flowed gauge potential has an expansion:

$$B_\mu = \sum_{k=1}^{\infty} g_0^k B_{\mu,k}, \qquad B_{\mu,k}|_{t=0} = \delta_{k1} A_\mu. \tag{3.28}$$

When inserted in the expectation value of the observable it gives:

$$\mathcal{E}(t) = \langle E(t) \rangle = \frac{1}{2} \langle \partial_\mu B^a_\nu(t) \partial_\mu B^a_\nu(t) - \partial_\mu B^a_\nu(t) \partial_\nu B^a_\mu(t) \rangle + O(B^4) \tag{3.29}$$

The Fourier representation of the B-field is:

$$B^a_{\mu,1}(t,x) = \int \frac{d^D p}{(2\pi)^D} e^{ipx} e^{-tp^2} \tilde{A}_\mu{}^a(p), \tag{3.30}$$

The observable is a linear combination of derivatives applied to the B-field propagator; the latter, in infinite spacetime volume, at finite flow times s, t, it has the expression:

$$\langle B^a_\mu(s,x) B^b_\nu(t,y) \rangle = \delta^{ab} \int \frac{d^4 p}{(2\pi)^4} e^{ip(x-y)} \bar{D}_{\mu\nu}(p; s, t; \alpha, \lambda) + O(g_0^2), \tag{3.31}$$

where

$$\bar{D}(p; s, t; \alpha, \lambda) = H(s, p, \alpha) D(p, \lambda) H(t, -p, \alpha)^T, \tag{3.32}$$

$D(p, \lambda)$ is defined in (2.25) and we use a matrix notation for the Lorentz indices $\mu, \nu = 0, \dots, 3$, with H^T indicating the transpose matrix. The free heat kernel is

$$H(t, p, \alpha) = \exp(-tK(p, \alpha)), \tag{3.33}$$

K is the Yang-Mills action kernel (3.33) and $\alpha > 0$ is the gauge parameter of the flow time evolution. The action density at leading order reads:

$$\mathcal{E} = \frac{g_0^2}{2} (N^2 - 1) \int \frac{d^D p}{(2\pi)^D} e^{-2tp^2} (p^2 \delta_{\mu\nu} - p_\mu p_\nu) \bar{D}(p, \lambda)_{\mu\nu} + O(g_0^4), \tag{3.34}$$

where the $\bar{D}$-propagator eq. (3.32) contains the B_μ-fields, while the D-propagator contains the gauge fields A_μ. In Fourier space, the B- and A-fields are related by:

$$\tilde{B}_\mu(t, p) = \sum_\nu H_{\mu\nu}(t, p, \alpha) \tilde{A}_\nu(p)\,, \tag{3.35}$$

where the heat kernel is given in (3.33). Setting $D = 4 - 2\epsilon$, one obtains:

$$\mathcal{E} = \frac{g_0^2}{2} \frac{N^2 - 1}{(8\pi t)^{\frac{D}{2}}} (D - 1) \left\{ 1 + g_0^2 (2t)^\epsilon \frac{\Gamma(2 - 2\epsilon)}{\Gamma(2 - \epsilon)} \omega_1 + \dots \right\}, \tag{3.36}$$

where

$$\omega_1 = \frac{1}{16\pi^2} (4\pi e^{-\gamma_E})^\epsilon \left\{ N \left(\frac{5}{3\epsilon} + \frac{31}{9} \right) - N_f \left(\frac{2}{3\epsilon} + \frac{10}{9} \right) + O(\epsilon) \right\}, \tag{3.37}$$

$\gamma_E = 0.577...$ is Euler's constant and N_f is the number of flavours. The bare coupling g_0 is related to the renormalised coupling g in the $\bar{MS}$ scheme by [67]:

$$g_0^2 = g^2 \mu^{2\epsilon} (4\pi e^{-\gamma_\epsilon})^{-\epsilon} \left\{ 1 - \frac{1}{\epsilon} b_0 g^2 + O(g^4) \right\} \tag{3.38}$$

where

$$b_0 = \frac{1}{16\pi^2} \left\{ \frac{11}{3} N - \frac{2}{3} N_f \right\} \tag{3.39}$$

and μ is the subtraction scale at which the theory is renormalised. The expectation value of the action density, at lowest order, is then expressed in terms of the renormalised coupling as:

$$\langle E(t) \rangle = \frac{3(N^2-1)g^2}{128\pi^2 t^2} \left\{ 1 + \bar{c}_1 g^2 + \bar{c}_2 g^4 + O(g^6) \right\}, \tag{3.40}$$

where the terms in $\frac{1}{\epsilon}$ cancel and the coefficients:

$$\bar{c}_1 = \frac{1}{16\pi^2} \left\{ N \left(\frac{11}{3} L + \frac{52}{9} - 3\ln 3 \right) - N_f \left(\frac{2}{3} L + \frac{4}{9} - \frac{4}{3} \ln 2 \right) \right\}, \tag{3.41}$$

while

$$\bar{c}_2 = \frac{k_2}{16\pi^2} \tag{3.42}$$

and the numerical value of k_2 is given in [68].

The observable $\mathcal{E}_0(t)$ we are going to use in this work is the coefficient of the leading order in the perturbative expansion of $\mathcal{E}$:

$$\mathcal{E}(t) = \mathcal{E}_0(t) g_0^2 + O(g_0^4), \tag{3.43}$$

which in terms of the derivatives of gradient flowed fields is the combination:

$$\mathcal{E}_0(t) = \frac{1}{2} \langle \partial_\mu B^a_{\nu,1}(t) \partial_\mu B^a_{\nu,1}(t) - \partial_\mu B^a_{\nu,1}(t) \partial_\nu B^a_{\mu,1}(t) \rangle. \tag{3.44}$$

Later we define it in finite volume in such a way that it will depend not only on the smearing radius introduced by the flow equation but also on the lattice size L. Its asymptotic value in infinite volume is:

$$t^2 \mathcal{E}_0(t) = \frac{3}{16\pi^2}, \tag{3.45}$$

for $N = 3$. As we will see, the finite volume is a useful tool as it allows to use the step scaling and then to apply the non-perturbative renormalisation.

In this section, we gave an explicit demonstration that the observable $\langle E(t) \rangle$ is finite at positive flow time, after the renormalisation of the gauge coupling. Such property is what allows for interesting applications that we list in the next section.

3.4 Uses of the gradient flow

We set the ground by defining the gradient flow, and we have also introduced the simplest gauge invariant object, which defines the observable we use to perform our tests. There are various interesting applications we mention here.

For example, the non-perturbative renormalisation of the running coupling can be studied combining a gradient flowed observable, such as the action density introduced, with the step scaling technique. Another application of the GF including the matter fields, is the spontaneous breaking of chiral symmetry in QCD where the flow time dependent condensate may serve as chiral order parameter in QCD at non-zero temperatures. Also, the GF can be used to understand the emergence of topological sectors in taking the continuum limit of QCD. Finally, there is an attempt in computing the electro-weak transition matrix elements using the effective hamiltonian approach. Such applications are an example of both the successful as well as the potentially powerful applications which motivate our work.

3.4.1 Small flow time expansion

We have seen that the advantage of using the GF is that the ultraviolet divergences are suppressed. By looking at the small flow time expansion [28] we can better understand how the divergences are suppressed. The generic flowed observable $O(t, x)$ can be related to the renormalised local fields $O^R(x)$ at flow time $t = 0$. The GF smears the gauge field. The more t goes toward zero the more local the field. The expansion has the form:

$$O(t, x) \sim \sum_k c_k(t) O_k^R(x) \quad \text{for } t \to 0, \tag{3.46}$$

where the coefficients $c_k(t)$ can be asymptotically determined using the renormalisation group theory [27]. The expansion is valid for correlation functions at nonzero separation,

where the fields are renormalised. A graphical representation is given in Fig. 3.3.

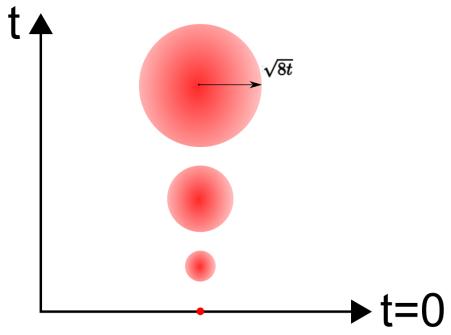

Figure 3.3: Small flow time expansion, the smaller the flow time t, the more local the operator.

This expansion is similar to the operator product expansion, and the coefficients $c_k(t)$ can be computed in perturbation theory, as one does for the Wilson coefficients. The small flow time expansion [28] is useful to compute quantities such as the energy-momentum tensor (EMT), and the chiral condensate.

3.4.2 Scale setting and renormalisation of the coupling constant

Gauge invariant operators are composite. In a pure gauge theory, the easiest observable which satisfies gauge invariance, defined in terms of the gradient flowed fields $B_\mu(t,x)$, is the action density defined in eq. (3.26). The expectation value $\langle E(t,x)\rangle$ has two successful applications which have been studied.

- First, the scale setting [4] can be done using the dimensionless quantity $t^2\langle E(t,x)\rangle$ which is ideal as it can be computed with high statistical precision and does not require any extrapolation to a physical quantity [69]. One can define a reference scale t_0 via the equation:

$$t^2\langle E(t)\rangle|_{t=t_0} = 0.3. \tag{3.47}$$

  In Fig. 3.4 an extrapolation of the dimensionless ratio between $\sqrt{8t_0}$ and the Sommer radius r_0 is shown. The grey points show the presence of strong discretisation effects, while for the black point there is an accidental cancellation [4].

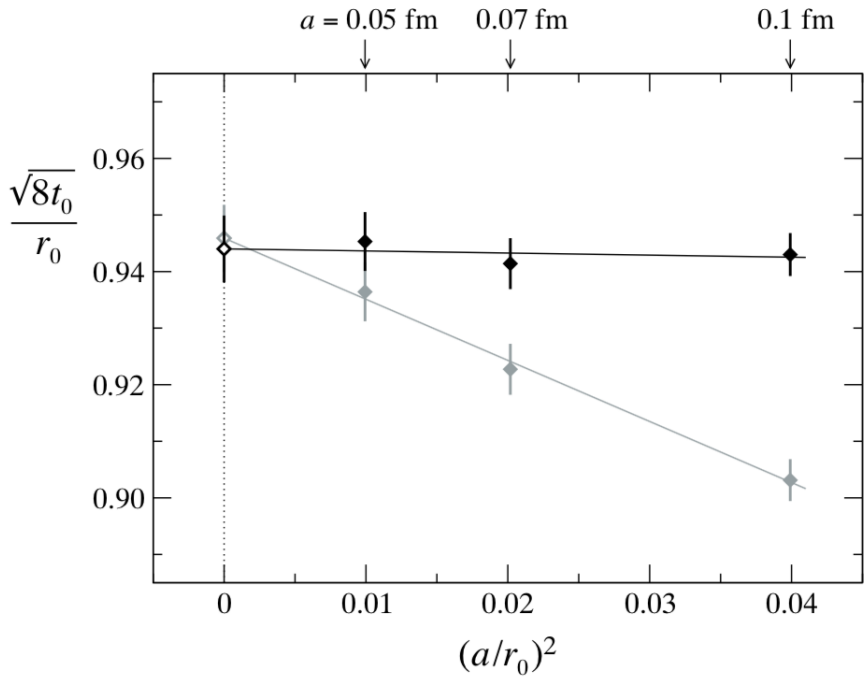

Figure 3.4: Extrapolation of the dimensionless ratio $\frac{\sqrt{8t_0}}{r_0}$ of reference scales to the continuum limit taken from [4], where t_0 has been defined through the gradient flow observable $E(t)$ in eq. (3.47), while r_0 is the Sommer radius defined by the static potential (see [5]). The comparison is between the clover (black) and plaquette (grey) discretisations of the observable $E(t)$ used to define t_0. At tree-level, the clover discretisation looks less affected by cutoff effects, but this is an accidental cancellation where the cutoff effects coming from action (Wilson, pure gauge) and flow (Wilson) cancel those relative to the observable[4].

Another possibility to set the scale is to use the reference w_0 defined by[69]:

$$t\frac{d}{dt}t^2\langle E(t)\rangle|_{t=w_0^2} = 0.3, \tag{3.48}$$

where the observable is replaced by its derivative with respect to the flow time[3];

- Second, the coupling that can be defined non-perturbatively in terms of GF observables, with SF boundary conditions [7, 70]. By inverting the perturbative expansion of the expectation value of the energy density $\langle E(t,x)\rangle$ eq. (3.40), one can give the following non-perturbative definition:

$$\bar{g}^2_{GF} = \mathcal{N}^{-1}t^2\langle E(t,x)\rangle \tag{3.49}$$

[3]The advantage of this choice is that it gives rise to smaller cutoff effects in comparison with t_0.

where the normalisation factor $\mathcal{N}$ ensures that:

$$\bar{g}^2_{GF} = g_0^2 + O(g_0^4). \tag{3.50}$$

This definition of the coupling allows its measurement using lattice simulations [7].Once the coupling is computed at some energy scale, it is difficult to bridge the large scale difference, which is connecting the perturbative regime to the hadronic scale, where the lattice performs best. A very elegant way to overcome this difficulty is to perform step-scaling studies, to connect the non-perturbative regime to the perturbative one, at high energies. As we pointed out, $\langle E(t,x)\rangle$ does not require renormalisation at $t > 0$; the flow time has dimension of length squared $t = [L^2]$ and by setting

$$c = \frac{\sqrt{(8t)}}{L}, \tag{3.51}$$

the coupling results depend only on one scale, the lattice size L. This allows the step scaling studies to be performed. By identifying the renormalisation scale with the size of the box $\mu = \frac{1}{L}$ it is possible to study the running of the gauge coupling. This technique defines the finite-size scaling method. The so-called step scaling

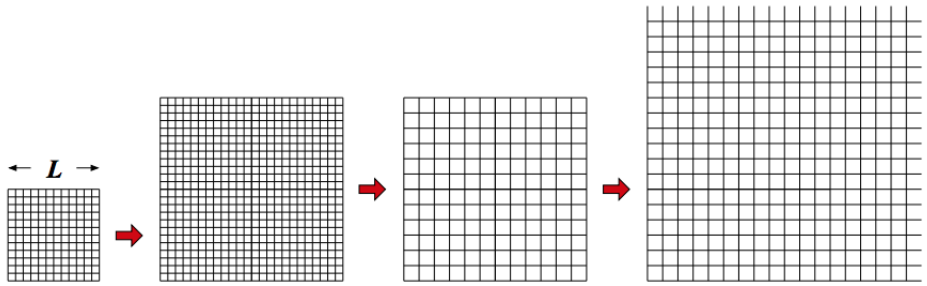

Figure 3.5: Step scaling studies performed by fixing the coupling $g^2(L) = u$ and determining L/a and g_0 (such that $g^2(L)$ is kept fixed at the value u. For these values of the lattice spacing a one computes the coupling on a lattice $2L/a$ and measure $g^2(2L)$which is the step scaling function; finally one does the extrapolation to the continuum limit $a \to 0$ (Fig. taken from [6]).

function (see Fig. 3.5) measures how much the value of the coupling changes when the volume is doubled $L \to 2L$:

$$\sigma(u,2) = \bar{g}^2(2L)|_{\bar{g}^2(L)=u}. \tag{3.52}$$

The step scaling function is a discrete version of the beta function which appears in

the renormalisation group equation and describes how the coupling varies within the renormalisation scale. The procedure of performing the scaling step at different resolutions and taking the continuum extrapolation $\frac{a}{L} \to 0$ defines the non-perturbative renormalisation.

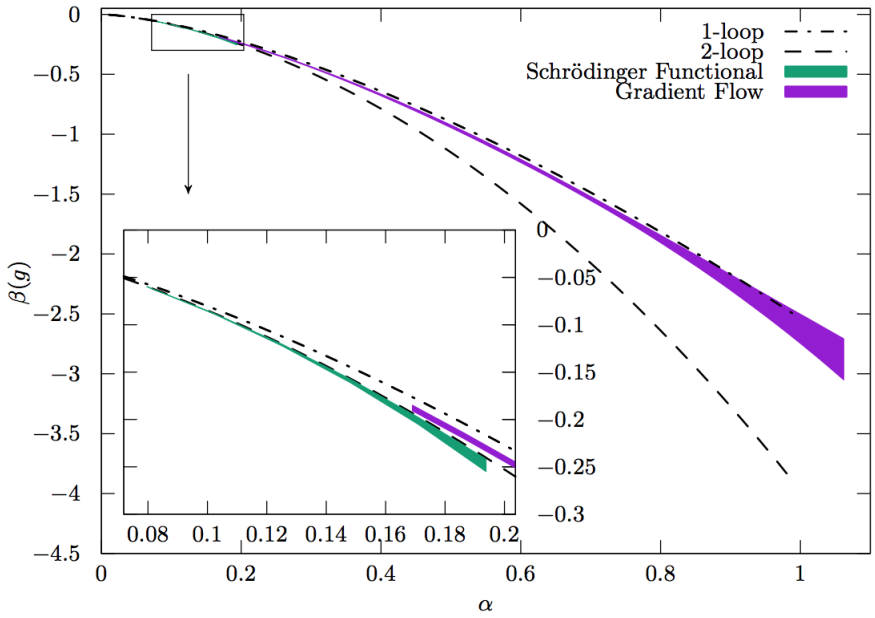

Figure 3.6: Beta function relative to two different definitions of the coupling, GF and SF. The figure shows the connection between the two, they are computed in QCD with $N_f = 3$. The GF coupling is computed in the energy range between 200 MeV and 4 GeV (large coupling region) [7]. At higher energies the SF coupling works better and it agrees with the perturbative result as one must expect. We see the 1-loop and 2-loop result, the 3-loop value already does not change much from the 2-loop result. Going at even higher energies where the coupling is small (less than 0.1), one can confidently make a connection with perturbation theory.

The study of the GF coupling is performed in the energy range between 200 MeV and 4 GeV, and its connection with the SF coupling is shown in Fig. 3.6 [7]. The SF coupling better performs at high energies, where perturbation theory can be applied with confidence (see [71, 72] and references therein) .

On the other hand, the perturbation theory is quite hard; in this context, numerical stochastic perturbation theory (NSPT) serves as a very powerful tool to automatise them. NSPT is based on the Langevin equation, but it has recently been technically improved using the stochastic molecular dynamics equations (generalized Hybrid Monte Carlo) [73, 74] leading to the understanding of the relation between the renormalised coupling and the bare coupling, at two loops.

3.4.3 Axial current renormalisation constant and chiral condensate

A possible extension of the flow equation which includes matter fields has been defined in eq. (3.10) and eq. (3.11). There are no significant complications introduced by the inclusion of the quark fields, concerning the theoretical analysis on one side and the practical implementation on the other side. Following [27] one can see that, once the renormalisation of the parameters of QCD has been carried out, the correlation function of gauge-invariant local fields, at positive flow time, requires only a multiplicative renormalisation of the gradient flowed quark fields. Simple Ward identities are satisfied by the correlation functions of flowed fields, being the flow equations chiral invariant [28]. The equivalence with the local theory in $D+1$ dimensions can be shown at all orders in perturbation theory. The renormalisation requires further counterterms, but bulk counterterms are not needed (see [27], the correlation functions are given by tree diagrams). There is only one additional counterterm required which is equivalent to a multiplicative renormalisation. The observable used to probe these properties is the chiral condensate defined by:

$$\langle \bar{\psi}(x)\psi(x)\rangle \tag{3.53}$$

where $\psi(x)$ indicates the quark field. It is an order parameter for the spontaneous chiral symmetry breaking mechanism. We can define the scalar and pseudoscalar densities in terms of the flowed fields $\chi(t,x)$ and $\bar{\chi}(t,x)$:

$$S_t^{rs}(x) = \bar{\chi}_r(t,x)\chi_s(t,x), \qquad P_t^{rs}(x) = \bar{\chi}_r(t,x)\gamma_5\chi_s(t,x), \tag{3.54}$$

where r,s are flavour indices. By evaluating the expectation value $\langle S_t^{rs}(x)\rangle$, one can evaluate the chiral condensate. Another application, studied in [28], is the renormalisation of the axial current and the $O(a)$ improvement is discussed [18, 75–78]. First, the effective Symanzik action is given, it includes the clover term and an additional one containing the Lagrange multiplier field introduced to formulate the local theory in $D+1$ dimensions. Also the effective local fields are improved. The PCAC relation is discussed and the renormalised pseudo-scalar meson decay constants can be obtained. In addition, there are further uses of the flow (e.g. the flavour singlet channel can be computed). Beyond that, also QCD-like theories near the conformal window and gauge theories based on other gauge groups and different fermion representations can be studied using such a powerful tool.

3.4.4 The energy momentum tensor

The energy momentum tensor on the lattice requires renormalisation as the Poincaré symmetry is broken by the regulator. Given the YM action, the EMT in dimensional regularisation, where we set $D = 4 - 2\epsilon$, is defined by (see for example [79]):

$$T_{\mu\nu}(x) = \frac{1}{g_0^2}\left[F^a_{\mu\rho}(x)F^a_{\nu\rho}(x) - \frac{1}{4}\delta_{\mu\nu}F^a_{\rho\sigma}(x)F^a_{\rho\sigma}(x)\right], \tag{3.55}$$

where $F_{\mu\rho}(x)$ is the field strength tensor defined in terms of the gauge field $A_\mu(x)$. The renormalisation can be done by imposing the Ward identities related to translations [80] and these identities can be probed using flowed observables [79, 81]. In section 3 of [79] a $D+1$ dimensional analogue of the EMT is expressed in terms of GF observables:

$$U_{\mu\nu}(t,x) = G^a_{\mu\rho}(t,x)G^a_{\nu\rho}(t,x) - \frac{1}{4}\delta_{\mu\nu}G^a_{\rho\sigma}(t,x)G^a_{\rho\sigma}(t,x), \tag{3.56}$$

where $G_{\mu\rho}(t,x)$ is a field strength tensor defined in terms of the gauge field $B_\mu(t,x)$. These observables have an asymptotic series, the small flow time expansion, with renormalised operators and finite coefficients. The EMT is a basic quantity in physics and it is relevant to study the scaling behaviour of quantum field theory in the strongly coupled regime; it also appears in Einstein's equation and in the equation of state of QCD [82, 83].

3.4.5 The topological charge and effective interactions

QCD gauge fields A_μ carry a non-zero topological charge which results in quite interesting topological properties; how the different topological sectors emerge when sending the lattice spacing to zero can be studied using the GF on the lattice. As topology is a non-perturbative issue the lattice is the ideal tool to study it. In particular using the gluonic definition of the topological charge it is possible to see exactly how the different topological sectors emerge, starting from the flowed link field $V_{\mu(t,x)}$ and perfoming a change of variables in the QCD functional integral [4] [84] [85]. Another application, in the limit of a large number of colours, is the Witten-Veneziano formula, which might explain the mass of the η' meson [86, 87].

The flow can be usefully employed for effective interactions. Low-energy hadronic processes are particularly difficult because the strong coupling at this scale ($\sim O(1GeV)$) is so large that it does not allow for a perturbative expansion to be valid. We do not go into the details of such uses, we refer to [88].

3.5 Finite volume. The Schrödinger Functional

In this thesis, we work with the Schrödinger Functional (SF) which has been introduced in the continuum theory and then on the lattice for gauge theories in [89]. The significant advantage of this formulation is that it allows one to connect the analytical perturbative regime to the numerical non-perturbative one. Using different boundary condition, such as periodic in all directions, renders perturbation theory very difficult because of the complicated structure of the QCD vacuum. The SF boundary conditions ensure that there is a unique minimum of the action which makes the perturbative expansion feasible. The renormalisability of the theory has been studied by Symanzik in [41] for scalar fields. In QCD one-loop renormalisability as been verified for a pure gauge theory in [89] and for QCD in [90] [91]. In finite volume $V = L^3T$ we can have more constraints, define more observables and we can use step scaling techniques, as seen in Sec. 3.4.2. This is relevant for studying the physics of the strong interaction as it allows one to connect the evolution of the renormalised gauge coupling from the perturbative high-energy regime to the non-perturbative one. In fact, through the use of a background field, one can define the so-called SF coupling, [89, 90, 92, 93], and compute it on the lattice. In the present work we choose zero background field and we introduce the coupling defined in terms of the GF observables we examine, the so-called GF coupling the connection between the two couplings has been shown in Fig. 3.6. In the path integral representation, defined on a Euclidean spacetime, the SF is a partition function which has the quantum mechanical interpretation of a propagation kernel for going from a field configuration at time $x_0 = 0$ to another at time $x_0 = T$.

We are not going into the details of the SF formulation in this regard, as here we consider zero background field, and we only want to impose such boundary conditions on the gradient flowed fields $B_\mu(t, x)$[4]:

$$B_\mu(x + \hat{k}L, t) = B_\mu(x, t) \tag{3.57}$$

and

$$B_k(x, t)|_{x_0=0,T} = 0. \tag{3.58}$$

This way the gauge field is periodic in the spatial directions, identified by the unit vector $\hat{k}$,

[4]In the literature on the SF the field B_μ indicates the background field, we want to stress again that here the background field is zero, and B_μ is the gauge field depending on the additional parameter, the flow time.

and its spatial components satisfy Dirichlet boundary conditions in time. The boundary conditions of the time component of the gauge field are not fixed but naturally emerge through the gauge fixing condition [70]. In addition, we analyse the so-called open-SF (SF-open) boundary conditions, which are defined by taking Neumann conditions, rather than Dirichlet at $x_0 = 0$ ($x_0 = T$):

$$\partial_0 B_k(t, x) = 0, \quad x_0 = 0 \text{ (or } x_0 = T). \tag{3.59}$$

3.6 How to impose SF/open boundary conditions from an orbifold reflection

The first step we wish to take is to study the perturbative expansion of the observable under examination. As we see in Sec.(3.3), it contains the propagators of the gauge fields $B_\mu(t, x)$, evolved in flow time. Before moving on, we derive the expression of such propagators using an orbifold reflection. It is advantageous to introduce this formulation as it makes the numerical computation of the observable of interest much faster. The benefit comes from the relic of translation invariance in the initial periodic set-up. Let us consider the simple case of a $2T$-periodic scalar field $\varphi(x_0)$ to explain this point. We define a reflection:

$$R: \quad \varphi(x_0) \to \varphi(-x_0), \tag{3.60}$$

about $x_0 = 0$. Since $R^2 = 1$, we can classify the states as eigenstates of the reflection operator which have eigenvalues $\lambda = \pm 1$, depending on wether they are even or odd components:

$$(R\varphi_\pm)(x_0) = \pm\varphi_\pm(x_0). \tag{3.61}$$

This means we can define the projectors:

$$(P_\pm\varphi)(x0) = \varphi_\pm(x0), \tag{3.62}$$

and we can split the function $\varphi(x_0)$ into even and odd components:

$$\varphi(x_0) = \varphi_+(x_0) + \varphi_-(x_0), \tag{3.63}$$

in such a way that

$$\varphi_-(0) = 0 = \varphi'_+(0). \tag{3.64}$$

Dirichlet and Neumann conditions at $x_0 = 0$ are satisfied for the odd and even parts of φ, respectively (see A2). Also, by imposing $2T$-periodicity we ensure the same boundary conditions at $x_0 = T$, while $2T$-antiperiodic boundary conditions imply interchanged Neumann and Dirichlet conditions at $x_0 = T$. By applying a Fourier transform to the function $\varphi(x_0)$:

$$\varphi(x_0) = \frac{1}{2T}\sum_{p_0} e^{ip_0x_0}\tilde{\varphi}(p_0) = \underbrace{\frac{1}{2T}\sum_{p_0}\cos(p_0x_0)\tilde{\varphi}(p_0)}_{\varphi_+(x_0)} + \underbrace{\frac{1}{2T}\sum_{p_0} i\sin(p_0x_0)\tilde{\varphi}(p_0)}_{\varphi_-(x_0)}, \tag{3.65}$$

we see that the parity of the function is contained in the functions $\cos(p_0x_0)$ and $\sin(p_0x_0)$, while $\tilde{\varphi}(p_0)$ remains unchanged. It is possible to extend this consideration to the four components of a gauge field and it is also possible to define the orbifold reflection on the lattice, where it is necessary to introduce the reflection with respect to both the link and the site.

3.7 Propagator of the B-fields in finite volume with SF/open boundary conditions

By setting the spacetime volume finite, $V = L^3 2T$, where L and T are the spatial and temporal extents respectively, the integrals become sums over momenta, which can be computed numerically. In this case, the B-field propagator is:

$$\langle B^a_\mu(x,t)B^b_\nu(y,s)\rangle^{PER} = \frac{\delta^{ab}}{L^3 2T}{\sum_{\mathbf{p}p_0}}' e^{ip(x-y)}\bar{D}_{\mu\nu}(p,t,s;\lambda,\alpha), \tag{3.66}$$

assuming periodic boundary conditions in the four directions. The primed sum indicates that we exclude the zero momentum term ($p = (0,0,0,0)$), and we use this notation everywhere in the following. The fact that we need to exclude the zero mode, comes from the gauge fixing we need to perform in order to invert the action kernel obtain the propagator.

As we have seen in Sec. 3.6 it is possibile to introduce either SF or SF-open boundary

conditions using an orbifold projection. We define the projectors:

$$P_{\pm} = \frac{1}{2}\left(1 \pm R\right) \tag{3.67}$$

where R has been defined in (3.61). By applying the following projectors to the propagator:

$$P_{-}\langle B_k^a(t, x_0, \mathbf{p}) B_l^b(s, y_0, -\mathbf{p})\rangle P_{-} = \frac{\delta^{ab}}{L^3 2T} {\sum_{\mathbf{p}p_0}}' \sin(p_0 x_0)\sin(p_0 y_0) e^{i\mathbf{p}(\mathbf{x}-\mathbf{y})} \bar{D}_{kl}(p, t, s; \lambda, \alpha), \tag{3.68}$$

$$P_{+}\langle B_0^a(t, x_0, \mathbf{p}) B_0^b(s, y_0, -\mathbf{p})\rangle P_{+} = \frac{\delta^{ab}}{L^3 2T} {\sum_{\mathbf{p}p_0}}' \cos(p_0 x_0)\cos(p_0 y_0) e^{i\mathbf{p}(\mathbf{x}-\mathbf{y})} \bar{D}_{00}(p, t, s; \lambda, \alpha), \tag{3.69}$$

$$P_{-}\langle B_k^a(t, x_0, \mathbf{p}) B_0^b(s, y_0, -\mathbf{p})\rangle P_{+} = \frac{\delta^{ab}}{L^3 2T} {\sum_{\mathbf{p}p_0}}' \sin(p_0 x_0)\cos(p_0 y_0) e^{i\mathbf{p}(\mathbf{x}-\mathbf{y})} \bar{D}_{k0}(p, t, s; \lambda, \alpha), \tag{3.70}$$

where $p_0 = n_0 \frac{\pi}{T}$ with $n_0 = \pm 1, \pm 2, ...$, the SF boundary condition [70] are satisfied:

$$\forall p: \quad \tilde{B}_k(\mathbf{p}, x_0, t)\Big|_{x_0=0,T} = 0, \tag{3.71}$$

$$\mathbf{p} \neq 0: \quad \partial_0\, \tilde{B}_0(\mathbf{p}, x_0, t)\Big|_{x_0=0,T} = 0, \tag{3.72}$$

$$\mathbf{p} = 0: \quad \tilde{B}_0(\mathbf{0}, x_0, t)\Big|_{x_0=0} = 0, \quad \partial_0\, \tilde{B}_0(\mathbf{0}, x_0, t)\Big|_{x_0=T} = 0. \tag{3.73}$$

In order to impose SF-open boundary conditions:

$$\forall p: \quad \tilde{B}_k(\mathbf{p}, x_0, t)\Big|_{x_0=0} = 0 = \partial_0 \tilde{B}_k(\mathbf{p}, x_0, t)\Big|_{x_0=T}, \tag{3.74}$$

the only difference with respect to SF boundary conditions is that at $x_0 = T$ the time-derivative of the spatial components must be zero. This depends on the set of momenta being summed over: $p_0 = \left(n_0 + \frac{1}{2}\right)\frac{\pi}{T}$ with $n_0 = 0, \pm 1, \pm 2, ...$ [60]. Moreover, one can use the parity of the functions $\sin(p_0 x_0)\sin(p_0 y_0)$ and $\cos(p_0 x_0)\cos(p_0 y_0)$ to rewrite twice the sum over non-negative values of n_0.

3.8 Continuum value of $\mathcal{E}_0$ and its derivatives in time. Colour magnetic and electric components

Once introduced the SF boundary conditions (and also either SF-open or open-SF boundary conditions), in finite volume we no longer have time translation invariance, it is useful

to split the observable into colour magnetic and electric components:

$$\mathcal{E}_0 = \mathcal{E}_0^{mag} + \mathcal{E}_0^{el} = \frac{1}{4} G^a_{kl} G^a_{kl} + \frac{1}{4} \left(G^a_{0k} G^a_{0k} + G^a_{k0} G^a_{k0} \right). \tag{3.75}$$

The magnetic component only contains the spatial components of the field strength:

$$\mathcal{E}_0^{mag} = \frac{1}{2} \langle \partial_k B^a_{l,1} \partial_k B^a_{l,1} - \partial_k B^a_{l,1} \partial_l B^a_{k,1} \rangle, \tag{3.76}$$

while the electric part depends on the mixed components:

$$\mathcal{E}_0^{el} = \langle \partial_0 B^a_{k,1} \partial_0 B^a_{k,1} - \partial_0 B^a_{k,1} \partial_k B^a_{0,1} \rangle, \tag{3.77}$$

and we stress again that this is relevant when using SF boundary conditions as they break translation invariance in time.

At this stage, we can insert the expression for the B-field propagators in the expectation value of the observable we are computing $\langle E(t,x) \rangle$, which at $O(g_0^2)$ has the expression given by the eq. (3.44). Also, we apply a Fourier transformation (see (A1.2)) and multiply by t^2 in order to have a dimensionless combination:

$$t^2 \mathcal{E}_0^{mag} = \frac{g_0^2 c^4 L^4}{64 \cdot 2} \frac{\delta^{aa}}{2TL^3} \sum_{\mathbf{p}p_0}{}' \, sin^2(p_0 x_0) \left(\sum_l \mathbf{p}^2 \bar{D}_{ll} - \sum_{kl} p_k p_l \bar{D}_{kl} \right). \tag{3.78}$$

By inserting the expression of the propagator, after some algebraic work, we see that the dependence on the gauge parameter cancels as expected and we have [70]:

$$t^2 \mathcal{E}_0^{mag} = \frac{g_0^2 (N^2-1) c^4}{64\rho} \sum_{n_0 \mathbf{n}}{}' \, sin^2 \left(\frac{2\pi n_0}{T} x_0 \right) \frac{\mathbf{n}^2}{\frac{n_0^2}{4\rho^2} + \mathbf{n}^2} \, e^{-c^2\pi^2 (\frac{n_0^2}{4\rho} + \mathbf{n}^2)}, \tag{3.79}$$

where $\rho = \frac{T}{L}$. As we said the term $n = (0,0,0,0)$ is not included. Also, in the numerical evaluation, by fixing the precision to five significant digits we need to take at least fifteen terms (the smaller c the more terms we need to take). Similarly for the electric component we obtain:

$$t^2 \mathcal{E}_0^{el} = \frac{g_0^2 (N^2-1) c^4}{128\rho} \sum_{n_0 \mathbf{n}}{}' \, cos^2 \left(\frac{2\pi n_0}{T} x_0 \right) \frac{\frac{3n_0^2}{4\rho^2} + \mathbf{n}^2}{\frac{n_0^2}{4\rho^2} + \mathbf{n}^2} \, e^{-c^2\pi^2 (\frac{n_0^2}{4\rho} + \mathbf{n}^2)}. \tag{3.80}$$

In finite volume, the constant c is defined by the ratio between the smearing radius $\sqrt{8t}$ and the lattice size L, eq. (3.51). We computed these quantities numerically and we use them in Chap. (5). We wrote a C++ code and we cross-checked our evaluation with `Mathematica` [94]. The profiles in Euclidean time of these observables are shown in

Figs. 3.7 and 3.8 for 3 different values of $c = 0.2, 0.3, 0.4$.

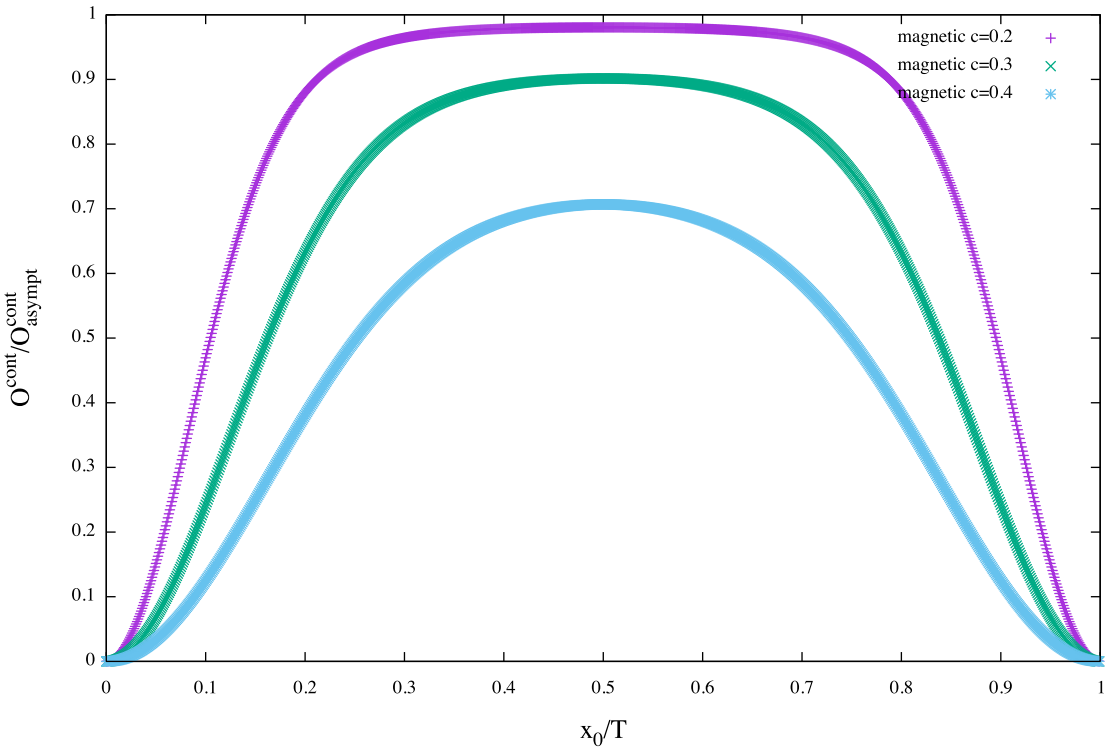

Figure 3.7: The magnetic component of $\mathcal{E}_0$, for 3 different values of $c = 0.2, 0.3, 0.4$. We can see from the plot that we have different observables taking the following two values $\frac{x_0}{T} = 0.25, 0.5$. The function plotted is normalised to the infinite volume asymptotic value (eq. (3.45)) $O^{cont}_{asympt} = \frac{1}{2}\frac{3}{16\pi^2}$ (the factor $\frac{1}{2}$ is to take in account that we split $E = E_{mag} + E_{el}$), with zero at the extremes because we impose Dirichlet conditions. The smaller the value of c, the larger the plateau in the plot. For $c \to 0$ the value of the observable goes towards its asymptotic value.

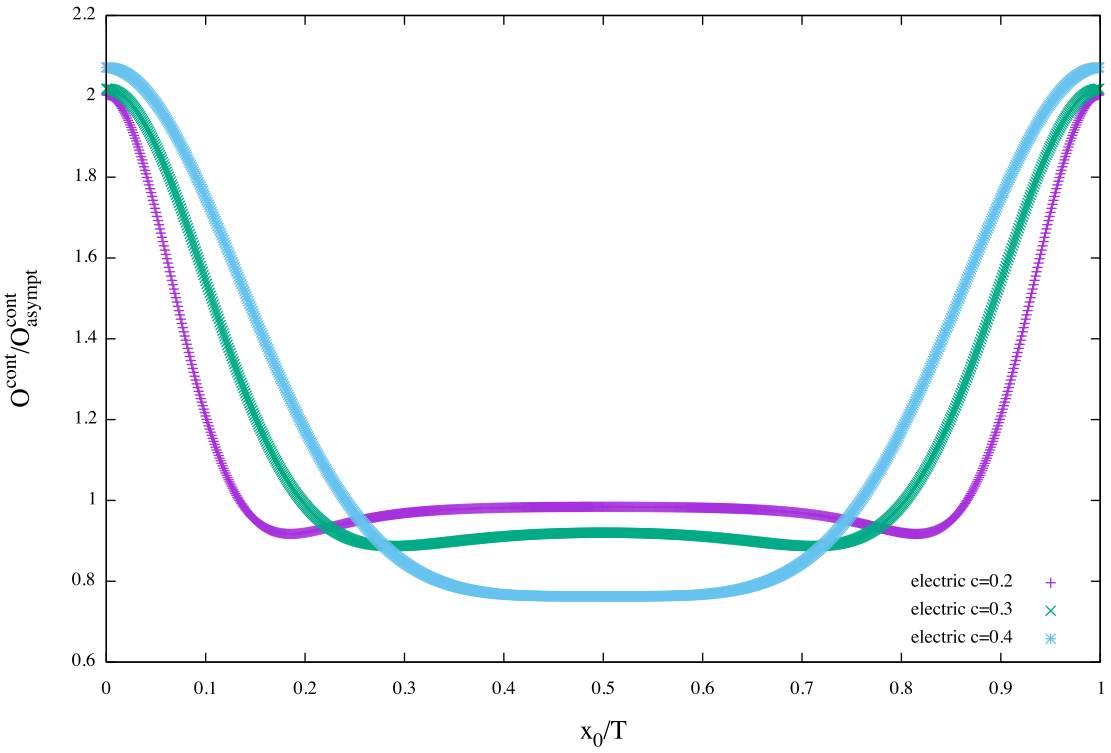

Figure 3.8: The electric component of $\mathcal{E}_0$, for 3 different values of $c = 0.2, 0.3, 0.4$. Similarly to the magnetic component case, we can pick different observables taking the following two values $\frac{x_0}{T} = 0.25, 0.5$. The function in the plot is normalised to its asymptotic value (eq. (3.45)) $O^{cont}_{asympt} = \frac{1}{2}\frac{3}{16\pi^2}$ (the factor $\frac{1}{2}$ is to take in account that we split $E = E_{mag} + E_{el}$). The smaller the value of c, the larger the plateau in the plot. For $c \to 0$ the value of the observable goes toward its asymptotic value.

We also evaluate the second time-derivative of these two components. All these observables can be made dimensionless by multiplying by the right power of the temporal extension T, to yield the following expressions:

$$T^2\partial_0^2 t^2\mathcal{E}_0^{mag} = \left(\frac{8c^4}{64\rho}\right) {\sum_n}' e^{-c^2\pi^2\left(\mathbf{n}^2+\frac{n_0^2}{4\rho^2}\right)} \frac{\mathbf{n}^2}{\mathbf{n}^2+\frac{n_0^2}{4\rho^2}} 2(\pi n_0)^2\left[\cos^2\left(\frac{\pi n_0 x_0}{T}\right) - \sin^2\left(\frac{\pi n_0 x_0}{T}\right)\right] \quad (3.81)$$

$$T^2\partial_0^2 t^2\mathcal{E}_0^{el} = \left(\frac{8c^4}{128\rho}\right) {\sum_n}' e^{-c^2\pi^2\left(\mathbf{n}^2+\frac{n_0^2}{4\rho^2}\right)} \frac{\mathbf{n}^2+\frac{3n_0^2}{4\rho^2}}{\mathbf{n}^2+\frac{n_0^2}{4\rho^2}} 2(\pi n_0)^2\left[\sin^2\left(\frac{\pi n_0 x_0}{T}\right) - \cos^2\left(\frac{\pi n_0 x_0}{T}\right)\right] \quad (3.82)$$

The profiles in Euclidean time of the continuum expressions for the second derivatives given in eq. (3.81) and eq. (3.82) are shown in Figs. 3.9 and 3.10.

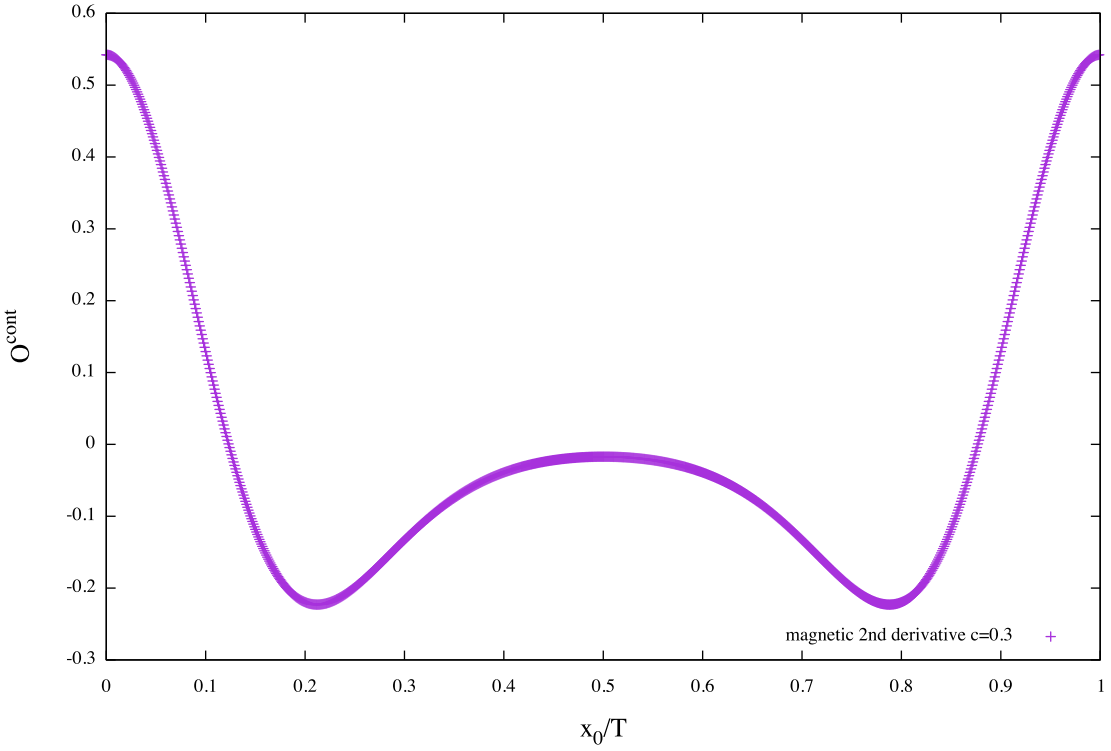

Figure 3.9: Profile in Euclidean time of the magnetic second derivative at $c = 0.3$ with SF boundary conditions.

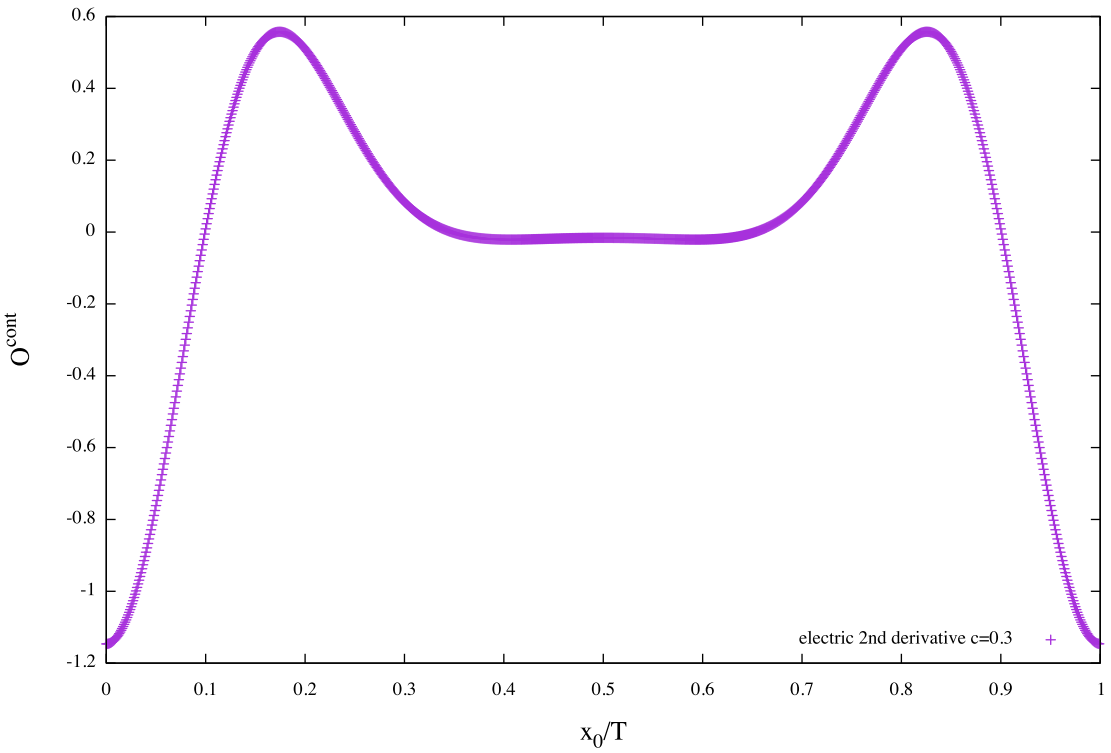

Figure 3.10: Profile in Euclidean time of the electric second derivative at $c = 0.3$ with SF boundary conditions.

3.9 SF-open boundary conditions

We evaluate the two components of $t^2\mathcal{E}_0$ with SF-open boundary conditions, their profile in Euclidean time is shown in Figs. (3.11) and (3.12).

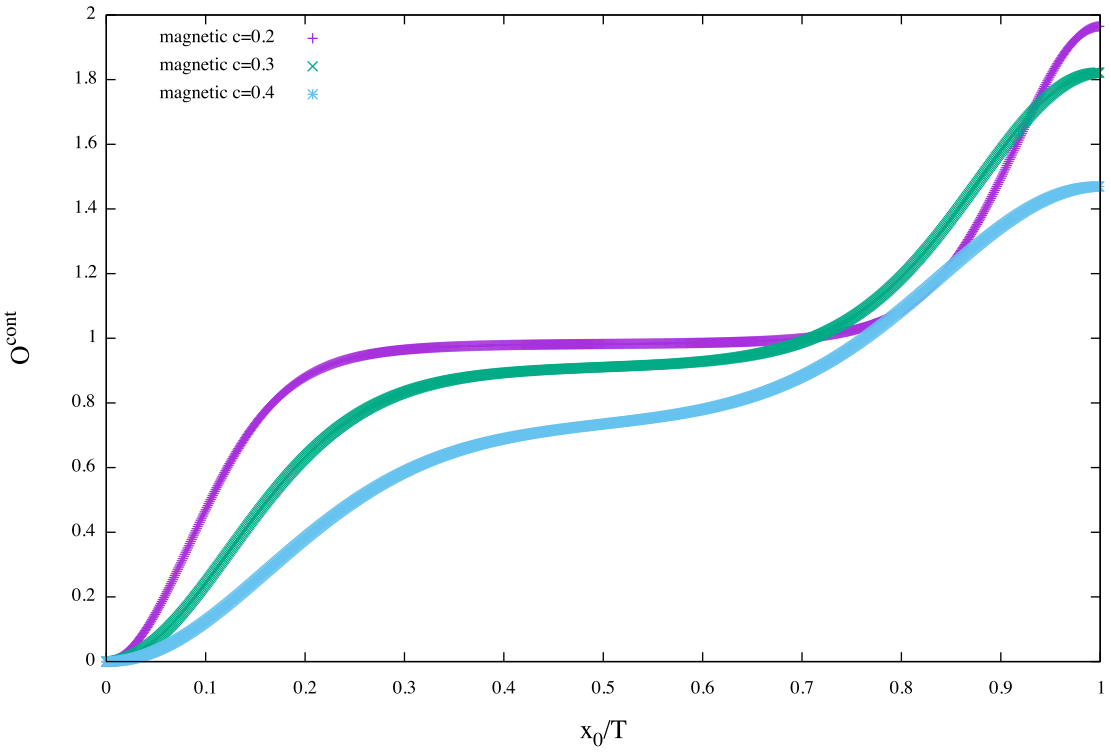

Figure 3.11: The magnetic component of $t^2\mathcal{E}_0$, for 3 different values of $c = 0.2, 0.3, 0.4$, with SF-open boundary conditions. The smaller the value of c, the larger the plateau in the plot. For $c \to 0$ the value of the observable goes toward its asymptotic value.

We also compute the first time-derivatives of such observables. The magnetic and electric components with SF-open boundary conditions read:

$$t^2\mathcal{E}_0^{mag} = \frac{g_0^2(N^2-1)c^4}{64\rho}\sum_{n_0\mathbf{n}}\cos^2\left(\frac{2\pi n_0}{T}x_0\right)\frac{\mathbf{n}^2}{\frac{n_0^2}{4\rho^2}+\mathbf{n}^2}\,e^{-c^2\pi^2(\frac{n_0^2}{4\rho}+\mathbf{n}^2)}, \tag{3.83}$$

$$t^2\mathcal{E}_0^{el} = \frac{g_0^2(N^2-1)c^4}{128\rho}\sum_{n_0\mathbf{n}}\sin^2\left(\frac{2\pi n_0}{T}x_0\right)\frac{\frac{3n_0^2}{4\rho^2}+\mathbf{n}^2}{\frac{n_0^2}{4\rho^2}+\mathbf{n}^2}\,e^{-c^2\pi^2(\frac{n_0^2}{4\rho}+\mathbf{n}^2)}. \tag{3.84}$$

and the profile of their first time-derivatives is shown in Figs. (3.13) and (3.14). The difference between SF and SF-open is that in the second case the sums are performed by including the term $n = (0,0,0,0)$ but with weight $\frac{1}{2}$ (double primed sign), the sine and cosine functions are exchanged, and the range of momenta is $p_0 = \left(n_0 + \frac{1}{2}\right)\pi T$.

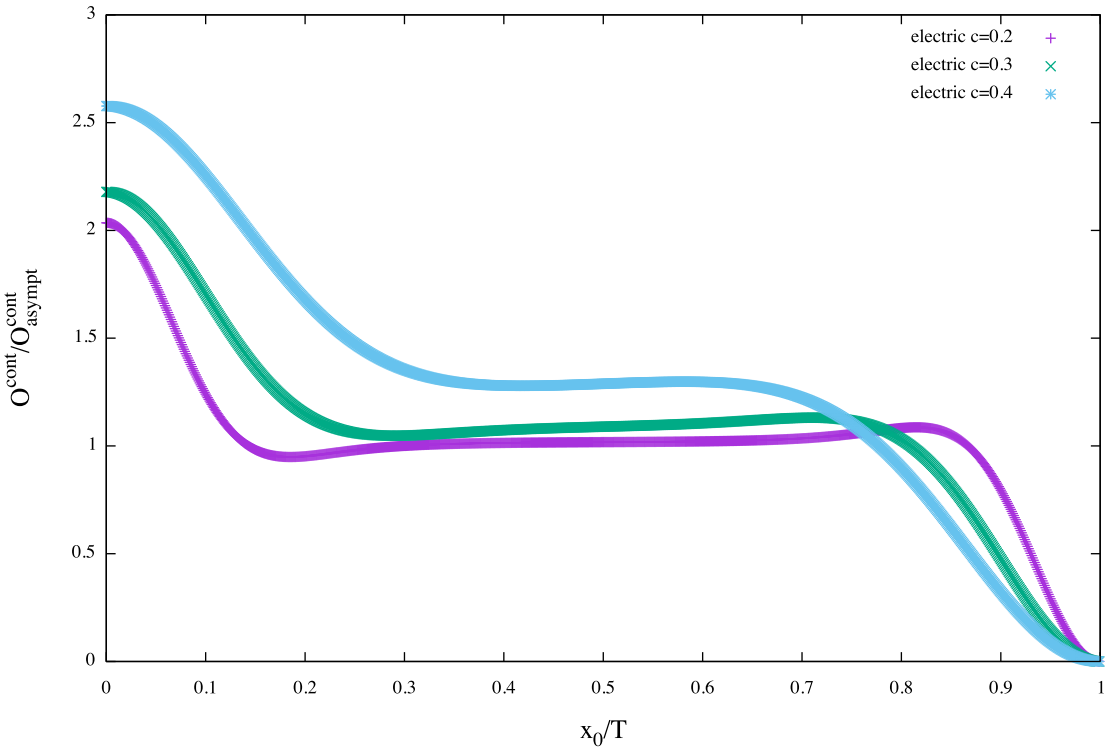

Figure 3.12: The electric component of $t^2\mathcal{E}_0$, for 3 different values of $c = 0.2, 0.3, 0.4$, with SF-open boundary conditions. The smaller the value of c, the larger the plateau in the plot. For $c \to 0$ the value of the observable tends toward its asymptotic value in infinite volume.

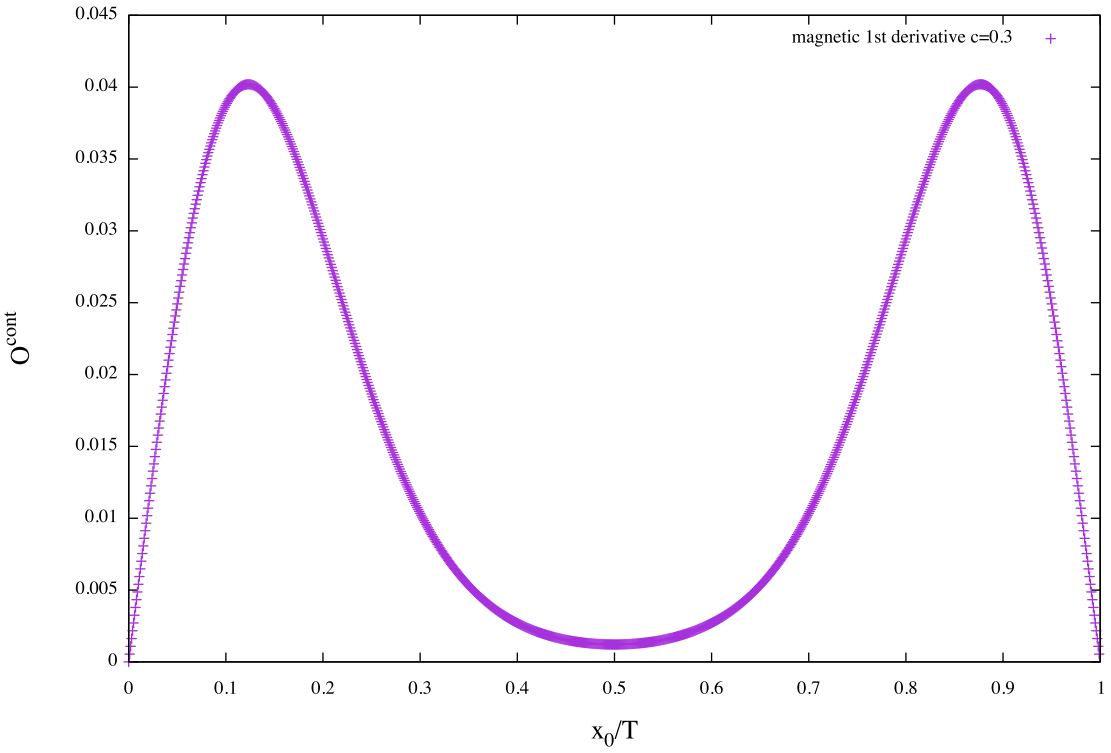

Figure 3.13: The first derivative of the magnetic component of $t^2\mathcal{E}_0$, for $c = 0.3$, with SF-open boundary conditions. Its asymptotic value is zero.

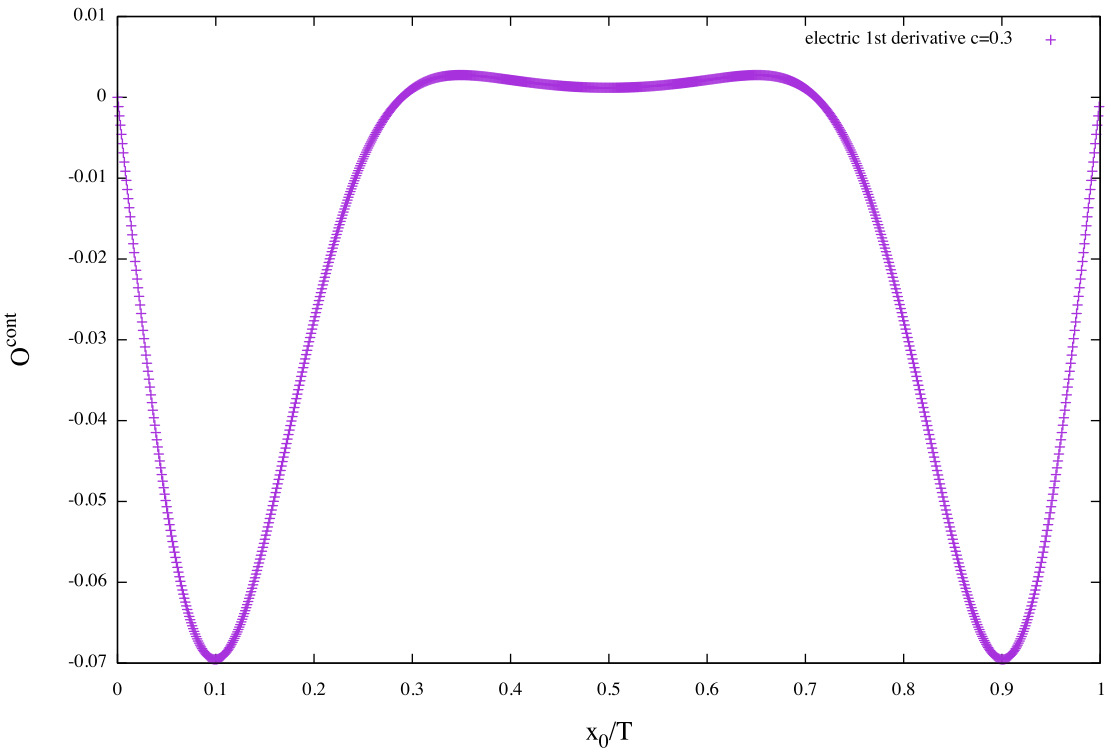

Figure 3.14: The first derivative of the electric component of $t^2\mathcal{E}_0$, for $c = 0.3$, with SF-open boundary conditions. Its asymptotic value is zero.

3.10 Orbifolding on the lattice

We have seen in Sec. 3.6 that it is advantageous to impose boundary conditions using an orbifolding projection. On the lattice, we define the projectors either with respect to the link reflection:

$$R^{(L)} : \phi(x_0) \to \phi(-x_0 - a), \tag{3.85}$$

as

$$\Pi^0_\pm = \frac{1}{2}(1 \pm R^{(L)}), \tag{3.86}$$

or with respect to the site reflection:

$$R^{(S)} : \phi(x_0) \to \phi(-x_0), \tag{3.87}$$

as

$$\Pi^k_\pm = \frac{1}{2}(1 \mp R^{(S)}). \tag{3.88}$$

By applying these projectors to the propagator we get:

$$\Pi^0_+ D_{00}(x_0, y_0, \mathbf{p}, \lambda)\Pi^0_+ = \frac{1}{2T}{\sum_{p_0}}' \sin[p_0 x_0]\, D_{00}(p, \lambda)\, \sin[p_0 y_0]\,, \tag{3.89}$$

$$\Pi^k_+ D_{kl}(x_0, y_0, \mathbf{p}, \lambda)\Pi^l_+ = \frac{1}{2T}{\sum_{p_0}}' \cos\left[p_0\left(x_0 + \frac{a}{2}\right)\right] D_{kl}(p, \lambda)\, \cos\left[p_0\left(y_0 + \frac{a}{2}\right)\right], \tag{3.90}$$

$$\Pi^k_+ D_{k0}(x_0, y_0, \mathbf{p}, \lambda)\Pi^0_+ = \frac{1}{2T}{\sum_{p_0}}' \sin[p_0 x_0]\, D_{k0}(p, \lambda)\, \cos\left[p_0\left(y_0 + \frac{a}{2}\right)\right] e^{ip_0\frac{a}{2}}, \tag{3.91}$$

and

$$\Pi^0_+ D_{0k}(x_0, y_0, \mathbf{p}, \lambda)\Pi^k_+ = \frac{1}{2T}{\sum_{p_0}}' \cos\left[p_0\left(x_0 + \frac{a}{2}\right)\right] e^{-ip_0\frac{a}{2}} D_{0k}(p, \lambda)\, \sin[p_0 y_0]\,, \tag{3.92}$$

where $D(p, \lambda)$ is defined in (2.25), but on a finite lattice the range of momenta is determined by the lattice size and $p_0 = \frac{\pi}{T} n_0$ with $n_0 = -\frac{T}{a}, ..., 0, ..., \frac{T}{a} - 1$, assuming $2T$ periodicity in time. The same equations hold for the propagator of the flowed gauge fields, defined in (3.32). The range of summation can be reduced by noting that the functions are even expressions in p_0. The prime symbol indicates that the term with $p = 0$ has to be excluded from the sum, in case it occurs. The B field propagator on the lattice is

given by:

$$\langle B_k(x,t)B_l(y,s)\rangle^{SF} = \frac{1}{L^3T}\sum_{\mathbf{p}p_0} \sin(p_0x_0)\sin(p_0y_0)\, e^{i\mathbf{p}(\mathbf{x}-\mathbf{y})}\bar{D}_{kl}(p,t,s;\lambda,\alpha), \tag{3.93}$$

$$\langle B_0(x,t)B_0(y,s)\rangle^{SF} = \frac{1}{L^3T}\sum_{\mathbf{p}p_0} \cos\left(p_0\left(x_0+\frac{a}{2}\right)\right)\cos\left(p_0\left(y_0+\frac{a}{2}\right)\right) e^{i\mathbf{p}(\mathbf{x}-\mathbf{y})}\bar{D}_{00}(p,t,s;\lambda,\alpha), \tag{3.94}$$

$$\langle B_0(x,t)B_k(y,s)\rangle^{SF} = \frac{1}{L^3T}\sum_{\mathbf{p}p_0}(-2i)\cos\left(p_0\left(x_0+\frac{a}{2}\right)\right)\sin(p_0y_0)\, e^{-ip_k\frac{a}{2}}e^{i\mathbf{p}(\mathbf{x}-\mathbf{y})}\bar{D}_{0k}(p,t,s;\lambda,\alpha), \tag{3.95}$$

and

$$\langle B_k(x,t)B_0(y,s)\rangle^{SF} = \frac{1}{L^3T}\sum_{\mathbf{p}p_0}(2i)\sin(p_0x_0)\cos\left(p_0\left(y_0+\frac{a}{2}\right)\right) e^{ip_k\frac{a}{2}}e^{i\mathbf{p}(\mathbf{x}-\mathbf{y})}\bar{D}_{k0}(p,t,s;\lambda,\alpha). \tag{3.96}$$

We have imposed the boundary conditions using an orbifold projection.

The expression of:

$$\bar{D}_{\mu\nu}(p,t,s;\lambda,\alpha) = H(t,\alpha)D_{\mu\nu}(p,\lambda)H(s,\alpha)^T \tag{3.97}$$

on the lattice is different depending on two choices. First, the flow we choose, either Wilson flow defined in the next section or Zeuthen flow, which is defined in Chap. 4 defines the two different kernels K_W and K_Z which are used in the heat kernel eq. (3.33). Second, depending on the action we employ on the lattice, either W or LW we have two different kernels eq.(2.22) and (2.23) which inverted give the two expressions $D^W_{\mu\nu}(p,\lambda)$ and $D^{LW}_{\mu\nu}(p,\lambda)$.

3.11 Gradient flow equation on the lattice. Wilson flow

The lattice formulation of the GF equation is given in terms of the link variables $U_\mu(x)$ and $V_\mu(t,x)$, and a discretisation of the gauge action. There is some freedom in putting the equation on the lattice which leads to different cutoff effects. The simplest choice is the Wilson gauge action, defined in eq. (2.12), which defines the *Wilson flow*:

$$\begin{aligned} \partial_t V_\mu(t,x) &= -g_0^2\left\{\partial_{x,\mu}S_{WG}[V]\right\}V_\mu(t,x) \\ V_\mu(t,x) &= U_\mu(x) \end{aligned} \tag{3.98}$$

where $\partial_{x,\mu}$ is a Lie-Algebra valued differential operator. We will see in Chap. 4 how to put the equation on the lattice in such a way that it will no longer have $O(a^2)$ cutoff effects.

To sum up the content of this chapter:

1. We introduced the differential equation which defines the GF: the gauge field is defined in such a way that it depends upon an additional parameter, the flow time. The perturbative solution of the equation offers an intuitive picture of how this operation implies a smearing of the gauge field. Such an operation removes the utraviolet divergences in composite operators defined in terms of the flowed fields.

2. The theory has been reformulated in $4+1$ dimensions to ensure locality is recovered. The fifth dimension is the flow time. Such a formulation allows one to study the renormalisability of the theory and to apply the Symanzik effective theory.

3. We have reported the result that the perturbative expansion of the action density, at positive flow time, in infinite volume, is finite at all orders in perturbation theory. Also, the value is known up to three loops, and we refer to the result in the literature. This is the relevant property which allows for the applications of the GF observables that we list. There are two examples in which the use of GF observables lead to a better precision: the coupling constant and the scale setting. This is relevant in the search for new physics. In addition, the chiral condensate can be evaluated in terms of GF observables, the energy momentum tensor can be renormalised on the lattice and also, by computing the topological charge, the emergence of topological sector is more transparent.

4. We defined the action density in finite volume. The SF boundary conditions have been introduced. In particular, we have seen how to obtain such boundary conditions from an orbifolding projection. This set-up is advantageous as it contains the relic of translation invariance which makes the numerical computation faster. In addition the SF-open boundary conditions have been defined, and in this set-up they are obtained from SF by simply summing over a different set of momenta (and exchanging with each other even and odd functions).

5. The expressions for the continuum values of the two components (colour magnetic and electric) of the action density, is given at $O(g_0^2)$ in perturbation theory, in finite volume with SF and SF-open boundary conditions. We also compute the first and second derivatives. The numerical computation of the listed observables has been carried out and the continuum values are used in Chap. 5 to normalise the lattice observables.

6. Finally, the flow equation on the lattice is given in terms of the Wilson action, which defines the Wilson flow.

4 Symanzik improvement of the gradient flow

In this chapter we study how to minimise the lattice artifacts in order to make reliable extrapolations to the continuum limit. In fact, regularising the theory on a lattice implies the presence of cutoff effects. This is the major source of systematic uncertainties in a lattice computation, and it is essential to understand how to remove it to make the best use out of the available computational power. We briefly review what the universality of the continuum limit is (see for example [95]) and why it is extremely useful studying different discretisations on the lattice, which correspond to the same quantity in the continuum. This is relevant because it allows us to design the quantities we need, e.g. the action in the path integral, the flow equation and the observables we want to measure. Such quantities are designed in order to reduce as much as possible the error introduced by the discretisation [96]. However, in doing that we increase the complexity of the expressions, so in practice the best thing to do is to maintain a balance between such complexity and small cutoff effects [97]. The Symanzik improvement programme is a systematic way designed to accelerate the convergence to the continuum limit. It consists in giving an effective description of the lattice theory, close to the continuum, by including counterterms of a fixed order in the lattice spacing a. Here, we classify the sources of the cutoff effects and see how to realise the $\mathcal{O}(a^2)$ improvement for a particular class of observables. As we analyse in this chapter, the fact that we use a pure gauge action[1], within the symmetry of the observables discretisations, and the use of the so-called Zeuthen flow allow us to apply Symanzik improvement in such a way that, when we have a complete basis of counterterms, the observables are free from $\mathcal{O}(a^2)$ cutoff effects and they approach their continuum limit as a^4.

The magnetic component of the action density is computed in literature, we add the computation of the electric component as well in Sec. 4.3. This requires the inclusion of

[1]The pure gauge action has $O(a^2)$ leading discretisation effects, while the fermionic part is $O(a)$.

a total derivative term in time, as there is no longer periodicity in this direction. Also, we report the expressions for the action density to be computed on the lattice at leading order in perturbation theory in Sec. 4.4.

4.1 Universality of the continuum limit

Universality finds its theoretical basis on the Wilsonian formulation of the renormalisation group. We can think that the original action with a cutoff Λ lives in an infinite-dimensional space of actions:

$$S = k_i S_i, \tag{4.1}$$

where the coefficients k_i are called couplings and $S_i = \sum_x \mathcal{L}_i$ are local operators, functions of the fields and their derivatives, which respect the symmetries of the lattice. This is the most general local theory we can write down and it is quite complicated as it has many coupled degrees of freedom but it is possible to reduce the number of degrees of freedom performing a change in the couplings. In other words, we can apply a renormalisation group transformation R_λ defined as a mapping

$$S \to S^{(\lambda)} \tag{4.2}$$

such that both S and $S^{(\Lambda)}$ describe the same physics at large distances. This means that $S^{(\Lambda)}$ is obtained from S by integrating out degrees of freedom with momenta close to the value of the cutoff Λ. The cutoff is decreased by a factor $\lambda > 1$:

$$\Lambda \to \frac{1}{\lambda}\Lambda. \tag{4.3}$$

This transformation can be described as a change of couplings:

$$k_i \to k_i^{(\Lambda)}. \tag{4.4}$$

We are interested in the so called fixed points S^*, defined by:

$$R_\lambda S^* = S^*, \tag{4.5}$$

as they determine the universality classes of the action. Near the fixed point, the action can be linearised in such a way that

$$k_\alpha = k_\alpha^* + \delta k_\alpha \tag{4.6}$$

and the transformed couplings become:

$$k_\alpha^\Lambda = k_\alpha^* + \lambda^{d_\alpha}\delta k_\alpha. \tag{4.7}$$

Here d_α can be either negative, null or positive corresponding to irrelevant, marginal and relevant terms, respectively. Irrelevant terms do not affect the long-distance physics.

The important conclusion we want to draw here is that the critical behavior is determined only by a few relevant operators in the vicinity of the fixed points:

$$S = S^* + \sum_{\text{relevant } \alpha} k_\alpha S_\alpha. \tag{4.8}$$

On a fixed point the coupling does not change by definition and this means that the physics is constant. In Statistical Mechanics this is called critical point, and here the correlation length goes to infinity

$$\frac{\xi}{a} \to \infty, \tag{4.9}$$

where the exponential decay of the two-point correlator is given by:

$$\xi \sim m_{phys}^{-1}. \tag{4.10}$$

The empirical fact that many systems near the critical points behave in similar ways is what we call universality, which means that the long range properties do not depend on the microscopic details of the interaction.

4.2 Symanzik effective field theory

The idea of Symanzik is based on the fact that, close to the continuum limit, the QCD theory on the lattice can be described by a local effective filed theory in which we include the lagrangian of QCD in the continuum $\mathcal{L}_0$ as well as operator insertions $\mathcal{L}_i$ with $i = 1, 2, ...$:

$$S_{eff} = \int d^4x \{\mathcal{L}_0 + a\mathcal{L}_1 + a^2\mathcal{L}_2\}. \tag{4.11}$$

The $\mathcal{L}_i$ have dimension $4+i$ and respect the symmetries of the lattice theory. With these constraints, it is possible to classify all the possible operators which appear in $\mathcal{L}_i$. For instance, the counterterm to the W action should be chosen such that the order a term in the action of the effective continuum theory is cancelled. In order to have an on-shell

improvement at $O(a)$, the action must include the so-called the Sheikholeslami-Wohlert term [44, 45], where the coefficient c_{SW} has been properly tuned:

$$S_{eff} = S_0 + a^5 c_{SW} \frac{i}{4} \sum_x (g_0) \bar{\psi}(x) \sigma_{\mu\nu} \hat{F}_{\mu\nu} \psi(x), \tag{4.12}$$

where S_0 is the standard W action, $\hat{F}_{\mu\nu}$ is a lattice regularization of the field strength tensor $F_{\mu\nu}$. The *clover* discretisation is defined by:

$$\hat{F}_{\mu\nu} = \frac{1}{8a^2}\{Q_{\mu\nu}(x) - Q_{\nu\mu}(x)\} \tag{4.13}$$

and represented in Fig. 4.1, where

$$\begin{aligned} Q_{\mu\nu}(x) = {} & U_\mu(x) U_\nu(x + a\hat{\mu}) U_\mu(x + a\hat{\nu})^{-1} U_\nu(x)^{-1} \\ & + U_\nu(x) U_\mu(x - a\hat{\mu} + a\hat{\nu})^{-1} U_\nu(x - a\hat{\mu})^{-1} U_\mu(x - a\hat{\mu}) \\ & + U_\mu(x - a\hat{\mu})^{-1} U_\nu(x - a\hat{\mu} - a\hat{\nu})^{-1} U_\mu(x - a\hat{\mu} - a\hat{\nu}) U_\nu(x - a\hat{\nu}) \\ & + U_\nu(x - a\hat{\nu})^{-1} U_\mu(x - a\hat{\nu}) U_\nu(x + a\hat{\mu} - a\hat{\nu}) U_\mu(x)^{-1}. \end{aligned} \tag{4.14}$$

The coefficient $c_{SW} = 1$ at tree-level in perturbation theory, and has been computed

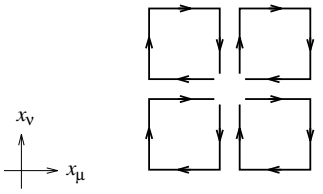

Figure 4.1: The clover leaf representation $\hat{F}_{\mu\nu}$ of $F_{\mu\nu}$.

at 1-loop order, but it is not very accurate. That is why it has been non-perturbatively determined by imposing the PCAC relation, which is the Ward identity associated to the chiral symmetry [44, 98]. Cutoff effects are generated not only by the action but also by the composite operators that one is interested in. For example, if we consider a gauge invariant (multiplicatively renormalisable) field $\phi(x)$, the connected n-point function, after renormalisation is given by:

$$G_n(x_1, ...x_n) = (Z_\phi)^n \langle \phi(x_1) ... \phi(x_n) \rangle_{con}, \tag{4.15}$$

where Z_ϕ is the renormalisation constant of the field $\phi(x)$. The Green function $G_n(x_1, ...x_n)$ has a well-defined continuum limit when the points $x_1 ... x_n$ are taken at finite distance one

from another. In the local effective theory the operator is given by an effective field:

$$\phi_{eff}(x) = \phi_0(x) + a\phi_1(x) + a^2\phi_2(x) + ..., \tag{4.16}$$

where the $\phi_i(x)$, similarly to the action counterterms, have the appropriate symmetries and dimensions. The lattice correlation functions are then given by:

$$\begin{aligned} G_n(x_1, ...x_n) &= \langle\phi(x_1)...\phi(x_n)\rangle_{con} \\ &- a\int d^4y\langle\phi(x_1)...\phi(x_n)\mathcal{L}_1(y)\rangle_{con} \\ &+ a\sum_{k=1}^{n}\langle\phi(x_1)...\phi_1(x_k)...\phi(x_n)\rangle_{con} + O(a^2) \end{aligned} \tag{4.17}$$

where the expectation values are evaluated with the lagrangian $\mathcal{L}_0$. All the fields used in the correlators have to be improved in order to obtain improved on-shell quantities. In the following we are interested in pure gauge quantities. In this case, the leading discretisation error is $O(a^2)$ and because of the symmetries of the problem there are no odd powers. The $O(a^2)$ improvement will lead to a $O(a^4)$ leading error in pure gauge theory.

4.2.1 Improved action

As we explained, we want to use the universality of the continuum limit in order to accelerate the convergence of the lattice quantity to its continuum value. The original idea of improvement consists in adding, to the desired quantity we want to improve, a complete set of higher-dimensional (irrelevant) operators, the coefficients of which are tuned in such a way that they cancel finite cut-off effects, to a desired order of a. The counterterms we add must respect the symmetries. In the case we are analysing they are gauge invariance and reflection symmetries. The higher dimensional operators are suppressed by powers of the lattice spacing, so they are irrelevant operators in the language of the renormalisation group, i.e. they vanish at the fixed point $a \to 0$. Both the action and the observable we want to compute have to be improved to the same order. The drawback of this program is that by adding irrelevant operators we increase the complexity of the quantity we discretise, i.e. the action and the observables. Some of the advantages of this formulation are: reducing discretisation errors allows us to work on coarser lattices for a given accuracy; the symmetries broken by the lattice spacing are better restored.

We use the local formulation defined in Sec. 3.2, in 5-dimensions, we translate the

expression of $S = S_4 + S_5$, eq. (3.22) and eq. (3.24), on the lattice and we apply the Symanzik improvement programme. As explained in [3], the action $S = S_4 + S_5$ on the lattice has the form:

$$S[V, L] = S_G[U, c_i] - 2a^4 \int_0^\infty dt \sum_{x,\mu} \mathrm{Tr} L_\mu(t, x) F_\mu(t, x), \tag{4.18}$$

where U are the link fields at the boundary $t = 0$; the initial condition for the flow equation is:

$$V_\mu(0, x) = U_\mu(x), \tag{4.19}$$

and F_μ is defined in such a way that the flow equation can be written in the compact form $F_\mu(t, x) = 0$. Given the action in the half space $t \geq 0$, the expectation value of the operator $O[V, L]$ is defined as usual,

$$\langle O \rangle = \frac{1}{\mathcal{Z}} \int D[V] D[L]\, O[V, L]\, e^{(-S[V,L])} \tag{4.20}$$

with normalisation

$$\frac{1}{\mathcal{Z}} \int D[V] D[L]\, e^{(-S[V,L])} = 1. \tag{4.21}$$

The starting point of the Symanzik programme is to write the action as a power expansion in a^2:

$$S_{eff} = S_0^{cont} + a^2 S_{(2)} + O(a^4); \tag{4.22}$$

also local observables are described by an effective continuum field which is expanded in powers of a^2:

$$O_{eff} = O_0 + a^2 O_{(2)} + O(a^4). \tag{4.23}$$

Concerning the action $S_{(2)}$ in eq. (4.22), we separate the contribution coming from the boundary $t = 0$, relative to the improvement of S_4, and the one coming from the bulk, we indicated the action in the bulk as S_5:

$$S_{(2)} = S_{2,\mathrm{fl}} + S_{2,\mathrm{b}}, \tag{4.24}$$

where "fl" and "b" stand for flow ($t > 0$) and boundary ($t = 0$). The next step in the

Symanzik improvement is to determine a basis of counterterms for the action; $S_{(2)}$ is a linear combination of all operators compatible with certain symmetries. By dimensional analysis, we see that the counterterms needed for the action at the boundary are all possible operators of dimension 6:

$$S_{2,\mathrm{b}} = \sum_i \int d^4x\, O_i^{d=6}(x), \tag{4.25}$$

$$S_{4(eff)} = -\frac{1}{2g_0^2} \int d^4x\, \mathrm{Tr}\left\{F_{\mu\nu}F_{\mu\nu}\right\} + \sum_i \int d^4x\, O_i^{d=6}(x), \tag{4.26}$$

while in the bulk they are dimension 8 operators:

$$S_{2,\mathrm{fl}} = \sum_i \int dt \int d^4x\, Q_i^{d=8}(t,x), \tag{4.27}$$

$$S_{5(eff)} = i \int \mathrm{Tr} L_\mu \left\{\partial_t B_\mu - D_\rho G_{\rho\mu}\right\} d^4x\, dt + \sum_i \int dt \int d^4x\, Q_i^{d=8}(t,x), \tag{4.28}$$

and then the same argument applies to the local observable (4.23). A relevant observation which has been done in [27]: there are no loops generated in the bulk, all the divergences are generated at $t = 0$, for $t > 0$ the theory is like a classical one; this implies that we only have to renormalise the action at $t = 0$, which is the YM action. S_4 contains the dimensionless coupling g, and we know that it is renormalisable. In chap. (4), we list all the possible counterterms $O_i^{d=6}$ of eq. (4.26), while for the bulk action they are determined by doing the so-called classical expansion:

$$S_{5(eff)} = S_5 + \sum_i \int dt \int d^4x\, Q_i^{d=8}(t,x). \tag{4.29}$$

In fact, using power counting and the BRS invariance of the theory, it can be shown that the correlation functions at positive flow time are finite, to all orders in PT. See [27] for further details.

In the following we list all the possible counterterms needed to realise the improvement of $S_{2,b}[B, L]$.

4.2.2 Determination of $S_{2,\mathrm{fl}}$: Zeuthen flow equation

By performing the classical a-expansion it turns out that the so-called "Zeuthen flow" equation successfully realises the $O(a^2)$ improvement in the bulk. The lattice expression of the action in the bulk is:

$$S(c_i) = -2\int_0^\infty dt \sum_x \mathrm{Tr}\left\{L_\mu(t,x)\left[a^2\partial_t V_\mu(t,x)V_\mu^{-1}(t,x) - g_0^2\partial_{x,\mu}S_{lat}(V)\right]\right\}, \quad (4.30)$$

where the dependence of the coefficients c_i is encoded in S_{lat}, which is the action on the lattice. In order to translate the flow equation (3.2) on the lattice we need to:

- Replace the gauge field $B_\mu(x,t)$ with the link field $V_\mu(t,x)$;

- Pick a discretisation of the action to put on the right hand side;

  - The W action is the simplest choice and it defines the Wilson flow:

    $$a^2\partial_t V_\mu(t,x) = -g_0^2\partial_{x,\mu}(S_W[V])V_\mu(t,x), \quad (4.31)$$

    On the lattice the representative of the gauge field is the link field and consequently the initial condition is given on it:

    $$V_\mu(0,x) = U_\mu(x); \quad (4.32)$$

  - The Lüscher-Weisz action and adding an $O(a^2)$ term we define the so called *Zeuthen flow* trough the equation:

    $$a^2\partial_t V_\mu(t,x) = -g_0^2(1+\frac{a^2}{12}D_\mu D_\mu^*)\partial_{x,\mu}(S_{LW}[V])V_\mu(t,x), \quad (4.33)$$

    with the same initial condition:

    $$V_\mu(0,x) = U_\mu(x). \quad (4.34)$$

4.2.3 Determination of $S_{2,b}[B, L]$: basis of counterterms for the action at the boundary, $t = 0$.

The basis of counterterms for the action at the boundary $t = 0$:

$$S_{2,b}[B, L] = \int d^4x \sum_i O_i^{d=6}(x) \tag{4.35}$$

is given by the following list of dimension 6-operators:

$$O_1(x) = \mathrm{Tr}\{J_{\mu\mu\rho}(x)J_{\mu\mu\rho}(x)\} \tag{4.36}$$
$$O_2(x) = \mathrm{Tr}\{J_{\mu\nu\rho}(x)J_{\mu\nu\rho}(x)\} \tag{4.37}$$
$$O_3(x) = \mathrm{Tr}\{J_{\mu\mu\nu}(x)J_{\rho\rho\nu}(x)\} \tag{4.38}$$
$$O_4(x) = \mathrm{Tr}\left\{L_\mu(0, x)J_{\nu\nu\mu}\right\} \tag{4.39}$$
$$O_5(x) = \mathrm{Tr}\left\{L_\mu(0, x)L_\mu(0, x)\right\} \tag{4.40}$$
$$O_6(x) = \partial_t \mathrm{Tr}\left\{G_{\mu\nu}G_{\mu\nu}\right\}|_{t=0} \tag{4.41}$$
$$O_7(x) = \mathrm{Tr}\left\{L_\mu(t, x)\partial_t B_\mu(t, x)\right\}|_{t=0} \tag{4.42}$$

where

$$J_{\mu\nu\rho} = D_\mu F_{\nu\rho}. \tag{4.43}$$

The number of linear independent counterterms is reduced by using the field equations and recognising the terms which already appear in the improved action[2]. Also, the 5-dimensional formulation is used for the theoretical analysis, in practice one integrates numerically the flow equation. It turns out that inserting O_4 is equivalent to shifting the initial condition for the link field:

$$V_\mu(t, x)|_{t=0} = e^{c_b g_0^2 \partial_{x,\mu} S_g[U]} U_\mu(x), \tag{4.44}$$

where c_b is the free improvement coefficient, which is the main character of this work we want to test numerically, and $S_g[U]$ a 4-dimensional action.

[2]The improvement of the pure gauge action has been implemented at tree-level and also to $O(g_0^2)$.

4.3 Improved observables

The counterterms needed to realise the Symanzik improvement of the observables are completely determined by the so-called classical a-expansion. It assumes that the lattice is an approximation of a continuum theory, so that the link field V_μ is related to the gauge field B_μ in the continuum by the path-ordered exponential:

$$V_\mu(t,x) = \mathcal{P} exp\left\{\int_0^1 du B_\mu(t, z(u))\right\}, \tag{4.45}$$

which has Taylor expansion in the lattice spacing a:

$$V_\mu(t,x) = 1 + aB_\mu(t,x) + \frac{1}{2}a(\partial B_\mu(t,x) + B_\mu^2(t,x)) + O(a^3). \tag{4.46}$$

It is convenient to work in a gauge introduced by Lüscher and Weisz in [32] which makes the expansion around $x = 0$ easier, e.g. the plaquette field

$$P_{\mu\nu}(t,x) = V_\mu(t,x)V_\nu(t,x+a\hat{\mu})V_\mu(t,x+a\hat{\nu})^\dagger V_\nu(t,x)^\dagger, \tag{4.47}$$

is simplified to a single link

$$P_{\mu\nu}(t,x) = V_\nu(t,a\hat{\mu}), \tag{4.48}$$

which is, in terms of the definition of the link field,

$$P_{\mu\nu}(t,x) = \mathcal{P} exp\left\{a\int_0^1 du B_\nu(t, a\hat{\mu} + (1-u)a\hat{\nu})\right\}. \tag{4.49}$$

In the continuum the energy density $E(t,x)$ is defined by:

$$E(x,t) = -\frac{1}{2}\,\mathrm{tr}\,\{G_{\mu\nu}(x,t)G_{\mu\nu}(x,t)\}; \tag{4.50}$$

on the lattice the two most popular discretisations are the so-called plaquette and clover, which have expressions, respectively,

$$E^{pl}(t,x) = -\frac{a^{-4}}{2}\sum_{\mu\nu}[\mathrm{tr}(P_{\mu\nu}(t,x) + P_{\mu\nu}(t,x)^\dagger) - 2N], \tag{4.51}$$

and

$$E^{cl}(t,x) = -\frac{1}{2}\mathrm{Tr}\,\{G^{cl}_{\mu\nu}G^{cl}_{\mu\nu}\}. \tag{4.52}$$

Performing the classical a-expansion of the plaquette $P_{\mu\nu}$ up to the order a^6 one obtains [3]:

$$\begin{aligned} E^{pl}(t,x) = E^{cont} &+ \frac{1}{24}a^2 \sum_{\mu\nu} \left[\mathrm{Tr}(D_\mu G_{\mu\nu}(t,x)^2) + \mathrm{Tr}(D_\nu G_{\mu\nu}(t,x))^2 \right] \\ &- \frac{1}{4}a \sum_{\mu\nu} (\partial_\mu + \partial_\nu \mathrm{Tr} G_{\mu\nu}(t,x)^2) \\ &- \frac{1}{24}a^2 \sum_{\mu\nu} \left(2\partial_\mu^2 + 2\partial_\nu^2 + 3\partial_\mu\partial_\nu \right) \mathrm{Tr} G_{\mu\nu}(t,x)^2) \\ &+ O(a^3), \end{aligned} \tag{4.53}$$

where there are odd powers of a because the definition of the plaquette discretisation is not symmetric, but we will use a symmetrised version (see eq. (4.58)). We can perform the same expansion for the four plaquettes in the clover definition, and we have:

$$\begin{aligned} E^{cl}(t,x) = E^{cont} &+ \frac{1}{6}a^2 \sum_{\mu\nu} \left[\mathrm{Tr}(D_\mu G_{\mu\nu}(t,x)^2) + \mathrm{Tr}(D_\nu G_{\mu\nu}(t,x))^2 \right] \\ &- \frac{1}{12}a^2 \sum_{\mu\nu} (\partial_\mu^2 + \partial_\nu^2) \mathrm{Tr} G_{\mu\nu}(t,x)^2 \\ &+ O(a^4), \end{aligned} \tag{4.54}$$

where there are only even power as the definition is symmetric. In the set-up we choose to work, SF (also, either open-SF or SF-open), we have translation invariance in space but not in time. This means that the total derivative terms do not contribute to the magnetic component, while they do to the electric one. This implies that the expectation value of the magnetic component will not contain odd powers of a.

The clover discretisation contains terms of $O(a^2)$ which have exactly the same structure which appears in the plaquette discretisation, but with a different coefficient. This implies that the $O(a^2)$ improved combination of the observable can be obtained by taking the following combination:

$$E^{imp}_{mag} = \frac{4}{3}E^{pl}_{mag} - \frac{1}{3}E^{cl}_{mag}. \tag{4.55}$$

The electric component of $E(t,x)$ contains the temporal components and we no longer have translation invariance in the temporal direction, indeed in either the SF or open-SF we impose Dirichlet or Neumann boundary conditions in time. This is the reason for which taking the combination $\tilde{E}_{el} = \frac{4}{3}E^{pl-sym}_{el} - \frac{1}{3}E^{cl}_{el}$ we have an additional $\mathcal{O}(a^2)$ term

containing the time derivative:

$$E_{el}^{imp} = \left(1 + ka^2\partial_0^2\right) E_{el}^{cont}, \tag{4.56}$$

and in order for it to be free from $O(a^2)$ cutoff effects we need to remove this additional term. Starting from the expression for the plaquette discretisation we get the electric component by taking the sum of the mixed components, i.e. $\mu = 0$, $\nu = k$ and viceversa, they give two identical contributions; we ignore the terms of high order (h.o.) in the field and the ones containing spatial derivatives ∂_k and we use the definition

$$E_{el}^{cont} = -\sum_k \mathrm{Tr}\left[G_{0k}(t,x)G_{0k}(t,x)\right]. \tag{4.57}$$

In order to eliminate the odd powers we take a symmetric definition

$$\begin{aligned} E_{el}^{pl-sym}(t,x) &= \frac{1}{2}\left(E_{el}^{pl}(t,\mathbf{x},x_0) + E_{el}^{pl}(t,\mathbf{x},x_0 - a)\right) \\ &= E_{el}^{cont} - \frac{1}{12}a\partial_0 E_{el}^{cont} - \frac{1}{12}a^2\partial_0^2 E_{el}^{cont} + \mathcal{O}(a^4). \end{aligned} \tag{4.58}$$

Similarly, taking the clover definition, which is already symmetric, we get

$$E_{el}^{cl}(t,x) = E_{el}^{cont} - \frac{1}{3}a\partial_0 E_{el}^{cont} + \frac{1}{6}a^2\partial_0^2 E_{el}^{cont} + \mathcal{O}(a^4). \tag{4.59}$$

Now the combination

$$\tilde{E}_{el} = \frac{4}{3}E_{el}^{pl-sym} - \frac{1}{3}E_{el}^{cl} \tag{4.60}$$

is given by

$$\begin{aligned} \tilde{E}_{el} = \frac{4}{3}&\left(E_{el}^{cont} - \frac{1}{12}a\partial_0 E_{el}^{cont} - \frac{1}{12}a^2\partial_0^2 E_{el}^{cont} + \mathcal{O}(a^4)\right) \\ -\frac{1}{3}&\left(E_{el}^{cont} - \frac{1}{3}a\partial_0 E_{el}^{cont} + \frac{1}{6}a^2\partial_0^2 E_{el}^{cont} + \mathcal{O}(a^4)\right) \end{aligned} \tag{4.61}$$

where the $O(a)$ terms cancel out and we have only one $O(a^2)$ term which contains the total derivative term:

$$\tilde{E}_{el} = E_{el}^{cont} + \frac{1}{6}a^2\partial_0^2 E_{el}^{cont}. \tag{4.62}$$

The $O(a^2)$ improved electric component of the action density is obtained by sub-

tracting the $O(a^2)$ term:

$$E_{el}^{imp} = \tilde{E} - \frac{1}{6}a^2\partial_0^2 E_{el}^{cont}. \tag{4.63}$$

4.4 Discretisations of the observables

We give the expressions for the discretised observables that we compute on the lattice: clover, plaquette and linear combinations of them.

4.4.1 Clover discretisation

We can discretise the observable $E(t,x)$

$$E^{cl}(t,x) = -\frac{1}{2}\mathrm{Tr}\langle G_{\mu\nu}^{cl} G_{\mu\nu}^{cl}\rangle \tag{4.64}$$

using the clover definition of the field strength

$$\begin{aligned} G_{\mu\nu}^{cl}(t,x) = \tfrac{1}{4a^2}\left[\tfrac{1}{2}(P_{\mu\nu}(t,x) + Q_{\mu\nu}(t,x) + R_{\mu\nu}(t,x) + S_{\mu\nu}(t,x) + \right. \\ \left. -(P_{\mu\nu}(t,x)^\dagger + Q_{\mu\nu}(t,x)^\dagger + R_{\mu\nu}(t,x)^\dagger + S_{\mu\nu}(t,x)^\dagger)\right], \end{aligned} \tag{4.65}$$

where the four plaquette $P_{\mu\nu}$, $Q_{\mu\nu}$, $R_{\mu\nu}$, $S_{\mu\nu}$ are represented in Fig. 4.1. In terms of link variables:

$$P_{\mu\nu}(t,x) = V_\mu(t,x)V_\nu(t,x+a\hat{\mu})V_\mu(t,x+a\hat{\nu})^\dagger V_\nu(t,x)^\dagger \tag{4.66}$$

and expanding in terms of the B fields:

$$P_{\mu\nu}(t,x) - P_{\mu\nu}(t,x)^\dagger = 2a\{[B_\mu(t,x) - B_\mu(t,x+a\hat{\nu})] - [B_\nu(t,x) - B_\nu(t,x+a\hat{\mu})]\}. \tag{4.67}$$

Similarly for the other plaquettes:

$$\begin{aligned} &Q_{\mu\nu}(t,x) - Q_{\mu\nu}(t,x)^\dagger = \\ &2a\{[B_\nu(t,x+a\hat{\mu}+a\hat{\nu}) - B_\nu(t,x-a\hat{\nu})] + [B_\mu(t,x-a\hat{\nu}) - B_\mu(t,x)]\} \end{aligned} \tag{4.68}$$

and

$$R_{\mu\nu}(t,x) - R_{\mu\nu}(t,x)^\dagger =$$

$$2a\{[B_\mu(t,x-a\hat{\mu}-a\hat{\nu}) - B_\mu(t,x-a\hat{\mu})] + [B_\nu(t,x-a\hat{\nu}) - B_\nu(t,x-a\hat{\mu}-a\hat{\nu})]\} \tag{4.69}$$

finally:

$$S_{\mu\nu}(t,x) - S_{\mu\nu}(t,x)^\dagger =$$

$$2a\{[B_\nu(t,x) - B_\nu(t,x-a\hat{\mu})] + [B_\mu(t,x-a\hat{\mu}) - B_\mu(t,x-a\hat{\mu}+a\hat{\nu})]\}. \tag{4.70}$$

In terms of derivatives on the lattice

$$P_{\mu\nu}(t,x) - P_{\mu\nu}(t,x)^\dagger = 2a\left(-a\partial_\nu B_\mu(t,x) + a\partial_\mu B_\nu(t,x)\right) \tag{4.71}$$

$$Q_{\mu\nu}(t,x) - Q_{\mu\nu}(t,x)^\dagger = 2a\left(a\partial_\mu B_\nu(t,x+a\hat{\nu}) - a\partial^*_\nu B_\mu(t,x)\right) \tag{4.72}$$

$$R_{\mu\nu}(t,x) - R_{\mu\nu}(t,x)^\dagger = 2a\left(-a\partial^*_\nu B_\mu(t,x-a\hat{\mu}) + a\partial^*_\mu B_\nu(t,x-a\hat{\nu})\right) \tag{4.73}$$

$$S_{\mu\nu}(t,x) - S_{\mu\nu}(t,x)^\dagger = 2a\left(a\partial^*_\mu B_\nu(t,x) - a\partial^*_\nu B_\mu(t,x-a\hat{\mu})\right) \tag{4.74}$$

By rewriting these quantities, the *clover discretisation* of $G_{\mu\nu}$ reads:

$$G^{cl}_{\mu\nu}(t,x) = \tilde{\partial}_\mu(1-\frac{1}{2}a\partial^*_\nu)B_\nu(t,x) - \tilde{\partial}_\nu(1-\frac{1}{2}a\partial^*_\mu)B_\mu(t,x). \tag{4.75}$$

in terms of lattice derivatives defined in (A1.22) and (A1.24).
If we put the expression for the B field propagator in this definition we obtain the magnetic and electric components:

$$\begin{aligned} E^{cl}_{mag} = \tfrac{1}{4L^3T}\textstyle\sum_p \sin(p_0x_0)^2 \Big[&\hat{p_0}^2\left(1-\tfrac{a^2}{4}\hat{p_0}^2\right)\left(1-\tfrac{a^2}{4}\hat{p_k}^2\right)\bar{D}_{kk} + \\ &+\hat{p_k}^2\left(1-\tfrac{a^2}{4}\hat{p_k}^2\right)\left(1-\tfrac{a^2}{4}\hat{p_0}^2\right)\bar{D}_{00} + \\ &-2\hat{p}_k\hat{p}_0\left(1-\tfrac{a^2}{4}\hat{p_0}^2\right)\left(1-\tfrac{a^2}{4}\hat{p_k}^2\right)\bar{D}_{k0}\Big]. \end{aligned} \tag{4.76}$$

where the propagator $\bar{D}$ is defined in eq. (3.97) and $\hat{p}$ and the lattice momenta are given in A1.7.

$$\begin{aligned} E^{cl}_{el} = \tfrac{1}{4L^3T}\textstyle\sum'_p \cos(p_0x_0)^2 \Big[&\hat{p_0}^2\left(1-\tfrac{a^2}{4}\hat{p_0}^2\right)\left(1-\tfrac{a^2}{4}\hat{p_k}^2\right)\bar{D}_{kk} + \\ &+\hat{p_k}^2\left(1-\tfrac{a^2}{4}\hat{p_k}^2\right)\left(1-\tfrac{a^2}{4}\hat{p_0}^2\right)\bar{D}_{00} + \\ &-2\hat{p}_k\hat{p}_0\left(1-\tfrac{a^2}{4}\hat{p_0}^2\right)\left(1-\tfrac{a^2}{4}\hat{p_k}^2\right)\bar{D}_{k0}\Big]. \end{aligned} \tag{4.77}$$

The primed summation symbol indicates that the terms at $p_0 = 0$ are given the weight $\frac{1}{2}$ and the sum is extend over positive values $p > 0$.

4.4.2 Plaquette discretisation

The plaquette lattice version of $E(t, x)$ is given by the formula

$$E^{pl}(t, x) = -\frac{1}{2} a^{-4} \sum_{\mu,\nu} \left[\mathrm{Tr} \left(P_{\mu\nu}(t, x) + P_{\mu\nu}(t, x)^\dagger - 6 \right) \right]. \tag{4.78}$$

At the order we are working this is equivalent to take the definition

$$E^{pl}(t, x) = -\frac{1}{2} \mathrm{Tr} \langle G^{pl}_{\mu\nu}(t, x) G^{pl}_{\mu\nu}(t, x) \rangle \tag{4.79}$$

using the field strength defined as

$$G^{pl}_{\mu\nu}(t, x) = \partial_\mu B_\nu(t, x) - \partial_\nu B_\mu(t, x) \tag{4.80}$$

where ∂_μ is the forward derivative.
If we put the expression for the B field propagator we get for the magnetic component:

$$E^{pl}_{mag} = \frac{1}{4 L^3 T} \sum_p \sin^2(p_0 x_0) \left(\hat{p}_k^2 \bar{D}_{ll} - 2 \hat{p}_k \hat{p}_l \bar{D}_{kl} + \hat{p}_l^2 \bar{D}_{kk} \right), \tag{4.81}$$

where the propagator $\bar{D}$ is defined in eq. (3.97) and $\hat{p}$ and the lattice momenta are given in A1.7. The electric component with plaquette discretisation is not symmetric with respect to x_0; one possibility is taking $E(x_0) + E(x_0 + a)$:

$$E^{pl}_{el} = \frac{1}{2 L^3 T} {\sum_p}' \left(\hat{p}_0^2 \bar{D}_{kk} - 2 \hat{p}_k \hat{p}_0 \bar{D}_{k0} - \hat{p}_k^2 \bar{D}_{00} \right) \left[\cos^2(p_0 x_0) \left(1 - \frac{a^2}{4} \hat{p}_0^2 \right) + \sin^2(p_0 x_0) \left(\frac{a^2}{4} \hat{p}_0^2 \right) \right]. \tag{4.82}$$

To sum up, in this chapter we reviewed the Symanzik effective theory.

1. First, the concept of universality is briefly reviewed. It consists in the observation that near the critical points physical systems behave similarly. This leads to the definition of a local effective field theory which includes in the action irrelevant operators. This procedure defines the Symanzik improvement programme.

2. Second, not only the action has to be improved but also any other local operator discretised on the lattice. In the case we examine the cutoff effects are generated by three sources: the action, the flow equation and the observable under consideration. As we consider a pure gauge theory and symmetric definitions of the observables, the leading contributions to cutoff effects are $O(a^2)$.

   The Wilson action and the Wilson flow are the simplest discretisations of the action and the flow equation one can think of. The tree-level improved action is the Lüscher-Weisz action, and the improved gradient flow equation is given by the so-called "Zeuthen flow".

3. In the local formulation of the theory, in $4+1$ dimensions, there is only one additional counterterm needed in order to remove the discretisation errors. It corresponds to a modified initial condition for the flow equation. In fact, the link field at zero flow time, not simply is the link field in the four-dimensional theory but it also includes the dependence upon a coefficient (called c_b), which is what we want to test numerically in perturbation theory.

4. The two components of the action density, color magnetic and electric, can be also $O(a^2)$ improved. For the magnetic component one has to notice that the structure of the $O(a^2)$ terms is the same, so by taking the right linear combination it is possible to remove them. In order to improve the electric component one has to add an additional term containing the total temporal derivative because of the non-translation invariance in the temporal direction.

5. Finally, we give the discretised expressions for the components of the action density that we compute on the lattice.

5 Perturbative model

The $O(a^2)$ Symanzik improvement has been discussed in the previous chapter, here we want to test it in perturbation theory at $O(g_0^2)$. We define the probes of a perturbative model by picking a set of observables defined by the expectation value of the action density $t^2\mathcal{E}_0(t,x)$, the electric and the magnetic fields defined in (3.76) and (3.77), at different flow and euclidean times. In Sect. (4.2.3) we explained that, in addition to the action, flow equation and discretisation of the observables, the value of the free improvement coefficient defined in eq. (4.44) needs to be tuned. Its asymptotic value in perturbation theory at tree level is zero [3]. At this value of the improvement coefficient, one expects that the choices of LW action, Z flow equation and the improved combination of the observables, lead to the fully realised $O(a^2)$ Symanzik improvement. The numerical test confirms this expectation.

Additionally, it is interesting to study what happens when the action is unimproved, namely when the W gauge action is used. In this case, there is not a complete basis of counterterms that allows the $O(a^2)$ Symanzik improvement to be applied and we can only determine the free improvement coefficient numerically for one particular observable. We study how this choice acts on the cutoff effects of other observables, by choosing a first set of observables and we measure the cutoff effects. We observe that the tuning of the improvement coefficient, which is now related to one particular observable, actually improves all the observable. By repeating the analysis on a second set of observables, which is qualitatively different as it includes the derivatives in time of $t^2\mathcal{E}_0(t,x)$, we see that the effects are different. The conclusion is that the improvement designed in such a way works only if we consider a set of observables similar among each other.

The analysis is interesting as it is the guide we use before embarking on a non-perturbative study, where the expression for an improved action is not available[1].

[1]The coefficients of the terms that we add in order to realise the improvement of the pure gauge action can only be computed in perturbation theory. For example, the LW improved action is known up to two loops.

Part of our work consists in writing a code to perform the numerical tests listed above (C++ code which uses the Armadillo library [99]).

Finally, we show that the determination of the free improvement coefficient is equivalent to the empirical non-perturbative improvement introduced in [33], which consists in a shift of the flow time. Then we conclude that the phenomenological improvement works only for a quite narrow choice of the set of observables, which leaves an interesting future study about whether this restriction is kept non-perturbatively.

This entire chapter is new material that has not appeared elsewhere. The source code we use is available at this link[2].

5.1 First numerical test: perturbative value of c_b for improved action, flow equation and observables

We know from [3] that at leading order in perturbation theory (order g_0^2), $O(a^2)$ cutoff effects can be fully removed only when the action, flow equation and observables are all improved. What we expect is that the c_b dependence in the initial condition for the flow equation (4.44), is such that $c_b = 0$ fully realises the $O(a^2)$ improvement for both electric and magnetic components. This is the first numerical test we perform here. We define a set of observables, O_i, in order to probe the improvement conditions. First, we consider the magnetic $\mathcal{E}_0^{mag}$ and electric $\mathcal{E}_0^{el}$ components of the energy density expectation value[3] which are represented in Figs. 3.7 and 3.8. We show the comparison between the continuum values and the computation of the observables on the lattice, for two lattice sizes $L = 16, 24$, Fig. 5.1, and we see that the profiles in euclidean time coincide.

Then we choose to define a set of observables by fixing different values of the two parameters that vary. The constant $c = \frac{\sqrt{8t}}{L}$ is the ratio between the spreading radius introduced by the flow and the lattice size: fixing the flow time t is equivalent to fixing the value of this constant. We study $c = 0.2, 0.3, 0.4$ as we wish to span a reasonable range but avoid the spreading radius getting too close to the boundaries of the lattice, as this would falsify our measurement. The other parameter we can vary is the Euclidean time and we study two values which, normalised to the temporal extent of the lattice, are $\bar{x}_0 = \frac{x_0}{T} = 0.5, 0.25$. The first, being in the middle of the lattice, is the less influenced by the boundaries.

[2] https://github.com/argiarubeo/perturbative-gf-coupling

[3] Here we refer to the lowest non-trivial order in perturbation theory, $O(g_0^2)$.

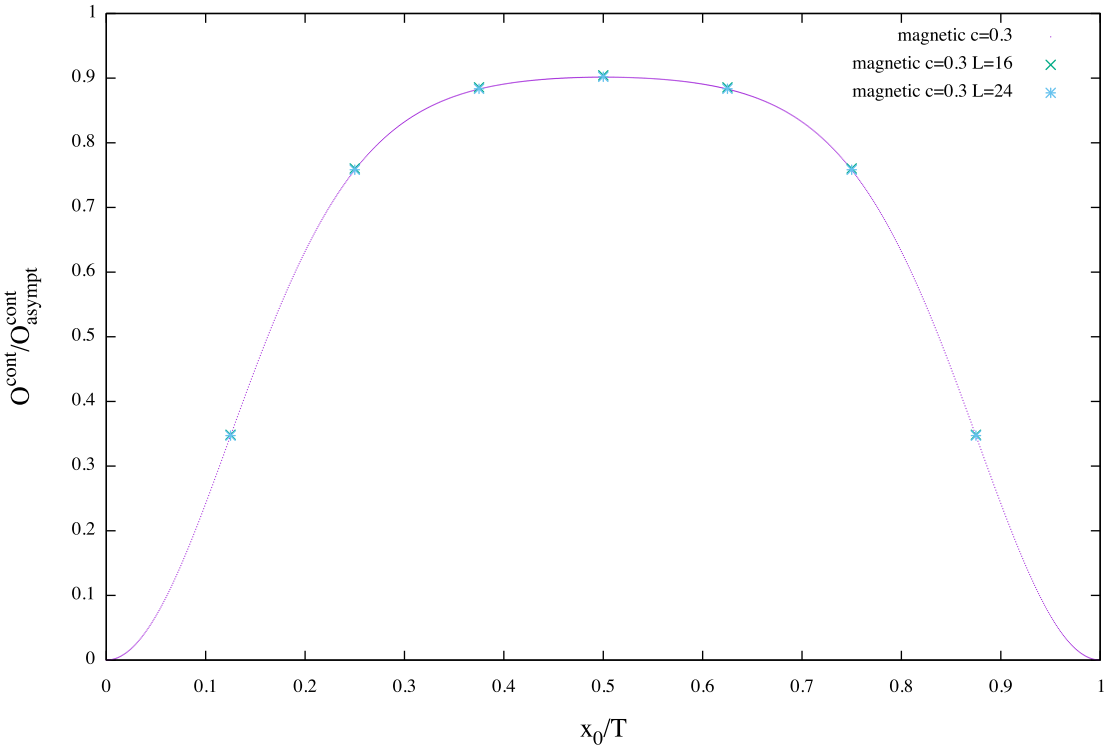

Figure 5.1: The magnetic component of $t^2\mathcal{E}_0$, for $c = 0.3$ as a function of the euclidean time normalised to the lattice extent in the temporal direction x_0/T. The function plotted is normalised to the infinite volume asymptotic value $O^{cont}_{asympt} = \frac{1}{2}\frac{3}{16\pi^2}$ (the factor $\frac{1}{2}$ is to take in account that we split $E = E_{mag} + E_{el}$), with zero at the extremes because we impose Dirichlet conditions. The points at $x_0/T = 0.125, 0.25, 0.375, 0.5, 0.625, 0.75, 0.875$ are the magnetic component of $t^2\mathcal{E}_0$ on the lattice at $O(g_0^2)$, for two different lattice sizes $L = 16, 24$.

The list of observables defined above contains twelve of them, we label the first six (magnetic field components, computed at $c = 0.2, 0.3, 0.4$ and each at $\bar{x}_0 = 0.5, 0.25$) as *set 1* (see Sec. A3), and the second six (same for the electric field components) as *set 2* (see Sec. A3). Set 1 includes the simplest observables to consider.

We perform the first numerical test on set 1, and we observe what we expect: the improvement is achieved only with LW improved action, Zeuthen improved flow and improved observables (magnetic component in this case). In Fig. 5.2 we plot the observable scaled by $\left(\frac{L}{a}\right)^2$ versus $\left(\frac{a}{L}\right)^2$, which means that the intercept of the function plotted with the y axis is the coefficient of the cutoff effects[4]. If we unimprove either the action, using W action, or the flow, using W flow, we can distinguish the cutoff effects coming from these two sources. They are the two lines with positive intercept in Fig. 5.2. Moreover, if we unimprove the observable, using either plaquette or clover discretisations, we get the

[4]It is easy to see this using a polynomial function in $\left(\frac{a}{L}\right)^2$, with no constant term, which corresponds to continuum value.

cutoff effects coming from these other two sources. As we pointed out in Sec. 4.3, both clover and plaquette discretisations have the same structure but the clover gives rise to effects which are four times larger, which is why we improve the magnetic component by taking the linear combination in eq. (4.55).

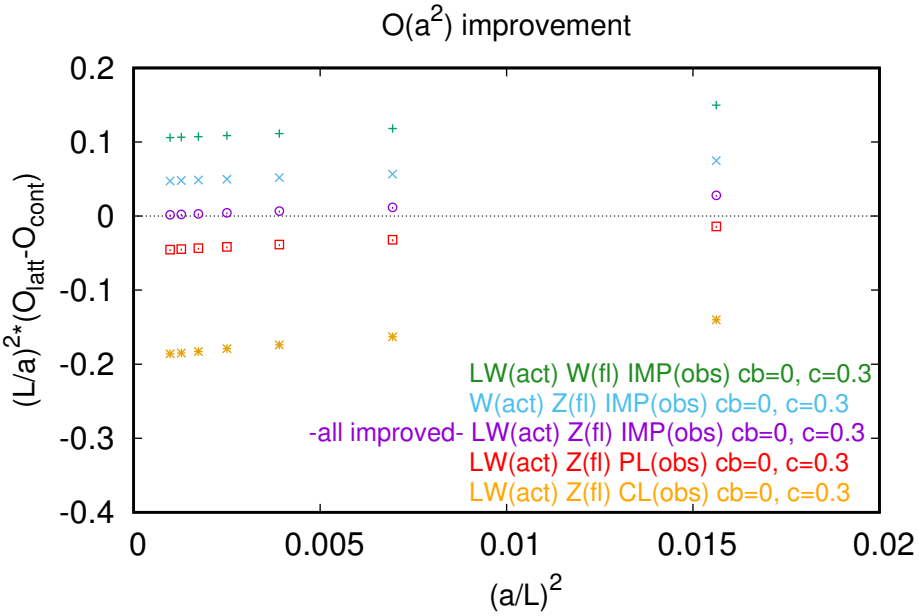

Figure 5.2: $O(a^2)$ improvement realised only for LW improved action, Zeuthen improved flow and improved observable. O_{lat} is the observable $t^2\mathcal{E}_0^{mag}$ (i.e. at $O(g_0^2)$ in perturbation theory) computed on the lattice at $c = 0.3$ and $\bar{x}_0 = 0.5$, while O_{cont} is its continuum value. The upper points correspond to either W action or W flow, while the points below are either plaquette or clover discretisations [8].

As previously mentioned, the constant $c = \frac{\sqrt{8t}}{L}$ measures how much the field is smeared, in units of the lattice size. Looking at different values of $c = 0.3, 0.4, 0.5$ in Fig. 5.4, somehow surprisingly, we do not see effects coming from the time boundaries.

We also check that the electric component behaves similarly: $c_b = 0$, such that the improved combination (4.63) is free from $O(a^2)$ effects when we use the LW improved action and the Zeuthen flow equation, Fig. 5.3.

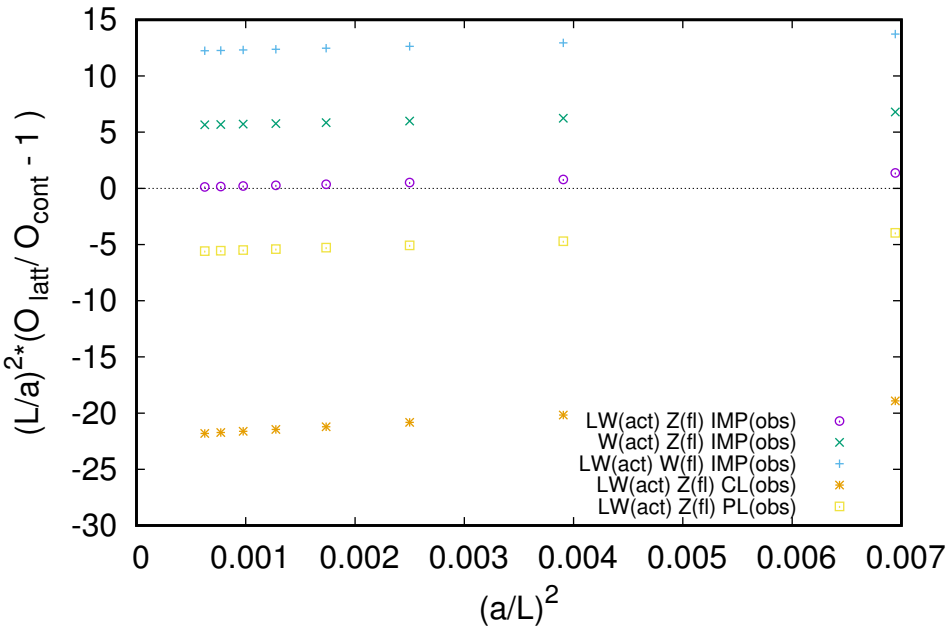

Figure 5.3: O_{lat} is the observable $t^2\mathcal{E}_0^{el}$ (i.e. at $O(g_0^2)$ in perturbation theory) computed on the lattice at $c = 0.3$ and $\bar{x}_0 = 0.5$, while O_{cont} is its continuum value. The upper points correspond to either W action or W flow, while the points below are either plaquette or clover discretisations.

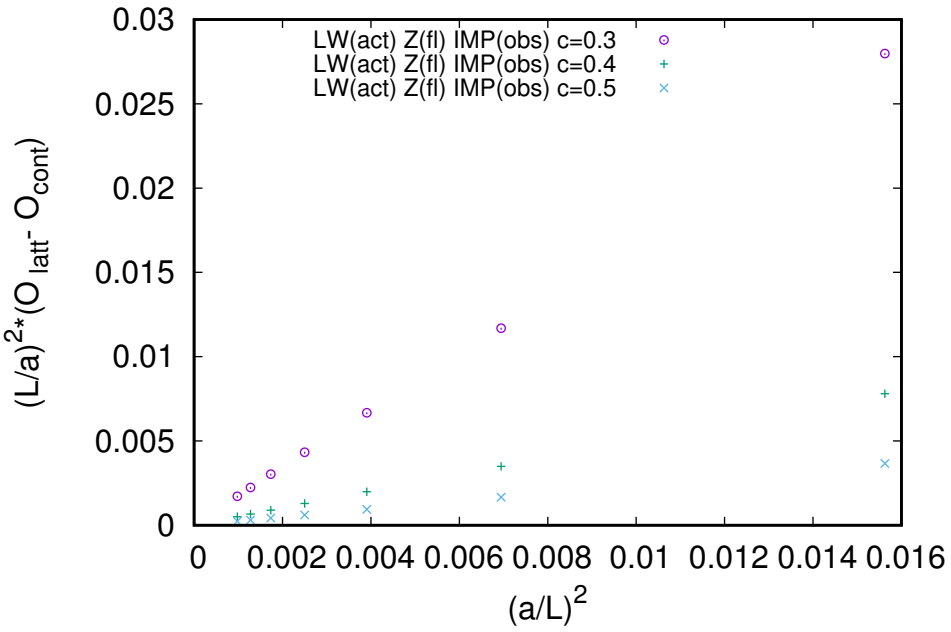

Figure 5.4: O_{lat} is the observable $t^2\mathcal{E}_0^{mag}$ (i.e. at $O(g_0^2)$ in perturbation theory), improved and computed at different values of $c = 0.3, 0.4, 0.5$, at $\bar{x}_0 = 0.5$ [8].

5.2 Numerical value of c_b^* computed with respect to the reference observable in the case of unimproved quantities

The next step we take in the perturbative analysis, is to consider an action which is not tree-level improved. By choosing the W action, we no longer have a complete basis of counterterms to realise the $O(a^2)$ Symanzik improvement; this implies that there is no way to compute $c_b = c_b^*$ such that every observable, in any set we choose, is free from $O(a^2)$ cutoff effects. In this set-up we can only compute what we call c_b^* phenomenologically, it is the c_b value for one particular observable. We call O_{ref} the reference observable which defines c_b^*, the coefficient which makes the cut-off effects of O_{ref} equal to zero. This means that we compute c_b^* numerically, by imposing that the coefficient of the $O(a^2)$ cutoff effects is zero.

Our goal is to define a reference observable O_{ref} by picking values for c and $\bar{x}_0$ such that they minimise the boundary effects. As long as the smearing radius is not too large and we choose the euclidean time coordinate in the middle of the lattice this is achieved; thus we choose the magnetic component at $c = 0.3$ and $\bar{x}_0 = 0.5$,

$$O_{ref} \equiv t^2 \mathcal{E}^0_{mag@0.3,T/2}, \quad \text{at } c = 0.3, x_0 = \frac{T}{2}. \tag{5.1}$$

At this stage it is interesting to study whether the cut-off effects are reduced for all the other observables in the set, by using $c_b = c_b^*$. The purpose of this procedure is that if the tuning of c_b to c_b^* actually would improve the other observables, then we know how to perform a phenomenological improvement perturbatively.

In tab. (5.1) we report the values of c_b^* computed by imposing $O_{lat} = O^{cont}$.[5] We compare the result with the infinite volume values (see [3]), reported in tab. (5.2): in the first row everything is improved and we know from the perturbative computation that $c_b^* = 0$; in the second row the action is not improved, so the particular improvement condition, which determines c_b^*, is to impose an $O(a^2)$-improvement of $O_{mag}(t)$ in infinite volume. We can check that increasing the lattice size, the value of c_b^* is going towards its continuum value, zero for the LW action, and $-\frac{1}{36}$ for the W action.

Once c_b^* is computed, we move on to study the effect of it on the other observables in the set. We now label as set 3 the union of set 1 and set 2 (see Sec. A3), which includes

[5]The precision of the numerical computation is set to be the fifth digit, (10^{-6}).

Table 5.1: Values of c_b^* for the magnetic component at $c = 0.3$ and $x_0 = \frac{T}{2}$. We consider two choices for the action: LW and W, and we impose $(O_{ref}^{lat} = O^{cont})$.

L	c_b^* (mag) $x_0 = \frac{T}{2}$ (W action)	c_b^* (mag) $x_0 = \frac{T}{2}$ (LW action)
12	-0.033088	-0.00706
16	-0.0305899	-0.00401
20	-0.029420	-0.00259
24	-0.028776	-0.00181
28	-0.028384	-0.00133
32	-0.028119	-0.00102
36	-0.02564	-0.0008
40	-0.02552	-0.0006

Table 5.2: Values of c_b, in infinite volume, for two choices of the action (LW and W). The W action is not $O(a^2)$ improved, then the counterterm basis is incomplete and c_b is fixed by the improvement condition imposed on the magnetic component at $c = 0.3$ and $x_0/T = 0.5$.

action	flow	observable	c_b
LW	Z	IMP	0
W	Z	IMP	$-\frac{1}{36}$

all 12 observables defined in Sec. (5.1). It is possible to repeat the argument unimproving the flow equation: without a complete basis of counterterms we choose one particular improvement condition and we study if this reduces the cutoff effects in the observables of the set considered. In Figs. (5.8)-(5.16) we observe that c_b^* actually reduces the size of the cutoff effects for all the observables considered in set 3. In Fig. 5.9 action, flow and observables are all improved. The green line corresponds to $O_{ref} = \mathcal{E}^0_{mag@0.3,T/2}$ which has zero cutoff effects and defines c_b^*. In tab. (5.3) we list all the possible choices for action, flow and observable (twelve in total). By comparing the spread of the observables at $c_b = 0$ (red) and the spread of the same observables at c_b^* (blue) we see how c_b^* reduces the cutoff effects. As we can see in tab. 5.3 a reduction by a factor two or three, and even six is realised by tuning c_b from zero to the value c_b^*.

We can do the same analysis by using the electric component $O^{lat} = t^2\mathcal{E}^0_{el}$ at $c = 0.3$ and $x_0 = \frac{T}{2}$. In tab. (5.4) we report the values of c_b^* obtained by imposing $O^{lat} = O^{cont}$.

We also list the values of c_b^* obtained for different choices of action, flow and observable discretisation.

Table 5.3: Spread of the observables plotted in the following Figs. at $c_b = 0$ (red), and c_b^* (blue). The spread is defined by taking from the plot the range spanned by the smallest lattice size we consider ($L = 12$) relative to different observables. The smaller the spread using c_b^* the larger the effect of tuning this coefficient in order to reduce the cutoff effects.

Action	Flow	Observable	Red spread $c_b = 0$	Blue spread c_b^*
W	W	IMP	0.29	0.043
W	W	PL	0.34	0.058
W	W	CL	0.055	0.015
W	Z	IMP	0.098	0.038
W	Z	PL	0.18	0.16
W	Z	CL	0.13	0.043
LW	W	IMP	0.20	0.034
LW	W	PL	0.26	0.05
LW	W	CL	0.099	0.026
LW	Z	IMP	0.05	0.05
LW	Z	PL	0.12	0.061
LW	Z	CL	0.17	0.053

Table 5.4: Values of c_b^* for the electric component at $c = 0.3$ and $x_0 = \frac{T}{2}$. We consider two choices for the action: W and LW, and we impose $O_{ref}^{lat} = O^{cont}$.

L	c_b^* (el) $x_0 = \frac{T}{2}$ (W action)	c_b^* (el) $x_0 = \frac{T}{2}$ (LW action)
12	-0.0388	-0.00809
16	-0.0361	-0.0046
20	-0.0347	-0.0030
24	-0.0340	-0.0021
28	-0.0335	-0.0015
32	-0.0332	-0.0012
36	-0.0330	-0.0009
40	-0.0328	-0.0007

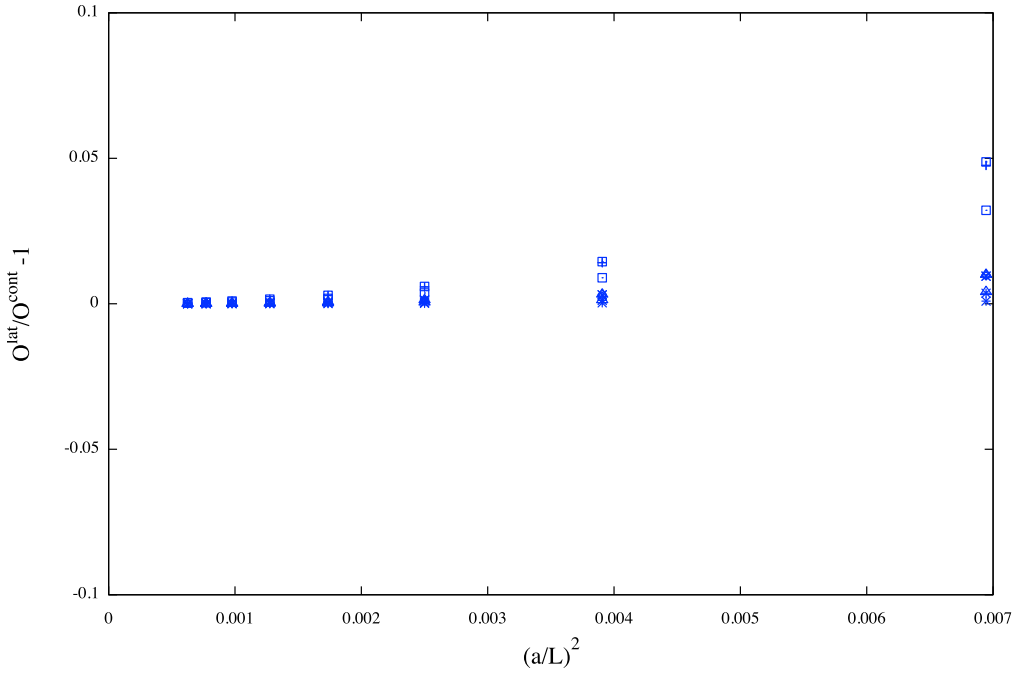

Figure 5.5: LW action, Z flow, and IMP observables of set 3 (see Sec. A3), at $O(g_0^2)$ in perturbation theory. $\frac{L}{a} = 12, 16, 20, 24, 28, 32, 36, 40$. This is the only case in which action flow and observables are improved, meaning that $c_b = 0 = c_b^*$. Note the finer scale compared to the other figures in this chapter.

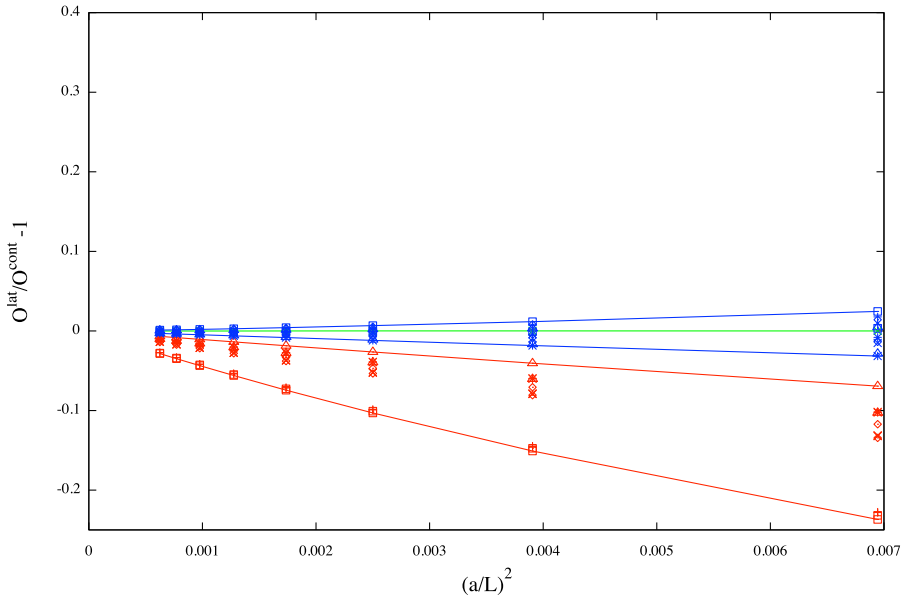

Figure 5.6: LW action, Z flow, and CL observables of set 3 (see Sec. A3), at $O(g_0^2)$ in perturbation theory. $\frac{L}{a} = 12, 16, 20, 24, 28, 32, 36, 40$. The green line is the reference observable which defines c_b^* (zero cutoff effects on $O_{ref} = \mathcal{E}_0^{mag}(c = 0.3, \frac{x_0}{T} = 0.5)$).The red points are the observables computed using $c_b = 0$. The blue points are the observables computed using c_b^*.

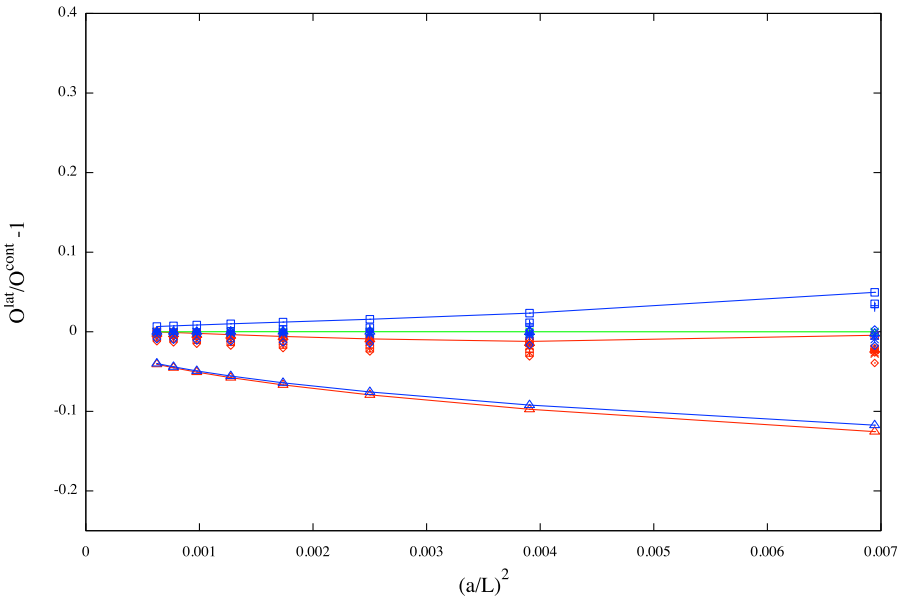

Figure 5.7: LW action, Z flow, and PL observables of set 3 (see Sec. A3), at $O(g_0^2)$ in perturbation theory. $\frac{L}{a} = 12, 16, 20, 24, 28, 32, 36, 40$. The green line is the reference observable which defines c_b^* (zero cutoff effects on $O_{ref} = \mathcal{E}_0^{mag}(c = 0.3, \frac{x_0}{T} = 0.5)$).The red points are the observables computed using $c_b = 0$. The blue points are the observables computed using c_b^*.

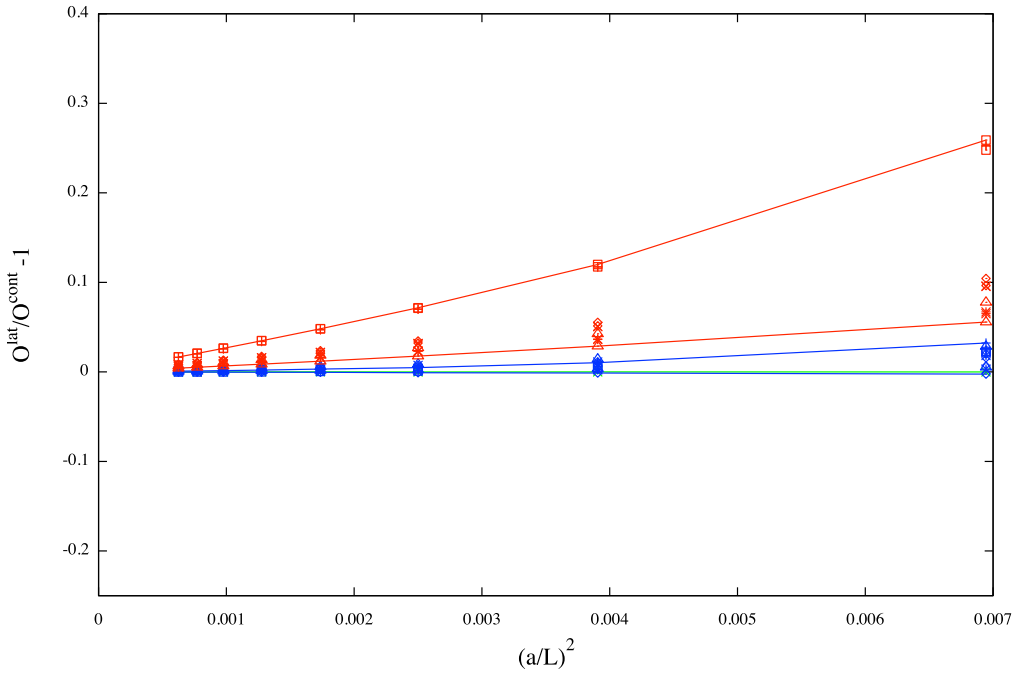

Figure 5.8: LW action, W flow, and IMP observables of set 3 (see Sec. A3), at $O(g_0^2)$ in perturbation theory. $\frac{L}{a} = 12, 16, 20, 24, 28, 32, 36, 40$. The green line is the reference observable which defines c_b^* (zero cutoff effects on $O_{ref} = \mathcal{E}_0^{mag}(c = 0.3, \frac{x_0}{T} = 0.5)$).The red points are the observables computed using $c_b = 0$. The blue points are the observables computed using c_b^*.

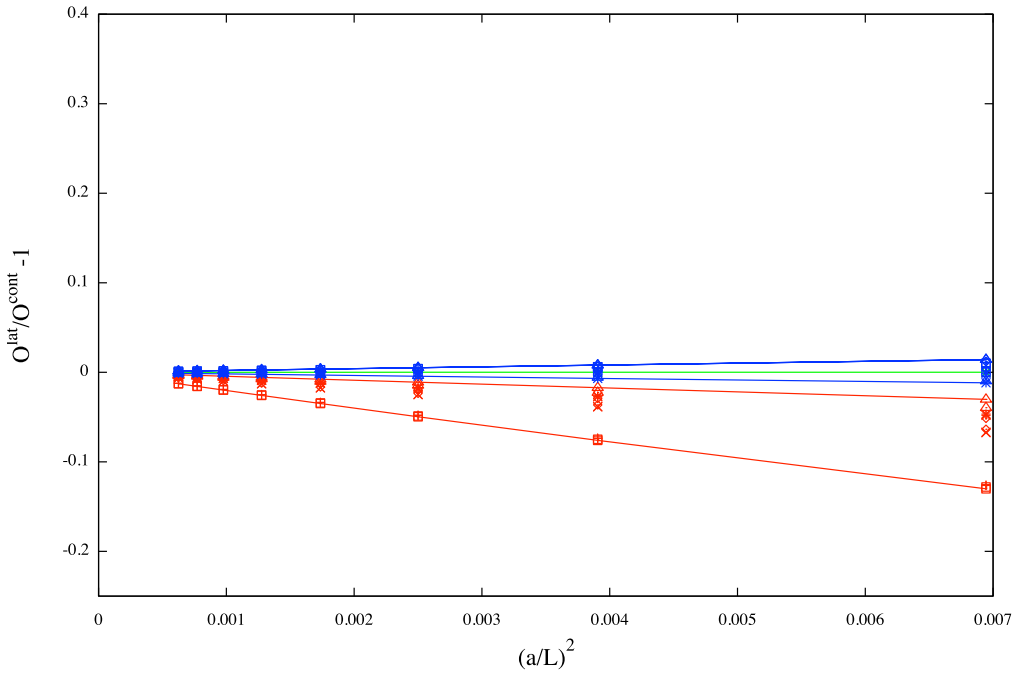

Figure 5.9: LW action, W flow, and CL observables of set 3 (see Sec. A3), at $O(g_0^2)$ in perturbation theory. $\frac{L}{a} = 12, 16, 20, 24, 28, 32, 36, 40$. The green line is the reference observable which defines c_b^* (zero cutoff effects on $O_{ref} = \mathcal{E}_0^{mag}(c = 0.3, \frac{x_0}{T} = 0.5)$).The red points are the observables computed using $c_b = 0$. The blue points are the observables computed using c_b^*.

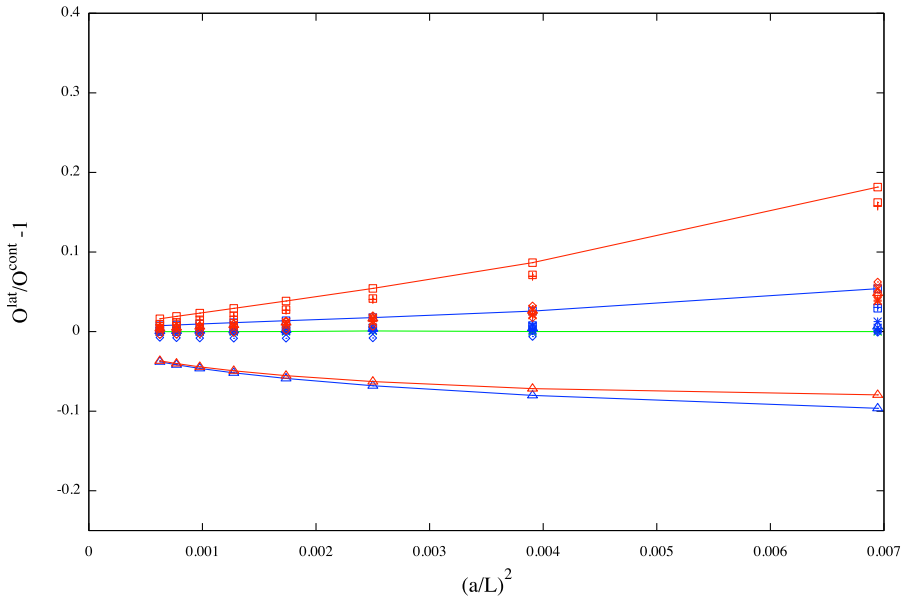

Figure 5.10: LW action, W flow, and PL observables of set 3 (see Sec. A3), at $O(g_0^2)$ in perturbation theory. $\frac{L}{a} = 12, 16, 20, 24, 28, 32, 36, 40$. The green line is the reference observable which defines c_b^* (zero cutoff effects on $O_{ref} = \mathcal{E}_0^{mag}(c = 0.3, \frac{x_0}{T} = 0.5)$).The red points are the observables computed using $c_b = 0$. The blue points are the observables computed using c_b^*.

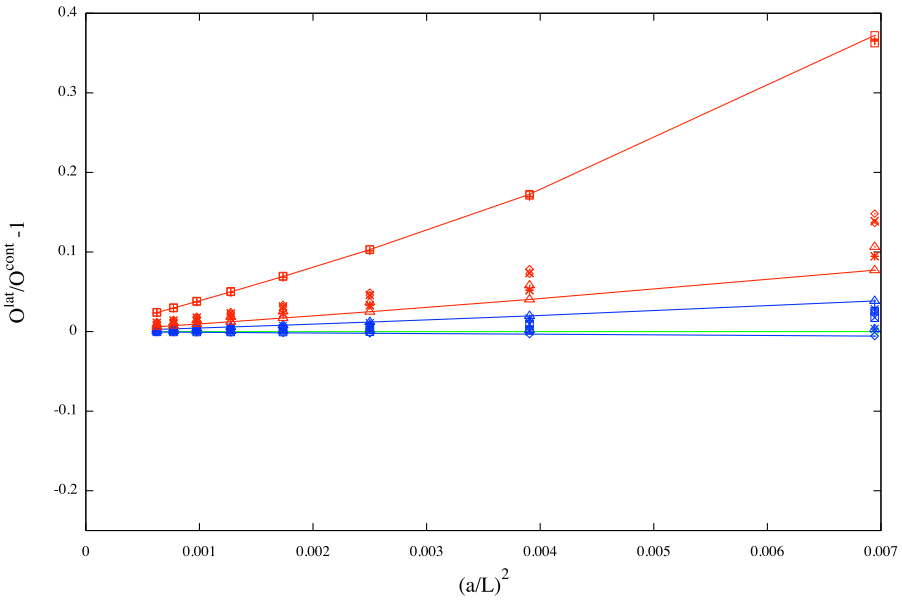

Figure 5.11: W action, W flow, and IMP observables of set 3 (see Sec. A3), at $O(g_0^2)$ in perturbation theory. $\frac{L}{a} = 12, 16, 20, 24, 28, 32, 36, 40$. The green line is the reference observable which defines c_b^* (zero cutoff effects on $O_{ref} = \mathcal{E}_0^{mag}(c = 0.3, \frac{x_0}{T} = 0.5)$).The red points are the observables computed using $c_b = 0$. The blue points are the observables computed using c_b^*.

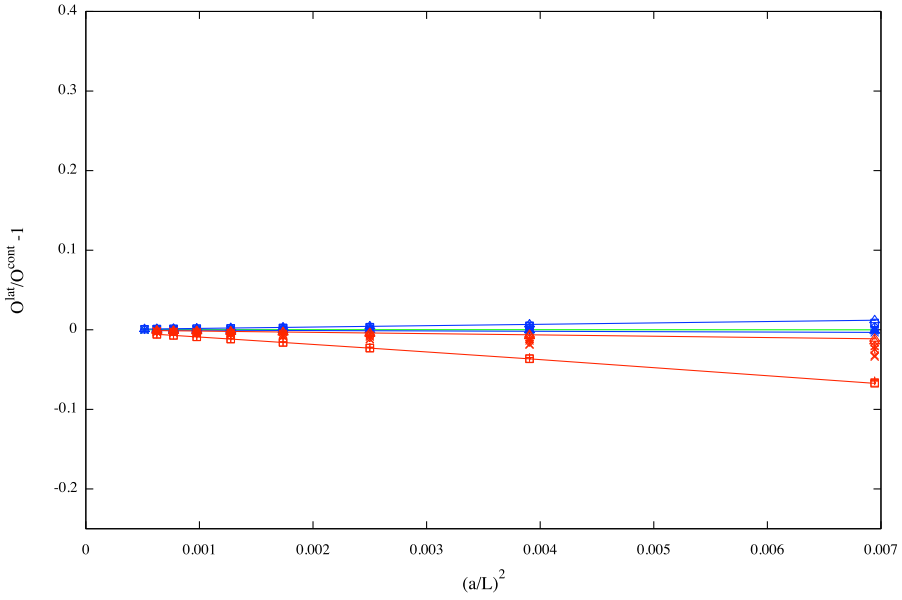

Figure 5.12: W action, W flow, and CL observables of set 3 (see Sec. A3), at $O(g_0^2)$ in perturbation theory. $\frac{L}{a} = 12, 16, 20, 24, 28, 32, 36, 40$ (also $L = 44$ at $c_b = 0$).The green line is the reference observable which defines c_b^* (zero cutoff effects on $O_{ref} = \mathcal{E}_0^{mag}(c = 0.3, \frac{x_0}{T} = 0.5)$).The red points are the observables computed using $c_b = 0$. The blue points are the observables computed using c_b^*.

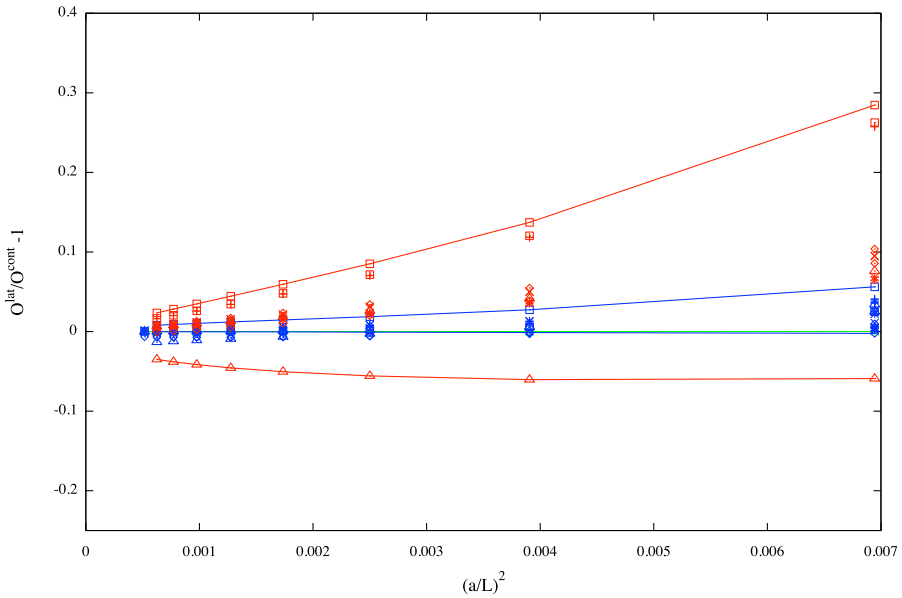

Figure 5.13: W action, W flow, and PL observables of set 3 (see Sec. A3), at $O(g_0^2)$ in perturbation theory. $\frac{L}{a} = 12, 16, 20, 24, 28, 32, 36, 40$ (also $L = 44$ at $c_b = 0$).The green line is the reference observable which defines c_b^* (zero cutoff effects on $O_{ref} = \mathcal{E}_0^{mag}(c = 0.3, \frac{x_0}{T} = 0.5)$).The red points are the observables computed using $c_b = 0$. The blue points are the observables computed using c_b^*.

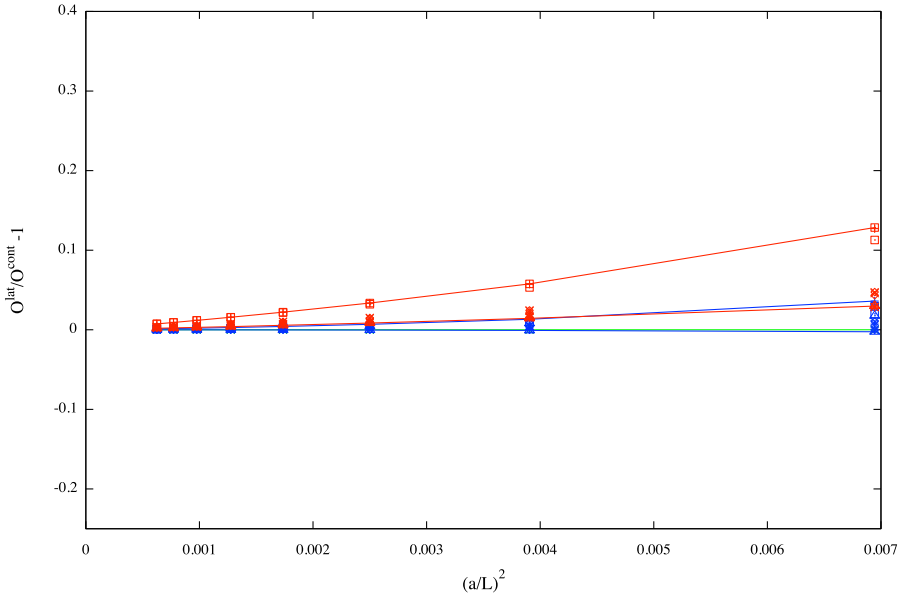

Figure 5.14: W action, Z flow, and IMP observables of set 3 (see Sec. A3), at $O(g_0^2)$ in perturbation theory. $\frac{L}{a} = 12, 16, 20, 24, 28, 32, 36, 40$. The green line is the reference observable which defines c_b^* (zero cutoff effects on $O_{ref} = \mathcal{E}_0^{mag}(c = 0.3, \frac{x_0}{T} = 0.5)$).The red points are the observables computed using $c_b = 0$. The blue points are the observables computed using c_b^*.

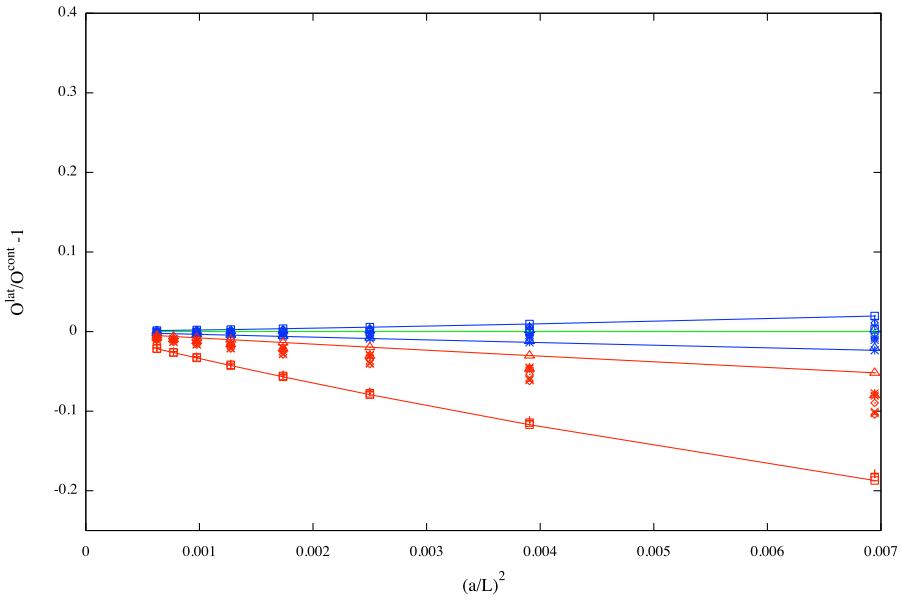

Figure 5.15: W action, Z flow, and CL observables of set 3 (see Sec. A3), at $O(g_0^2)$ in perturbation theory. $\frac{L}{a} = 12, 16, 20, 24, 28, 32, 36, 40$. The green line is the reference observable which defines c_b^* (zero cutoff effects on $O_{ref} = \mathcal{E}_0^{mag}(c = 0.3, \frac{x_0}{T} = 0.5)$).The red points are the observables computed using $c_b = 0$. The blue points are the observables computed using c_b^*.

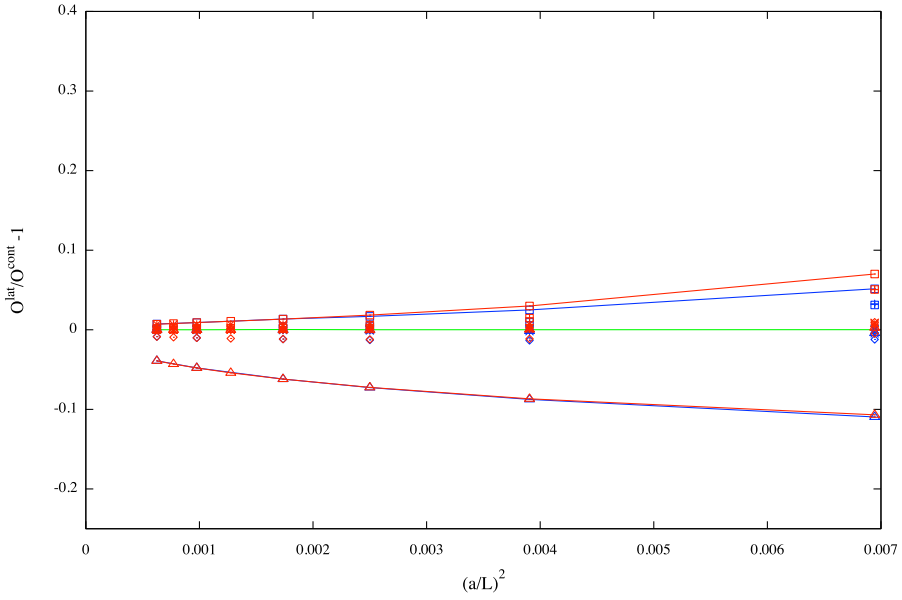

Figure 5.16: W action, Z flow, and PL observables of set 3 (see Sec. A3), at $O(g_0^2)$ in perturbation theory. $\frac{L}{a} = 12, 16, 20, 24, 28, 32, 36, 40$. The green line is the reference observable which defines c_b^* (zero cutoff effects on $O_{ref} = \mathcal{E}_0^{mag}(c = 0.3, \frac{x_0}{T} = 0.5)$).The red points are the observables computed using $c_b = 0$. The blue points are the observables computed using c_b^*.

5.2.1 Determination of c_b^* using different discretisations

We list (in tab. 5.5-5.8) the values that we obtain for the coefficient c_b^*, with all possible choices of the discretisations of action, flow equation and observable. We note that the order of magnitude is the same everywhere but for the particular choice W-Z-PL (Wilson action, Zeuthen flow, Plaquette observable), in this case c_b^* is smaller, meaning that we need to do less tuning in order to improve. Also, as we expect, for the choice LW-Z-IMP the coefficient is zero, up to the precision specified (10^{-5}).

The value of c_b^* quantifies how much we need to tune the coefficient in the initial condition in order to improve the observable. The larger the difference between c_b and c_b^* (Δc_b) the smaller the sensitivity of the observable O to a variation of c_b:

$$O(c_b + \Delta c_b) = O(c_b) + \frac{\partial O}{\partial c_b}\Delta c_b + ... \tag{5.2}$$

We observe a slight variation for different discretisations, but in this case there is not a significant difference. We see in the next section that by enlarging the set of observables, and picking the second derivative as a reference observable the order of magnitude of c_b^* changes (tab. 5.9). This observation implies that the second derivative is less sensitive to a change in the improvement coefficient c_b.

Table 5.5: Values of c_b^* for W action, W flow, and the three choices of the observables, improved, plaquette, clover.

L	c_b^* W-W-IMP	c_b^* W-W-PL	c_b^* W-W-CL
12	-0.0922	-0.0651	0.0252
16	-0.0907	-0.0630	0.0248
20	-0.0902	-0.0621	0.0247
24	-0.0902	-0.0615	0.0246
28	-0.0899	-0.0612	0.0246
32	-0.0899	-0.0610	0.0246
36	-0.0899	-0.0610	0.0246
40	-0.0899	-0.0610	0.0246

Table 5.6: Values of c_b^* for W action, Z flow, and the three choices of the observables, improved, plaquette, clover.

L	c_b^* W-Z-IMP	c_b^* W-Z-PL	c_b^* W-Z-CL
12	-0.03308	-0.0065	0.0828
16	-0.03058	-0.0032	0.0841
20	-0.02942	-0.0016	0.0848
24	-0.02877	-0.00001	0.0853
28	-0.02838	-0.0001	0.0854
32	-0.02811	-0.001	0.0859
40	-0.02552	-0.001	0.0864

Table 5.7: Values of c_b^* for LW action, W flow, and the three choices of the observables, improved, plaquette, clover.

L	c_b^* LW-W-IMP	c_b^* LW-W-PL	c_b^* LW-W-CL
12	-0.0656	-0.0386	0.0515
16	-0.0637	-0.0361	0.0515
20	-0.0632	-0.0350	0.0515
24	-0.0624	-0.0344	0.0515
28	-0.0624	-0.0344	0.0515
32	-0.0624	-0.0344	0.0515
40	-0.0624	-0.0344	0.0515

Table 5.8: Values of c_b^* for LW action, Z flow, and the two choices of the observables, improved, plaquette, clover. For the improved case $c_b^* = 0.0001$ for the lattice sizes spanning the range $\frac{L}{a} = 24 - 40$.

L	c_b^* LW-Z-PL	c_b^* LW-Z-CL
12	0.0198	0.1089
16	0.0235	0.1107
20	0.0253	0.1117
24	0.0264	0.1120
28	0.0270	0.1121
32	0.0270	0.1121
40	0.0270	0.1121

5.3 Larger set of observables to perform numerical tests

In the previous section we have seen that the improvement realised by tuning c_b for a reference observable, works for set 3, which includes the 12 observables defined in Sec. (5.1). It is interesting to test numerically if the same observation holds for a larger set of observables. We define the new set, *set 4* see Sec. A3, by including the second derivative in time, of both components, magnetic and electric. These observables measure the curvature of the original ones, and we include them in order to see how differently they behave with respect to E_{mag} and E_{el} themselves. At lowest order in perturbation theory, their continuum expressions are given in eq. (3.81) and eq. (3.82).

On the lattice, we want to use the $\mathcal{O}(a^2)$ improved second derivative operator, which has the expression:

$$D''^{(imp)}f(x_0) = -\frac{1}{12}f(x_0+2a) + \frac{4}{3}f(x_0+a) - \frac{5}{2}f(x_0) + \frac{4}{3}f(x_0-a) - \frac{1}{12}f(x_0-2a). \quad (5.3)$$

This is done in order to avoid cutoff effects coming from the non improved operator. The electric improved component already contains a second derivative in time, which involves the point (x), the nearest neighbour $(x+a)$, and the next-to-nearest neighbour $(x+2a)$. By applying this operator to it, we will get a dependence on $(x \pm 4a)$, which involves at most 8 lattice spacings. We need to either avoid simulating a lattice size which is too small (e.g. $L = 12$), alternatively we can choose $T = 2L$. In fact, we want to avoid being too close to the boundaries which effect the measurements.

We define a set of observables, *set 4* (explicitly listed in A3.4), by choosing the values of $c = 0.2, 0.3$ and $\bar{x_0} = 0.5$ for the improved derivatives of the two components colour electric and magnetic. We restricted che choice of the values for c and $\bar{x_0}$ as such choice avoids the boundary effect to influence our measurements. In fact the derivative operator in eq. (5.3) involves four lattice spacings and for a lattice size $L = 12$ either being at $\bar{x_0} = 0.25$ or having a smearing radius too large would not be a good choice.

We report the result of our study where we observe that the effect of using c_b^*, defined by setting zero cutoff effects on the magnetic component at $c = 0.3$ and $\bar{x_0} = 0.5$, does not significantly reduce the cutoff effects on set 4. We look at the different discretisation of the observable (IMP, PL, CL) using improved LW action and unimproved W flow, see Figs. 5.17, 5.18, 5.19. Then we analyse the different discretisation of the observable (IMP, PL, CL) using unimproved W plaquette action and improved Z flow, see Figs. 5.20, 5.21, 5.22.

The behaviour turns out to be the same for all possible choices of action, flow and observable, meaning that the observables are not significantly improved by c_b^*.

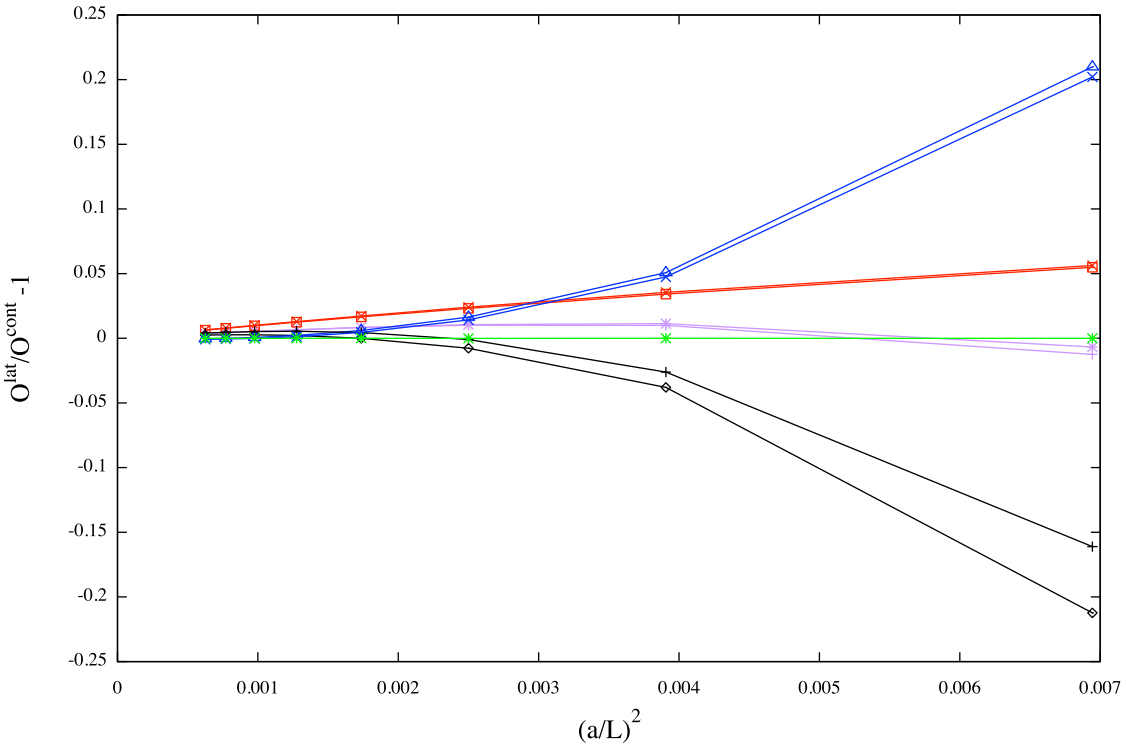

Figure 5.17: LW action, W flow, IMP observable of set 4 (see Sec. A3.4), at $O(g_0^2)$ in perturbation theory, with SF boundary conditions. The same colour represents the same observable. Two set of data points of the same colour represents both the values of $c_b = 0$ and c_b^* which does not significantly improve the observable. The green line (flat), is the definition of c_b^* which cancels the cutoff effects of the reference observable, namely $t^2\mathcal{E}_0^{mag}(c = 0.3, \frac{x_0}{T} = 0.5)$. The black and blue points refer to the electric component at $c = 0.2$ and $c = 0.3$, while the purple and red points represent the magnetic component at $c = 0.2$ and $c = 0.3$. $\frac{L}{a} = 12, 16, 20, 24, 28, 32, 36, 40$.

The observation that the improvement is not working when the reference observable is qualitatively different from the observable to improve (such as the component itself and its euclidean time-derivative) is consistent with the following fact. If we choose as reference observable $T^2\partial_0^2 t^2\mathcal{E}_0^{mag}(c = 0.3, \frac{x_0}{T} = 0.5)$, the c_b^* determined is at least one order of magnitude larger. In tab. 5.9, we report the comparison of such data for W action, Z flow and IMP observable, but it is observed for all possible choices. The value of c_b^* is very much dependent on the observable we pick, it does not change much by changing the euclidean and flow time but it changes if we take the euclidean time-derivatives.

We show the comparison between such difference in the effect on the second derivative and the observable itself, in two representative cases of unimproved action (Fig. 5.23) and unimproved flow (Fig. 5.24).

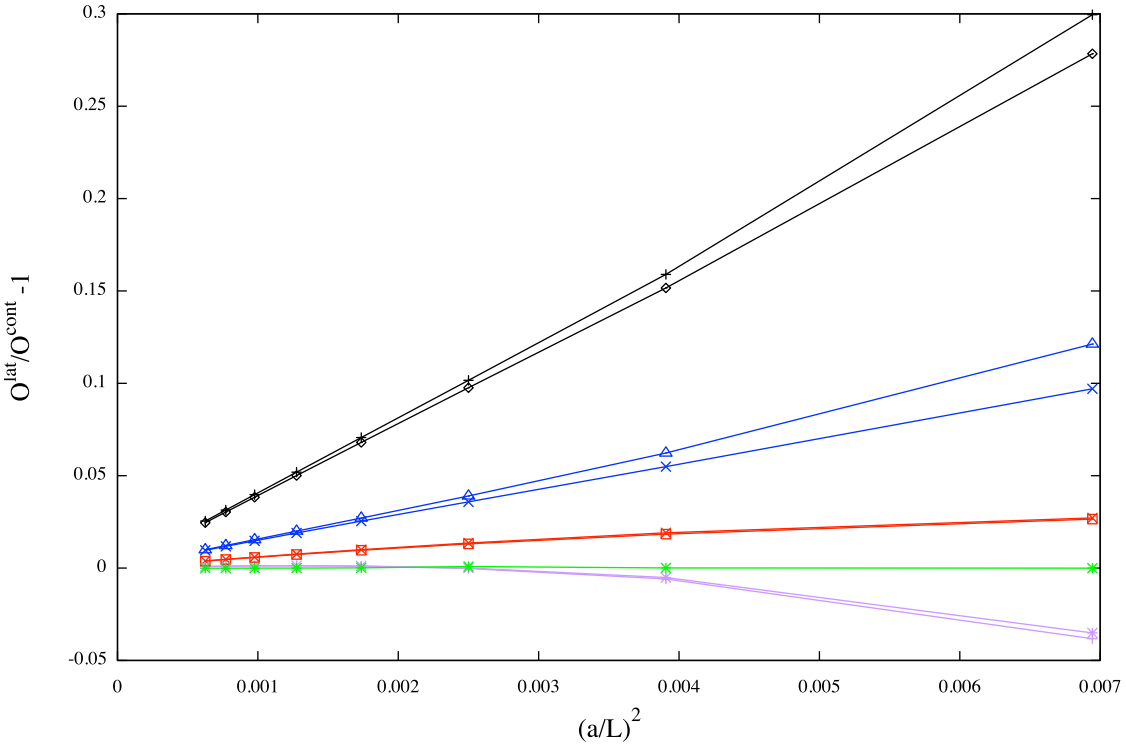

Figure 5.18: LW action, W flow, PL observable of set 4 (see Sec. A3.4), at $O(g_0^2)$ in perturbation theory, with SF boundary conditions. The same colour represents the same observable. Two set of data points of the same colour represents both the values of $c_b = 0$ and c_b^* which does not significantly improve the observable. The green line (flat), is the definition of c_b^* which cancels the cutoff effects of the reference observable, namely $t^2\mathcal{E}_0^{mag}(c = 0.3, \frac{x_0}{T} = 0.5)$. The black and blue points refer to the electric component at $c = 0.2$ and $c = 0.3$, while the purple and red points represent the magnetic component at $c = 0.2$ and $c = 0.3$. $\frac{L}{a} = 12, 16, 20, 24, 28, 32, 36, 40$.

Table 5.9: Values of c_b^* for W action, Z flow, and IMP observable. c_b^* refers to the reference observable $t^2\mathcal{E}_0^{mag}(c = 0.3, \frac{x_0}{T} = 0.5)$, while $(c_b^*)''$ is numerically computed by eliminating the cutoff effects of $T^2\partial_0^2 t^2\mathcal{E}_0^{mag}(c = 0.3, \frac{x_0}{T} = 0.5)$.

L	c_b^* W-Z-IMP	$(c_b^*)''$ W-Z-IMP
12	-0.033	-0.54
16	-0.030	-0.66
20	-0.029	-0.78
24	-0.028	-0.88
28	-0.028	-0.95
32	-0.028	-0.10
40	-0.025	-0.12

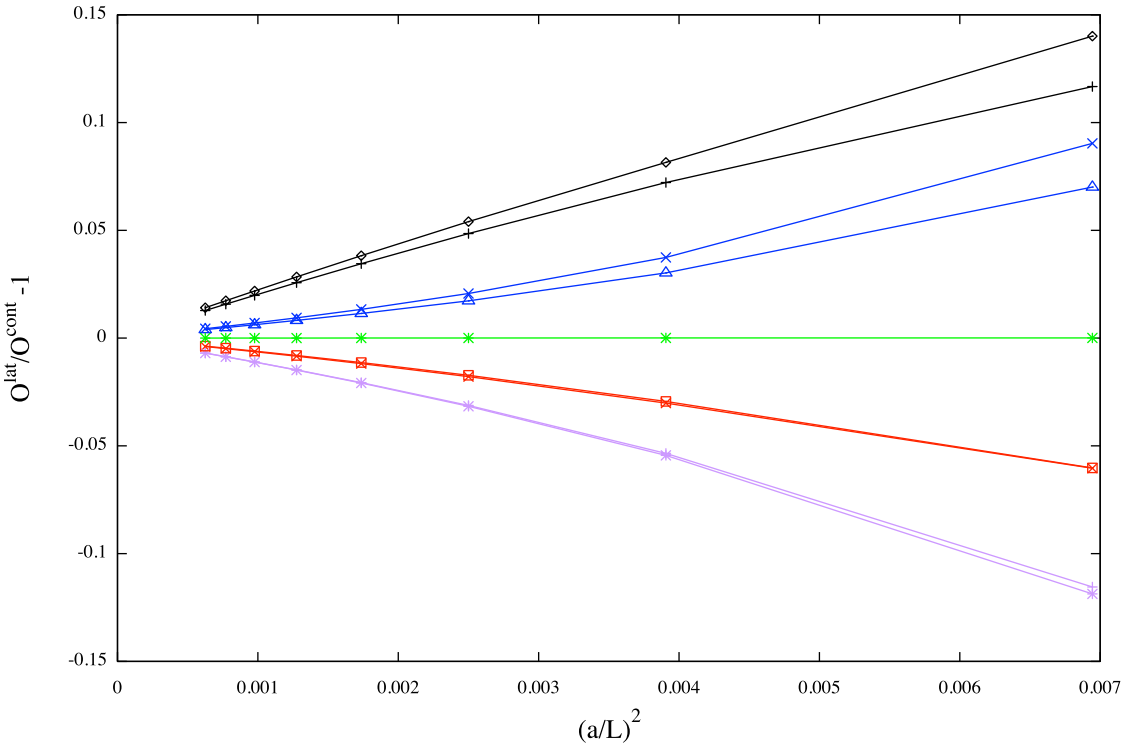

Figure 5.19: LW action, W flow, CL observable of set 4 (see Sec. A3.4), at $O(g_0^2)$ in perturbation theory, with SF boundary conditions. The same colour represents the same observable. Two set of data points of the same colour represents both the values of $c_b = 0$ and c_b^* which does not significantly improve the observable. The green line (flat), is the definition of c_b^* which cancels the cutoff effects of the reference observable, namely $t^2\mathcal{E}_0^{mag}(c = 0.3, \frac{x_0}{T} = 0.5)$. The black and blue points refer to the electric component at $c = 0.2$ and $c = 0.3$, while the purple and red points represent the magnetic component at $c = 0.2$ and $c = 0.3$. $\frac{L}{a} = 12, 16, 20, 24, 28, 32, 36, 40$.

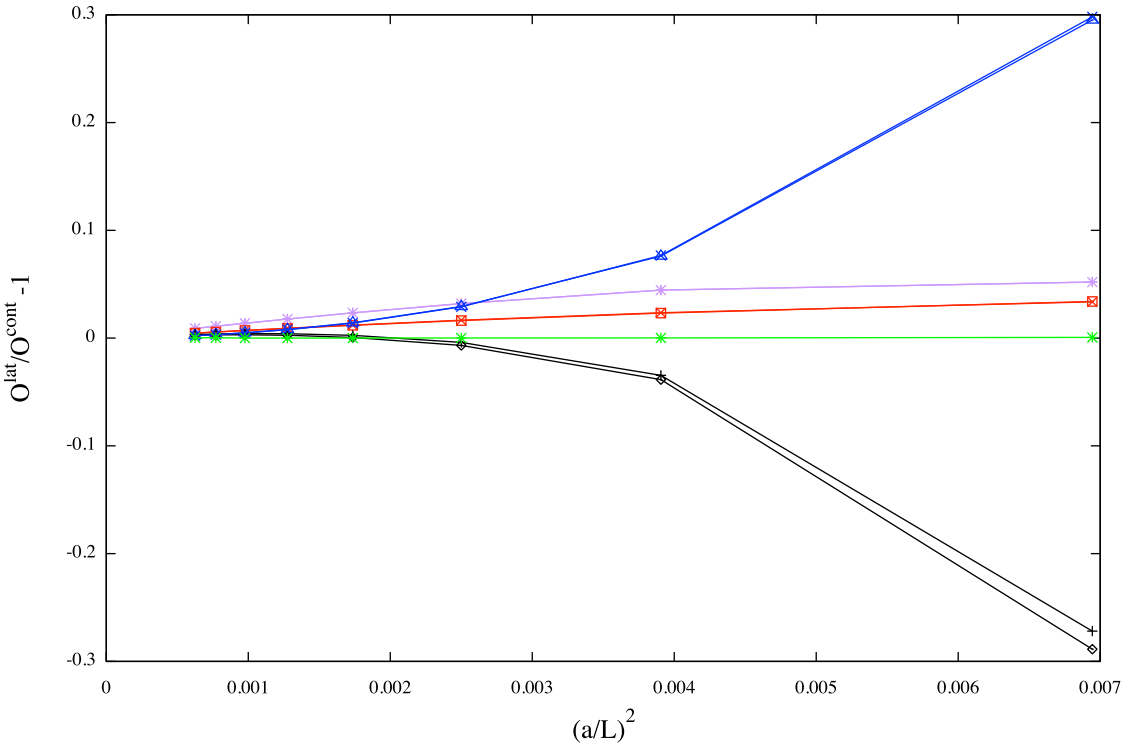

Figure 5.20: W action, Z flow, IMP observable of set 4 (see Sec. A3.4), at $O(g_0^2)$ in perturbation theory, with SF boundary conditions. The same colour represents the same observable. Two set of data points of the same colour represents both the values of $c_b = 0$ and c_b^* which does not significantly improve the observable. The green line (flat), is the definition of c_b^* which cancels the cutoff effects of the reference observable, namely $t^2\mathcal{E}_0^{mag}(c = 0.3, \frac{x_0}{T} = 0.5)$. The black and blue points refer to the electric component at $c = 0.2$ and $c = 0.3$, while the purple and red points represent the magnetic component at $c = 0.2$ and $c = 0.3$. $\frac{L}{a} = 12, 16, 20, 24, 28, 32, 36, 40$.

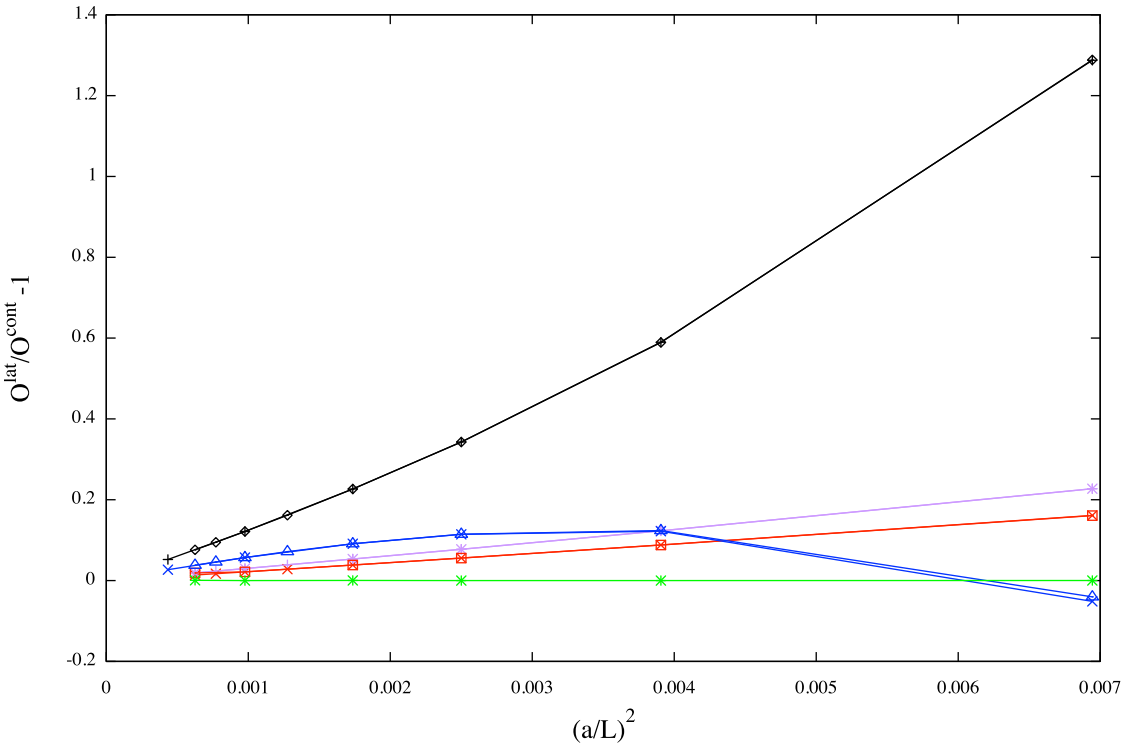

Figure 5.21: W action, Z flow, PL observable of set 4 (see Sec. A3.4), at $O(g_0^2)$ in perturbation theory, with SF boundary conditions. The same colour represents the same observable. Two set of data points of the same colour represents both the values of $c_b = 0$ and c_b^* which does not significantly improve the observable. The green line (flat), is the definition of c_b^* which cancels the cutoff effects of the reference observable, namely $t^2\mathcal{E}_0^{mag}(c = 0.3, \frac{x_0}{T} = 0.5)$. The black and blue points refer to the electric component at $c = 0.2$ and $c = 0.3$, while the purple and red points represent the magnetic component at $c = 0.2$ and $c = 0.3$. $\frac{L}{a} = 12, 16, 20, 24, 28, 32, 36, 40$.

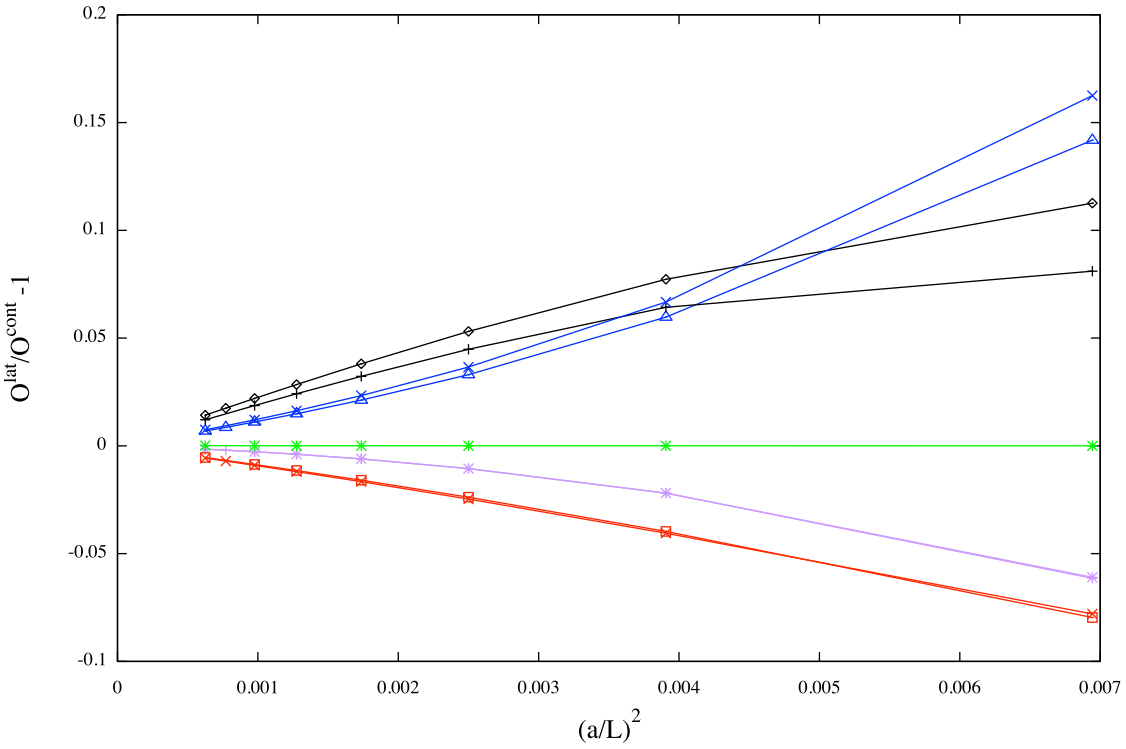

Figure 5.22: W action, Z flow, CL observable of set 4 (see Sec. A3.4), at $O(g_0^2)$ in perturbation theory, with SF boundary conditions. The same colour represents the same observable. Two set of data points of the same colour represents both the values of $c_b = 0$ and c_b^* which does not significantly improve the observable. The green line (flat), is the definition of c_b^* which cancels the cutoff effects of the reference observable, namely $t^2\mathcal{E}_0^{mag}(c = 0.3, \frac{x_0}{T} = 0.5)$. The black and blue points refer to the electric component at $c = 0.2$ and $c = 0.3$, while the purple and red points represent the magnetic component at $c = 0.2$ and $c = 0.3$. $\frac{L}{a} = 12, 16, 20, 24, 28, 32, 36, 40$.

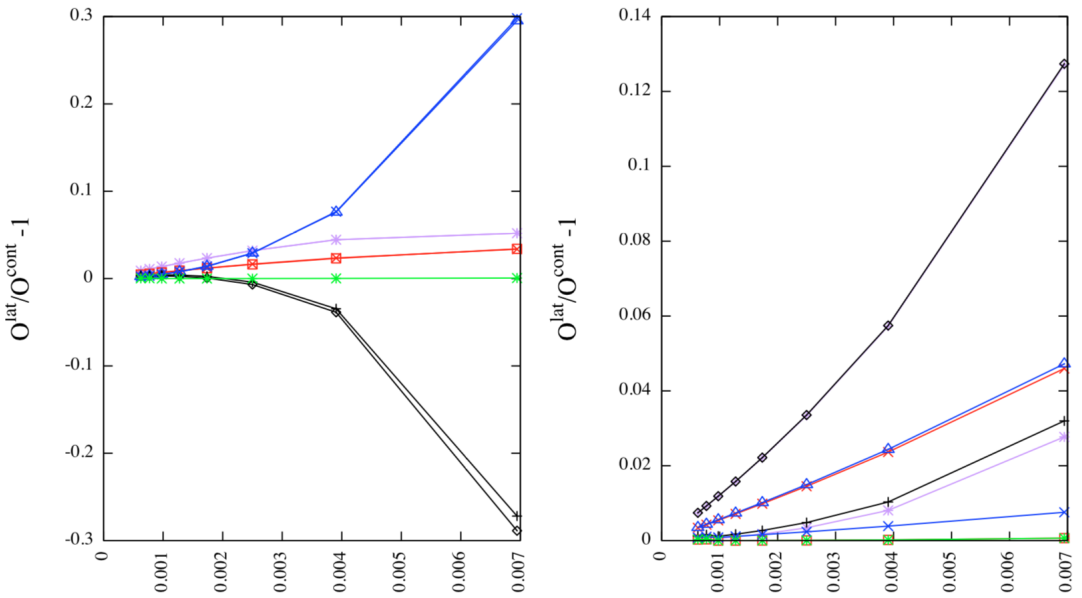

Figure 5.23: W action, Z flow, IMP observable of both second derivatives and observables themselves. We consider the electric and magnetic components at $c = 0.2, 0.3$ at $\frac{x_0}{T} = 0.5$. This result is valid at $O(g_0^2)$ in perturbation theory, with SF boundary conditions. The green line (flat), is the definition of c_b^* which cancels the cutoff effects of the reference observable, namely $t^2\mathcal{E}_0^{mag}(c = 0.3, \frac{x_0}{T} = 0.5)$. On the left side the observable lines with the same colour show a significant movement, they represent the same observable computed at $c_b = 0$ and c_b^*. On the right, the lines with the same colour do not show a large improvement, meaning that the effect of $c_b = 0$ and c_b^* is not significant. The black and blue points refer to the electric component at $c = 0.2$ and $c = 0.3$, while the purple and red points represent the magnetic component at $c = 0.2$ and $c = 0.3$. $\frac{L}{a} = 12, 16, 20, 24, 28, 32, 36, 40$.

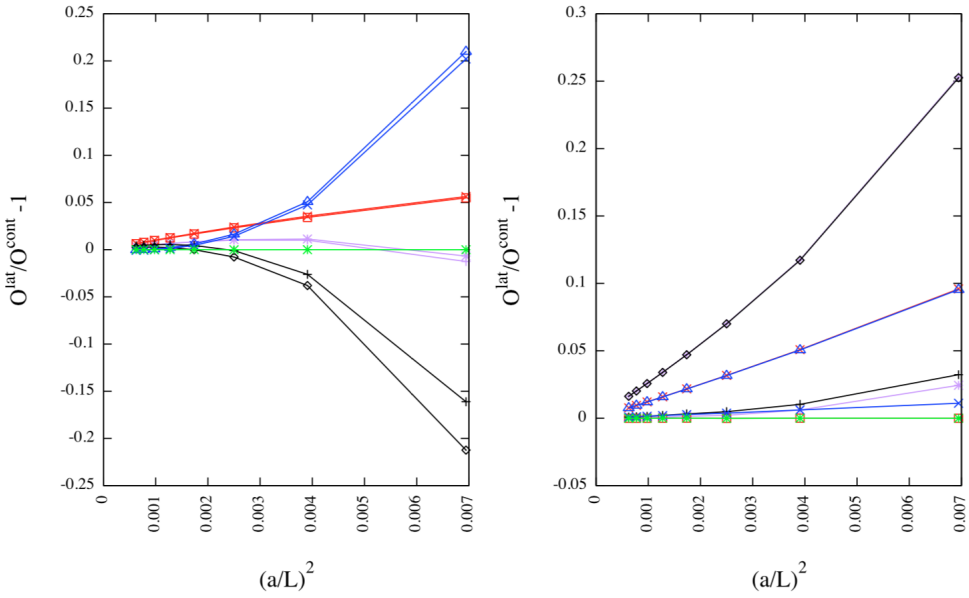

Figure 5.24: LW action, W flow, IMP observable of both second derivatives and observables themselves. We consider the electric and magnetic components at $c = 0.2, 0.3$ at $\frac{x_0}{T} = 0.5$. This result is valid at $O(g_0^2)$ in perturbation theory, with SF boundary conditions. The green line (flat), is the definition of c_b^* which cancels the cutoff effects of the reference observable, namely $t^2\mathcal{E}_0^{mag}(c = 0.3, \frac{x_0}{T} = 0.5)$. On the left side the observable lines with the same colour show a significant movement, they represent the same observable computed at $c_b = 0$ and c_b^*. On the right, the lines with the same colour do not show a large improvement, meaning that the effect of $c_b = 0$ and c_b^* is not significant. The black and blue points refer to the electric component at $c = 0.2$ and $c = 0.3$, while the purple and red points represent the magnetic component at $c = 0.2$ and $c = 0.3$. $\frac{L}{a} = 12, 16, 20, 24, 28, 32, 36, 40$.

5.4 Open-SF boundary condition

It is interesting to look at other observables. We take the first Euclidean time-derivative of the two components of the action density and we show their behaviour with SF-open boundary conditions. We remind the reader that SF-open boundary condition are defined by taking Neumann conditions at $T = 0$. It is interesting to study the differences, and such choice would be relevant for non-perturbative studies as it ensures avoiding the topological freezing problem. The profile of the magnetic and electric components of the action density at lowest order in perturbation theory, as functions of the Euclidean time are reported Figs. (3.13) and (3.14).

On the lattice we consider the improved first derivative operator, which reads:

$$D'^{(imp)} f(x_0) = -\frac{1}{12} f(x_0 + 2a) + \frac{2}{3} f(x_0 + a) - \frac{2}{3} f(x_0 - a) + \frac{1}{12} f(x_0 - 2a). \tag{5.4}$$

We compute the first improved derivative of the observables and we study the effect of c_b^* for different discretisations.

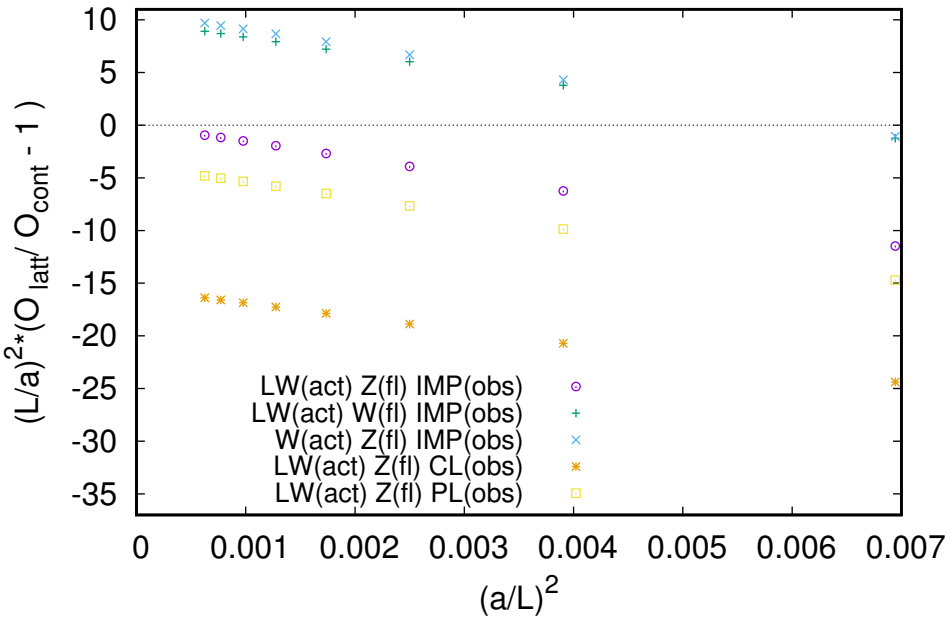

Figure 5.25: $O(a^2)$ improvement realised only for LW improved action, Zeuthen improved flow and improved observable. O_{lat} is the observable $T\partial_0 t^2 \mathcal{E}_0^{mag}$ (i.e. at $O(g_0^2)$ in perturbation theory) computed on the lattice at $c = 0.3$ and $\bar{x}_0 = 0.5$, while O_{cont} is its continuum value. The upper points correspond to either W action or W flow, while the points below are either plaquette or clover discretisations. $\frac{L}{a} = 12, 16, 20, 24, 28, 32, 36, 40$.

By making a comparison between the observable computed in SF and the first deriva-

tive computed in SF-open, we see that when all the three discretisations are improved, the coefficient of $O(a^2)$ effects is zero, as expected (for $c_b^* = 0$). By unimproving singularly each discretisation we observe that the coefficient of $O(a^2)$ effects is no longer zero.

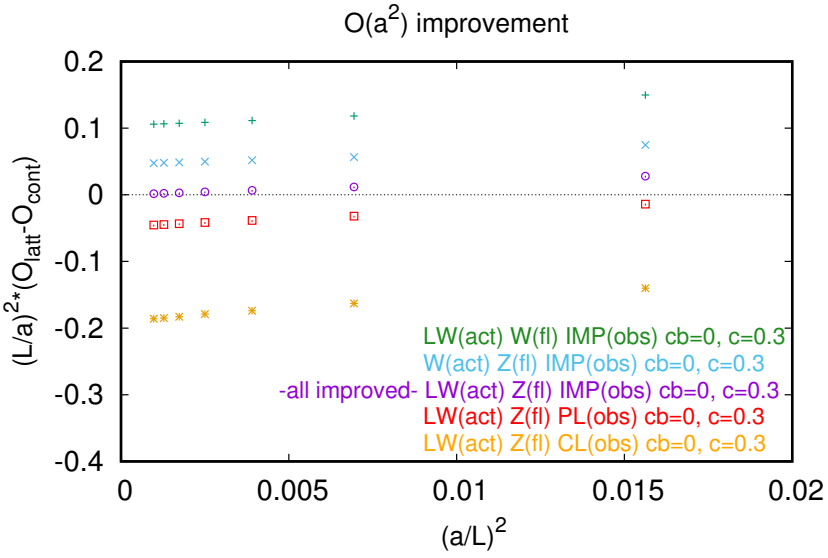

Figure 5.26: $O(a^2)$ improvement realised only for LW improved action, Zeuthen improved flow and improved observable. O_{lat} is the observable $t^2\mathcal{E}_0^{mag}$ (i.e. at $O(g_0^2)$ in perturbation theory) computed on the lattice at $c = 0.3$ and $\bar{x}_0 = 0.5$, while O_{cont} is its continuum value. The upper points correspond to either W action or W flow, while the points below are either plaquette or clover discretisations. $\frac{L}{a} = 12, 16, 20, 24, 28, 32, 36, 40$.

We study unimproved flow and both the action and the observables improved, see Fig. 5.27. We also analyse the unimproved action and both the flow and the observables improved, see Fig. 5.28. Finally, we unimprove the observables using both PL and CL discretisations with the action and the flow both improved, see Figs. 5.29 and 5.30.

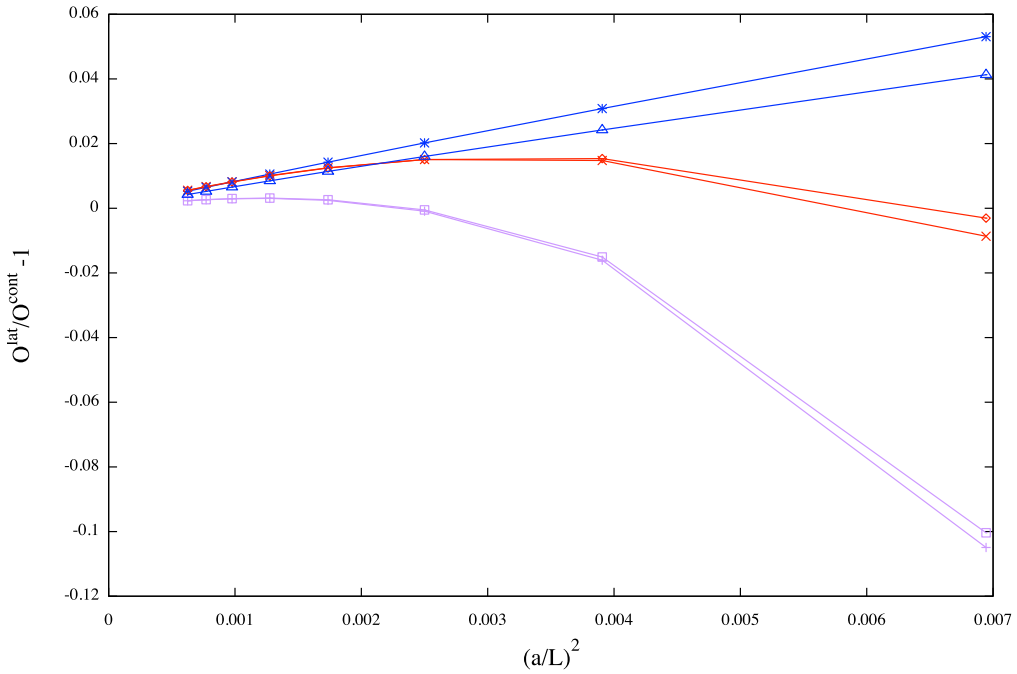

Figure 5.27: LW action, unimproved W flow, and IMP observables of the first derivative of the magnetic component at $c = 0.2, 0.3, 0.4$, at $O(g_0^2)$ in perturbation theory. The lattice sizes are $\frac{L}{a} = 12, 16, 20, 24, 28, 32, 36, 40$. The effect of c_b^* is to not reduce the cutoff effects.

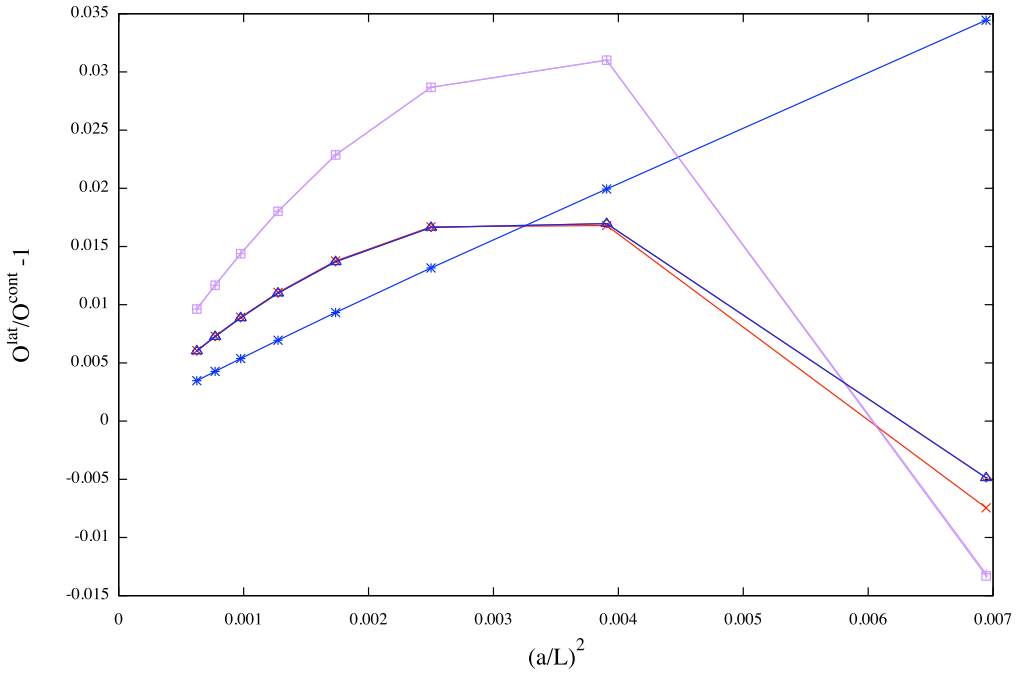

Figure 5.28: Unimproved W action, Z flow, and IMP observables of the first derivative of the magnetic component at $c = 0.2, 0.3, 0.4$, at $O(g_0^2)$ in perturbation theory. The lattice sizes are $\frac{L}{a} = 12, 16, 20, 24, 28, 32, 36, 40$. The effect of c_b^* is to not reduce the cutoff effects.

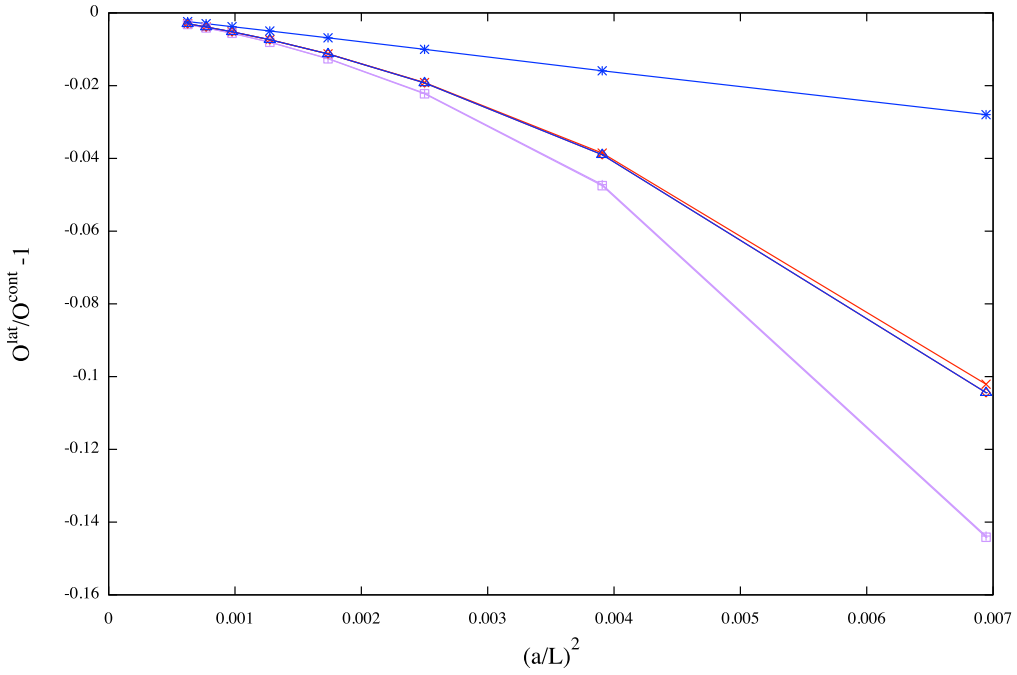

Figure 5.29: LW action, Z flow, and PL observables of the first derivative of the magnetic component at $c = 0.2, 0.3, 0.4$, at $O(g_0^2)$ in perturbation theory. The lattice sizes are $\frac{L}{a} = 12, 16, 20, 24, 28, 32, 36, 40$. The effect of c_b^* is to not reduce the cutoff effects.

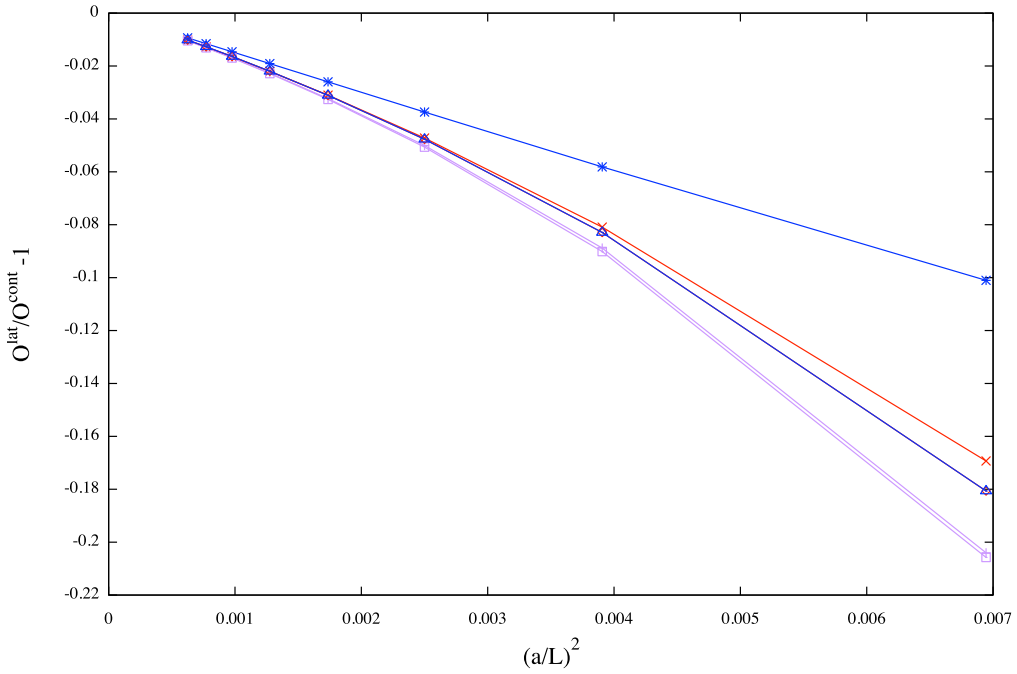

Figure 5.30: LW action, Z flow, and CL observables of the first derivative of the magnetic component at $c = 0.2, 0.3, 0.4$, at $O(g_0^2)$ in perturbation theory. The lattice sizes are $\frac{L}{a} = 12, 16, 20, 24, 28, 32, 36, 40$. The effect of c_b^* is to not reduce the cutoff effects.

5.5 Equivalence with the τ-shift in flow time

The determination of c_b^* has been shown to realise the improvement, to various extents depending on the choice of the observables. The value of c_b^* has been deduced by systematically applying the Symanzik improvement. As explained in Chap. 4, the insertion of a complete basis of counterterms leads to a rigorous proof that the improvement is regulated by the modification of the initial condition for the flow equation. On the other hand, there is an empirical way to improve the observable which has been introduced in [33], as a shift in the flow time called τ-shift. In the cited work the improvement is realised by noticing that a shift in the flow time actually reduces the effect of the discretisation. At lowest order in perturbation theory, it is straightforward to check that introducing a shift in the flow time is equivalent to tuning c_b^*, the coefficient in the initial condition for the flow equation. In fact, if we consider the gauge flowed field propagator:

$$\bar{D} = e^{(t+\tau)K_W} e^{c_b K_W} D \left(e^{(-t+\tau)K_W}\right)_T \left(e^{-c_b K_W}\right)_T , \tag{5.5}$$

where K_W is the W kernel (eq. (3.33)), as long as we use the same kernel multiplying c_b and the flow time, we obtain:

$$c_b = -\tau. \tag{5.6}$$

We have verified numerically that the equivalence holds. We also use the Zeuthen kernel:

$$\bar{D} = e^{(t+\tau)K_Z} e^{c_b K_W} D \left(e^{(-t+\tau)K_Z}\right)_T \left(e^{-c_b K_W}\right)_T , \tag{5.7}$$

in which case we see that (5.6) is not exactly satisfied. The difference is clearly visible in the points for the smaller lattice sizes plotted in Fig. 5.31 and Fig. 5.31, for the W and LW action, respectively.

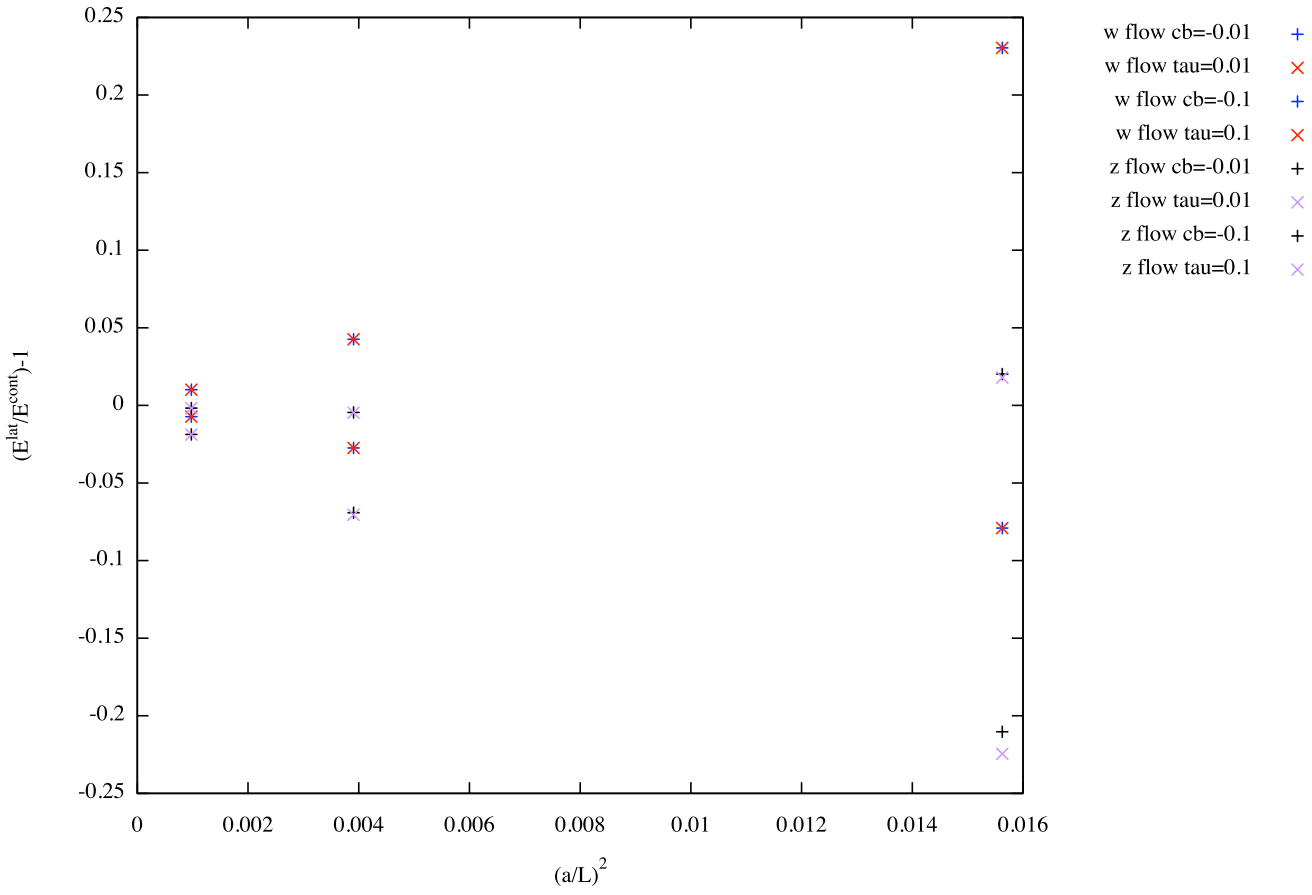

Figure 5.31: E_{lat} is the magnetic component at $c = 0.3$ and $\frac{x_0}{T} = 0.5$ for $L = 8, 16, 32$, where we use the LW action. Red and blue points coincide as they correspond to the W kernel, while purple and black points show the discrepancy due to the employment of the Zeuthen kernel.

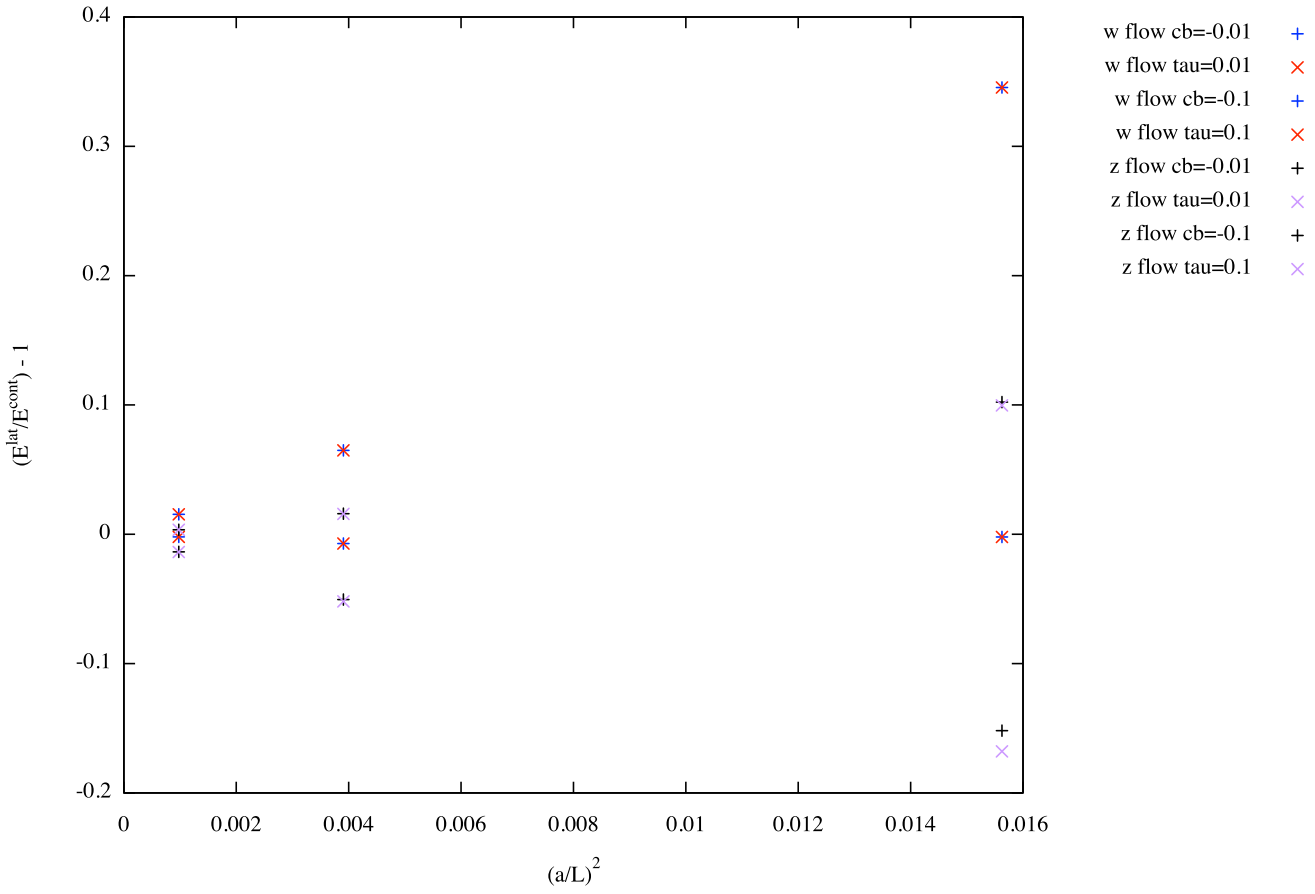

Figure 5.32: E_{lat} is the magnetic component at $c = 0.3$ and $\frac{x_0}{T} = 0.5$ for $L = 8, 16, 32$; we use the W action.

To summarise what was discussed in this chapter:

1. The numerical study at $O(g_0^2)$ in perturbation theory has been carried out. The fully realised $O(a^2)$ improvement of the magnetic component of the action density has been tested. When we say that the improvement is fully realised at $O(a^2)$ we mean that the cutoff effects coming from the action, the flow equation and the observable are eliminated. The only additional condition required is to set $c_b = 0$, this means we do not need to change the initial condition for the flow equation.

2. The improvement is fully realised also for the electric component, where we have to take into account that the temporal direction is not periodic. This implies the presence of a total derivative term in the temporal direction, that one need to subtract in order to have the improved observable.

3. In addition, we looked at the effect of the different discretisations of action, flow equation, and observable. In particular, we studied the behaviour of the observables within all the possible combination of action (W plaquette and LW), flow equation (W and Z) and observable (plaquette, clover and improved).

4. By picking the electric and magnetic components of the action density at different values of the flow and euclidean time, we defined a set of observables. In the case in which we do not have a complete set of counterterms to apply the Symanzik programme, we can only determine numerically the value of c_b^* that eliminates the cutoff effects from one particular observable of the set analysed. The coefficient c_b^* is defined with respect to a reference observable, we choose the magnetica component at $c = 0.3$ and $x_0/T = 0.5$. Then at fixed value of c_b^*, determined by the choice of the reference observable, we studied how this choice improves the other observables in the set. We saw that the improvement designed this way worked for the set made by the magnetic and electric components of the action density (set 1). In fact, by tuning c_b^* we observed a reduction of the cutoff effects in all the observables of this set.

5. We reported the result of tuning the improvement parameter c_b^* by picking different reference observable, which are given by the magnetic component for all possible combinations of the different choices we for the action (W plaquette and LW), the flow equation (W and Z) and the observable (plaquette, clover and improved).

6. We enlarged the set of observables to study the effect of using c_b^*. In order to take qualitatively different observables, we considered the Euclidean time-second derivatives in euclidean time of the magnetic and electric components of the action

density with SF boundary conditions. The result is that the choice of c_b^* does not work in improving the observables in this different set.

7. In addition, we considered the first Euclidean time-derivative of the magnetic component with SF-open boundary conditions. We observed that the improvement designed to be working by tuning c_b^* when there is not a complete basis of counterterms, does not work for this different set either.

8. We showed that the tuning of the c_b coefficient, which has a solid theoretical explanation based on the Symanzik effective theory, is equivalent to the phenomenological improvement which is the τ-shift. The latter consists in shifting the flow time by a quantity τ. At $O(g_0^2)$ in perturbation theory, it is trivial to show the equivalence.

6 Conclusions and Future Directions

This thesis began by explaining why lattice quantum chromodynamics is necessary to move forward in the quest to understand the phenomena described in terms of their fundamental degrees of freedom. The Standard Model of particle physics is the best description we have achieved in this direction, yet such a description requires both experimental and theoretical studies in order to be extended. Precision tests of the Standard Model require control of QCD effects, often at the percent level. This relies on input from lattice QCD; and it is therefore crucial to control systematic effects in lattice QCD caused by finite volume, renormalisation and finite lattice spacing effects in order to make progress in this field.

The gradient flow is a new promising tool which enables the definition of many gauge invariant, precisely measurable (in numerical simulations) flow observables. The relevant advantage is that such observables have the special property of being finite at positive flow time. This means that one can define composite operators which are renormalised after the standard renormalisation of fields and parameters. It has been established at all orders in perturbation theory that additional renormalisation, typically required for composite operators, is not needed. There are interesting applications, the most successful being the scale setting and the computation of the gradient flow coupling. Also, other potentially interesting studies are analysed in recent works, with one example being the renormalisation of the energy momentum tensor.

However, lattice artifacts of gradient flow observables are often observed to be large, in contrast to many standard observables computed in lattice simulations. For instance, extracting finite volume energy levels to either compute hadron spectra or constrain infinite volume hadron scattering amplitudes does not incur in such difficulties. Understanding how to make the extrapolation to the continuum limit of gradient flow observables more effective is the motivation of our work.

The systematic way to realise the improvement is known as the Symanzik improvement programme. In this context, the theory close to the continuum is described by an

effective field theory, in which irrelevant operators are added to the action. For a pure gauge theory the structure of the Symanzik improved theory and all its counterterms are known to leading order in perturbation theory [3]. We study the simplest observable, i.e. the action density $E(t)$, at leading order in perturbation theory. We use the finite volume as a tool in order to obtain a set of observables such that the constant defined by the ratio between the smearing radius and the lattice size, $c = \sqrt{(8t)}/L$, is an additional parameter, which labels different observables.

We use both the so-called Schrödinger Functional and Schrödinger Functional-open boundary conditions. They have the advantage that time and spatial directions are treated differently, thus enabling colour "electric" and "magnetic" components to be distinguished. In addition, the Euclidean time profile can be used to define additional finite volume specific observables. The observables used in this work are indeed specified by the components of the action density, at different values of both the euclidean and the flow times. Also, we include the first and second derivatives of such components, which are evaluated at different values of the flow time. By taking the finite differences, we define observables which are less local. This is the reason for choosing the euclidean time in the middle of the lattice, so that we can avoid boundary effects.

Using different sets of observables we have tested that the $O(a^2)$ improvement works as expected at leading order in perturbation theory, for all observables [8].

In QCD, an $O(a^2)$ improvement of the action is not practical as there are many six-dimensional four-quark operators as possible counterterms.

In pure gauge theory, using an unimproved four dimensional action we check whether the a^2 artefacts in flow specific observables can be made universally small by using the $O(a^2)$ improved setup (except for the action) and by tuning the only free flow-specific counterterm coefficient c_b (which is equivalent to the tau-shift by A. Hasenfratz [96]). At first sight a reduction by a factor two or three, and even six in the best case is indeed possible for a considerable subset of observables. A similar reduction is observed even in cases where the flow and the observables are unimproved. If the set is enlarged to include observables relating to the Euclidean time profile there is no improvement seen, or indeed very different values of the counterterm coefficient are required to reduce the a^2 effects for those observables.

Hence we have disproved our hypothesis that there is a hierarchy of cutoff effects between flow and non-flow observables, which would allow us to universally obtain a significant reduction of cutoff effects across all observables by tuning a single flow related counterterm coefficient.

When dealing with "similar" observables (e.g. action density in finite volume at different c-values) it may still be beneficial to use the tau-shift. This requires a reference observable in the continuum limit, we stared to look at, and then tuning c_b at all lattice spacings such that the reference observable is kept at the reference continuum value. One expects "similar" observables to have significantly reduced lattice artefacts. However, without further insight our study does not allow us to recommend a general strategy.

A1 Useful definitions

A1.1 Gauge group

The Lie algebra of the group $SU(N)$ can be defined as the space of N dimensional matrices X which satisfy

$$X^\dagger = -X, \qquad \mathrm{Tr}\, X = 0 \tag{A1.1}$$

where $X^\dagger$ is the adjoint matrix and $tr\, X$ is the trace of X.
We may choose a basis T^a, $a = 1, 2, ..., N^2 - 1$ such that the trace is normalized by the relation

$$\mathrm{Tr}\,(T^a T^b) = -\frac{1}{2}\delta^{ab}. \tag{A1.2}$$

A gauge field lives in the adjoint representation of the $SU(N)$ generators, then can be written as

$$A_\mu(x) = A^a_\mu(x)\, T^a \tag{A1.3}$$

and the field tensor $F_{\mu\nu}(x)$ is defined by the commutator of the covariant derivative

$$F_{\mu\nu}(x) = \partial_\mu A_\nu(x) - \partial_\nu A_\mu(x) + [A_\mu(x), A_\nu(x)]. \tag{A1.4}$$

A1.2 Fourier transform in the continuum

The Fourier transform of a generic function $f(x)$ is defined by

$$f(x) = \int \frac{d^D p}{(2\pi)^D}\ \tilde{f}(p)\ e^{ipx}, \tag{A1.5}$$

and the antitransform

$$\tilde{f}(p) = \int d^D x\ e^{-ipx} f(x) \tag{A1.6}$$

such that

$$\begin{aligned} f(x) &= \textstyle\int \frac{d^D p}{(2\pi)^D}\ e^{ipx}\ \int d^D x' e^{-ipx'} f(x') \\ &= \textstyle\int \frac{d^D p}{(2\pi)^D}\ \int d^D x' e^{-ip(x-x')} f(x') = \int d^D x'\ \delta^{(D)}(x-x') f(x'). \end{aligned} \tag{A1.7}$$

Then for a gauge field it is

$$\tilde{A}_\mu(p) = \int d^D x\ e^{-ipx} A_\mu(x) \tag{A1.8}$$

$$A_\mu(x) = \int \frac{d^D p}{(2\pi)^D}\ e^{ipx} \tilde{A}_\mu(p), \tag{A1.9}$$

and we will often use the short-hand $\int_p = \int \frac{d^D p}{(2\pi)^D}$.

A1.3 Fourier transform on an infinite lattice

On a lattice with lattice spacing a the x variable assumes discrete values $x = n\,a$ ($n \in \mathbb{Z}$) and the conjugate variable p is limited $p \in [-\frac{\pi}{a}, \frac{\pi}{a}]$ at the first Brillouin zone. Then the Fourier transform is defined by

- for a scalar field

$$\tilde{f}(p) = a^4 \sum_x e^{-ipx} f(x), \tag{A1.10}$$

$$f(x) = \int_{-\frac{\pi}{a}}^{\frac{\pi}{a}} \frac{d^4 p}{(2\pi)^4} e^{ipx} \tilde{f}(p); \tag{A1.11}$$

- for a vector field we have

$$\tilde{f}_\mu(p) = a^4 \sum_x e^{-ipx} e^{-ip_\mu \frac{a}{2}} f_\mu(x), \tag{A1.12}$$

$$f_\mu(x) = \int_{-\frac{\pi}{a}}^{\frac{\pi}{a}} \frac{d^4p}{(2\pi)^4} e^{ipx} e^{ip_\mu \frac{a}{2}} \tilde{f}_\mu(p). \tag{A1.13}$$

A1.4 Fourier transform on an finite lattice, in 1 dimension

On a finite lattice of size L we define the Fourier transform as:

$$\tilde{f}(p) = a \sum_x e^{-ipx} f(x), \tag{A1.14}$$

where $\frac{x}{a} = 0, ..., \frac{L}{a} - 1$

$$f(x) = \frac{1}{L} \sum_p e^{ipx} \tilde{f}(p); \tag{A1.15}$$

where $p = \frac{2\pi n}{L}$ and $n = 0, ..., \frac{L}{a} - 1$.

$$\begin{gathered} f(x) = \frac{a}{L} \sum_p e^{ipx} \sum_{x'} e^{-ipx'} f(x') = \\ = \frac{a}{L} \sum_{x'} \sum_p e^{ip(x-x')} f(x'), \end{gathered} \tag{A1.16}$$

we define the Kronecker delta as

$$\delta_{\frac{x}{a}, \frac{x'}{a}} = \frac{a}{L} \sum_{n=0}^{\frac{L}{a}-1} e^{ip(x-x')}. \tag{A1.17}$$

for which if $x - x' = 0$ we get $\frac{L}{a}$ while if $x - x' \neq 0$ we get zero.
If we consider the time interval with $2T$ periodicity, then $\frac{x_0}{a} = -\frac{T}{a}, ..., \frac{T}{a} - 1$ and if we can use the parity in the argument of the sum we can take twice the sum with the interval to $\frac{x_0}{a} = 0, ..., \frac{T}{a} - 1$ where the zero term has weight $\frac{1}{2}$.

A1.5 Fourier transform on an finite lattice, in 4 dimensions

On a hypercubic lattice of volume L^4 we define the Fourier transform as:

$$\tilde{f}_\mu(p) = a^4 \sum_{x_\mu} e^{-ipx} e^{-ip_\mu \frac{a}{2}} f_\mu(x), \tag{A1.18}$$

where $\frac{x_\mu}{a} = 0, ..., \frac{L}{a} - 1$.

$$f_\mu(x) = \frac{1}{L^4} \sum_{p_\mu} e^{ipx} e^{ip_\mu \frac{a}{2}} \tilde{f}_\mu(p); \tag{A1.19}$$

where we are assuming periodicity in the 4 directions which determines the values of momenta $p_\mu = \frac{2\pi n_\mu}{L}$ and $n_\mu = 0, ..., \frac{L}{a} - 1$. The Kronecker delta is

$$\delta^{(4)}_{\frac{x}{a}, \frac{x'}{a}} = \frac{a^4}{L^4} \sum_{n_\mu} e^{ip(x-x')} \tag{A1.20}$$

and the variables x and p are four-vectors.

A1.6 Derivative on the lattice

Forward and backward lattice derivatives act on a function as:

$$\partial_\mu f(x) = \frac{1}{a}[f(x + a\hat{\mu}) - f(x)] \tag{A1.21}$$

$$\partial^*_\mu f(x) = \frac{1}{a}[f(x) - f(x - a\hat{\mu})] \tag{A1.22}$$

where $\hat{\mu}$ denotes the unit vector in the μ direction,

$$\tilde{\partial}_\mu f(x) = \frac{1}{2} \left(\partial_\mu + \partial^*_\mu\right) f(x) \tag{A1.23}$$

$$\tilde{\partial}_\mu f(x) = \frac{1}{2a}[f(x + a\hat{\mu}) - f(x - a\hat{\mu})] \tag{A1.24}$$

We define the lattice Laplacian in 4 space-time dimensions

$$\Box = \sum_\mu \partial_\mu \partial^*_\mu \tag{A1.25}$$

which acts on a function as

$$\Box f(x) = \frac{1}{a^2}\sum_{\mu}\left[f(x+a\hat{\mu}) + f(x-a\hat{\mu}) - 2f(x)\right]. \tag{A1.26}$$

Integrating by parts on the lattice we have

$$\sum_{x}(\partial_\mu f(x))g(x) = -\sum_{x} f(x)\partial^*_\mu g(x). \tag{A1.27}$$

It is useful to introduce the following operators as well

$$\begin{aligned} t_\mu f(x) &= f(x+a\hat{\mu}) \\ t^*_\mu f(x) &= f(x-a\hat{\mu}), \end{aligned} \tag{A1.28}$$

which are related to the derivative by

$$\begin{aligned} a\partial_\mu &= t_\mu - 1 \\ a\partial^*_\mu &= 1 - t^*_\mu. \end{aligned} \tag{A1.29}$$

We can do something like an integration by parts

$$(t_\nu A_\mu(x), A_\mu(x)) = \sum_{x} A_\mu(x+a\hat{\nu})A_\mu = \sum_{x'} A_\mu(x')A_\mu(x-a\hat{\nu}) = (A_\mu(x), t^*_\nu A_\mu(x)) \tag{A1.30}$$

where we used $x' = x + a\hat{\nu}$. We see that the exponential is an eigenvector of this operator

$$t_\mu e^{ipx} = e^{ip(x+a\hat{\mu})} = e^{iap_\mu}e^{ipx} \tag{A1.31}$$

with eigenvalue e^{iap_μ}.
Furthermore, we can show that

$$t^*_\mu t_\mu = 1 \tag{A1.32}$$

because

$$t^*_\mu t_\mu f(x) = t^*_\mu f(x+a\hat{\mu}) = f(x); \tag{A1.33}$$

and

$$\partial_\nu + \partial_\nu^* = -a\partial_\nu^*\partial_\nu \tag{A1.34}$$

because

$$\left(\partial_\mu^* - \partial_\mu\right) f(x) = \partial_\mu^* f(x) - \partial_\mu f(x) = \tfrac{1}{a}\left[f(x) - f(x - a\hat{\mu})\right] - \tfrac{1}{a}\left[f(x + a\hat{\mu}) - f(x)\right]$$

$$= \tfrac{1}{a}\left[2f(x) - f(x - a\hat{\mu}) - f(x + a\hat{\mu})\right] \tag{A1.35}$$

and

$$\partial_\mu^*\partial_\mu f(x) = \partial_\mu^*\left[f(x + a\hat{\mu}) - f(x)\right]$$

$$= \tfrac{1}{a}\left[f(x + a\hat{\mu}) - f(x) - (f(x) - f(x - a\hat{\mu}))\right] = \tfrac{1}{a}\left[-2f(x) + f(x + a\hat{\mu}) + f(x - a\hat{\mu})\right]. \tag{A1.36}$$

A1.7 Momenta on the lattice

$$\hat{p}_\mu = \frac{2}{a}\,\sin\,\frac{a}{2}p_\mu \tag{A1.37}$$

$$\tilde{p}_\mu = \frac{1}{a}\,\sin\,ap_\mu \tag{A1.38}$$

A2 Dirichelet and Neumann boundary conditions

A2.1 Dirichelet/ Neumann boundary conditions

We defined in Sec. 3.6 the projector $P_{\pm} = (1 \pm R)$, where the reflection is defined by:

$$R: \quad \varphi(x_0) \to \varphi(-x_0) \tag{A2.1}$$

in order to split the function $\varphi(x)$ in even and odd components:

$$\varphi_(x) = \varphi_+(x) + \varphi_-(x). \tag{A2.2}$$

Dirichlet and Neumann conditions at $x_0 = 0$ are satisfied for the odd and even parts of φ, respectively:

$$\varphi_-(0) = 0 \tag{A2.3}$$

$$\varphi'_+(0) = 0 \tag{A2.4}$$

By imposing $2T$-periodicity we ensure the same boundary conditions at $x_0 = T$ are satisfied by $\varphi_-(x_0)$:

$$\varphi_-(T) = -\varphi_-(-T) = -\varphi_-(-T + 2T) = -\varphi_-(T) \tag{A2.5}$$

$$\varphi_-(T) = 0. \tag{A2.6}$$

By imposing $2T$-antiperiodic boundary conditions imply Neumann conditions at $x_0 = T$ for $\varphi_-(x_0)$. We can use that the derivative of a $2T$ (anti-)periodic function is $2T$ (anti-)periodic:

$$\varphi(x_0 + 2T) = \pm\varphi(x_0), \tag{A2.7}$$

$$\varphi'(x_0 + 2T) = \pm\varphi'(x_0), \tag{A2.8}$$

$$\varphi_-(T - x_0) = -\varphi_-(-(T - x_0)) = -\varphi_-(x_0 - T) \tag{A2.9}$$

$$\varphi'_-(T - x_0)(-1) = -\varphi'_-(x_0 - T) \tag{A2.10}$$

$$-\varphi'_-(T) = -\varphi'_-(-T) \tag{A2.11}$$

using anti-periodicity

$$-\varphi'_-(T) = \varphi'_-(-T + 2T) = \varphi'_-(T) \tag{A2.12}$$

which is

$$\varphi'_-(T) = 0 \tag{A2.13}$$

Now we show that φ'_+ satisfies Neumann boundary conditions also in T when the function is $2T$-periodic:

$$\varphi'_+(T) = -\varphi'_+(-T) \tag{A2.14}$$

using periodicity:

$$-\varphi'_+(-T + 2T) = -\varphi'_+(T) \tag{A2.15}$$

which is:

$$\varphi'_+(T) = 0, \tag{A2.16}$$

$$\varphi_+(T) = \varphi_+(-T), \tag{A2.17}$$

and using anti-periodicity

$$\varphi_+(T) = -\varphi_+(-T + 2T) = -\varphi_+(T), \tag{A2.18}$$

which is

$$\varphi_+(T) = 0. \tag{A2.19}$$

The result is summarised in Tab.A2.1 and by applying them to the components of the

Table A2.1: Dirichlet (D) and Neumann (N) conditions at $x_0 = 0$ are satisfied by the odd and even parts. $2T$-periodicity implies that the same boundary conditions are satisfied at $x_0 = T$, while $2T$-antiperiodicity implies that the boundary conditions are inverted at $x_0 = T$.

		$2T-$PER	
D	$\varphi_-(0) = 0$	D	$\varphi_-(T) = 0$
N	$\varphi'_+(0) = 0$	N	$\varphi'_+(T) = 0$
		$2T-$ANTI-PER	
D	$\varphi_-(0) = 0$	N	$\varphi'_-(T) = 0$
N	$\varphi'_+(0) = 0$	D	$\varphi_+(T) = 0$

gauge field we obtain SF, SF-open boundary conditions used in this work.

A3 Definition of the sets of observables

A3.1 Set 1

The list of observables which defines set 1 contains the colour magnetic field components, computed at $c = 0.2, 0.3, 0.4$ and each at $x_0/T = 0.5, 0.25$ with SF boundary conditions, six observables in total:

1. $\mathcal{E}_0^{mag}(c = 0.2, \frac{x_0}{T} = 0.5)$
2. $\mathcal{E}_0^{mag}(c = 0.3, \frac{x_0}{T} = 0.5)$
3. $\mathcal{E}_0^{mag}(c = 0.4, \frac{x_0}{T} = 0.5)$
4. $\mathcal{E}_0^{mag}(c = 0.2, \frac{x_0}{T} = 0.25)$
5. $\mathcal{E}_0^{mag}(c = 0.3, \frac{x_0}{T} = 0.25)$
6. $\mathcal{E}_0^{mag}(c = 0.4, \frac{x_0}{T} = 0.25)$.

A3.2 Set 2

The list of observables which defines set 2 contains the colour electric field components, computed at $c = 0.2, 0.3, 0.4$ and each at $x_0/T = 0.5, 0.25$ with SF boundary conditions, six observables in total:

1. $\mathcal{E}_0^{el}(c = 0.2, \frac{x_0}{T} = 0.5)$
2. $\mathcal{E}_0^{el}(c = 0.3, \frac{x_0}{T} = 0.5)$
3. $\mathcal{E}_0^{el}(c = 0.4, \frac{x_0}{T} = 0.5)$

4. $\mathcal{E}_0^{el}(c = 0.2, \frac{x_0}{T} = 0.25)$
5. $\mathcal{E}_0^{el}(c = 0.3, \frac{x_0}{T} = 0.25)$
6. $\mathcal{E}_0^{el}(c = 0.4, \frac{x_0}{T} = 0.25)$.

A3.3 Set 3

The list of observables which defines set 3 is the union of the elements in set 1 and set 2 set3 = {set1 $\bigcup$ set2}, in total there are 12 observables:

1. $\mathcal{E}_0^{mag}(c = 0.2, \frac{x_0}{T} = 0.5)$
2. $\mathcal{E}_0^{mag}(c = 0.3, \frac{x_0}{T} = 0.5)$
3. $\mathcal{E}_0^{mag}(c = 0.4, \frac{x_0}{T} = 0.5)$
4. $\mathcal{E}_0^{mag}(c = 0.2, \frac{x_0}{T} = 0.25)$
5. $\mathcal{E}_0^{mag}(c = 0.3, \frac{x_0}{T} = 0.25)$
6. $\mathcal{E}_0^{mag}(c = 0.4, \frac{x_0}{T} = 0.25)$
7. $\mathcal{E}_0^{el}(c = 0.2, \frac{x_0}{T} = 0.5)$
8. $\mathcal{E}_0^{el}(c = 0.3, \frac{x_0}{T} = 0.5)$
9. $\mathcal{E}_0^{el}(c = 0.4, \frac{x_0}{T} = 0.5)$
10. $\mathcal{E}_0^{el}(c = 0.2, \frac{x_0}{T} = 0.25)$
11. $\mathcal{E}_0^{el}(c = 0.3, \frac{x_0}{T} = 0.25)$
12. $\mathcal{E}_0^{el}(c = 0.4, \frac{x_0}{T} = 0.25)$.

A3.4 Set 4

The list of observables which defines set 4 is given by the second derivatives with SF boundary conditions:

1. $T^2\partial_0^2 t^2 \mathcal{E}_0^{mag}(c = 0.2, \frac{x_0}{T} = 0.5)$
2. $T^2\partial_0^2 t^2 \mathcal{E}_0^{mag}(c = 0.3, \frac{x_0}{T} = 0.5)$

3. $T^2\partial_0^2 t^2 \mathcal{E}_0^{el}(c = 0.2, \frac{x_0}{T} = 0.5)$

4. $T^2\partial_0^2 t^2 \mathcal{E}_0^{el}(c = 0.3, \frac{x_0}{T} = 0.5)$

A3.5 Set 5

The list of observables which defines set 5 is given by the first derivatives with SF-open boundary conditions:

1. $T\partial_0 t^2 \mathcal{E}_0^{mag}(c = 0.2, \frac{x_0}{T} = 0.5)$

2. $T\partial_0 t^2 \mathcal{E}_0^{mag}(c = 0.3, \frac{x_0}{T} = 0.5)$

3. $T\partial_0 t^2 \mathcal{E}_0^{el}(c = 0.2, \frac{x_0}{T} = 0.5)$

4. $T\partial_0 t^2 \mathcal{E}_0^{el}(c = 0.3, \frac{x_0}{T} = 0.5)$

Bibliography

[1] Review of particle physics. *Phys. Rev. D*, 98:030001, Aug 2018.

[2] Mattia Bruno et al. Simulation of QCD with $N_f = 2 + 1$ flavors of non-perturbatively improved Wilson fermions. *JHEP*, 02:043, 2015.

[3] A. Ramos and S. Sint. Symanzik improvement of the gradient flow in lattice gauge theories. *Eur. Phys. J.*, C76(1):15, 2016.

[4] Martin Lüscher. Properties and uses of the Wilson flow in lattice QCD. *JHEP*, 08:071, 2010. [Erratum: JHEP03,092(2014)].

[5] Rainer Sommer. Scale setting in lattice QCD. *PoS*, LATTICE2013:015, 2014.

[6] Martin Lüscher. Future applications of the Yang-Mills gradient flow in lattice QCD. *PoS*, LATTICE2013:016, 2014.

[7] Mattia Dalla Brida, Patrick Fritzsch, Tomasz Korzec, Alberto Ramos, Stefan Sint, and Rainer Sommer. Slow running of the Gradient Flow coupling from 200 MeV to 4 GeV in $N_f = 3$ QCD. *Phys. Rev.*, D95(1):014507, 2017.

[8] Argia Rubeo and Stefan Sint. Perturbative $O(a^2)$ effects in gradient flow couplings with SF and SF-open boundary conditions. *PoS*, LATTICE2016:388, 2016.

[9] Gilberto Colangelo et al. Review of lattice results concerning low energy particle physics. *Eur. Phys. J.*, C71:1695, 2011.

[10] G. Martinelli, C. Pittori, Christopher T. Sachrajda, M. Testa, and A. Vladikas. A General method for nonperturbative renormalization of lattice operators. *Nucl. Phys.*, B445:81–108, 1995.

[11] Mattia Dalla Brida, Tomasz Korzec, Stefan Sint, and Pol Vilaseca. High precision renormalization of the flavour non-singlet Noether currents in lattice QCD with Wilson quarks. 2018.

[12] R. Sommer. Nonperturbative renormalization of QCD. *Lect. Notes Phys.*, 512:65–113, 1998.

[13] David J. Gross and Frank Wilczek. Ultraviolet behavior of non-abelian gauge theories. *Phys. Rev. Lett.*, 30:1343–1346, Jun 1973.

[14] H. David Politzer. Reliable perturbative results for strong interactions? *Phys. Rev. Lett.*, 30:1346–1349, Jun 1973.

[15] Kenneth G. Wilson. Confinement of quarks. *Phys. Rev. D*, 10:2445–2459, Oct 1974.

[16] Karl Jansen, Chuan Liu, Martin Luscher, Hubert Simma, Stefan Sint, Rainer Sommer, Peter Weisz, and Ulli Wolff. Nonperturbative renormalization of lattice QCD at all scales. *Phys. Lett.*, B372:275–282, 1996.

[17] Michele Della Morte, Roland Hoffmann, Francesco Knechtli, Juri Rolf, Rainer Sommer, Ines Wetzorke, and Ulli Wolff. Non-perturbative quark mass renormalization in two-flavor QCD. *Nucl. Phys.*, B729:117–134, 2005.

[18] S. Aoki et al. Non-perturbative renormalization of quark mass in $N_f = 2 + 1$ QCD with the Schroedinger functional scheme. *JHEP*, 08:101, 2010.

[19] Michele Della Morte, Roberto Frezzotti, Jochen Heitger, Juri Rolf, Rainer Sommer, and Ulli Wolff. Computation of the strong coupling in QCD with two dynamical flavors. *Nucl. Phys.*, B713:378–406, 2005.

[20] S. Aoki et al. Precise determination of the strong coupling constant in N(f) = 2+1 lattice QCD with the Schrodinger functional scheme. *JHEP*, 10:053, 2009.

[21] Fatih Tekin, Rainer Sommer, and Ulli Wolff. The Running coupling of QCD with four flavors. *Nucl. Phys.*, B840:114–128, 2010.

[22] M. Guagnelli, J. Heitger, C. Pena, S. Sint, and A. Vladikas. Non-perturbative renormalization of left-left four-fermion operators in quenched lattice QCD. *JHEP*, 03:088, 2006.

[23] M. Creutz. Monte Carlo Study of Quantized SU(2) Gauge Theory. *Phys. Rev.*, D21:2308–2315, 1980.

[24] Martin Luscher, Peter Weisz, and Ulli Wolff. A Numerical method to compute the running coupling in asymptotically free theories. *Nucl. Phys.*, B359:221–243, 1991.

[25] Martin Luscher. Advanced lattice QCD. In *Probing the standard model of particle interactions. Proceedings, Summer School in Theoretical Physics, NATO Advanced Study Institute, 68th session, Les Houches, France, July 28-September 5, 1997. Pt. 1, 2*, pages 229–280, 1998.

[26] R. Narayanan and H. Neuberger. Infinite N phase transitions in continuum Wilson loop operators. *JHEP*, 03:064, 2006.

[27] Martin Luscher and Peter Weisz. Perturbative analysis of the gradient flow in non-abelian gauge theories. *JHEP*, 02:051, 2011.

[28] Martin Luscher. Chiral symmetry and the Yang–Mills gradient flow. *JHEP*, 04:123, 2013.

[29] Szabolcs Borsanyi et al. High-precision scale setting in lattice QCD. *JHEP*, 09:010, 2012.

[30] Stefan Sint and Alberto Ramos. On O(a^2) effects in gradient flow observables. *PoS*, LATTICE2014:329, 2015.

[31] K. Symanzik. Continuum limit and improved action in lattice theories : (i). principles and [phi]4 theory. *Nuclear Physics B*, 226(1):187 – 204, 1983.

[32] M. Luscher and P. Weisz. On-Shell Improved Lattice Gauge Theories. *Commun. Math. Phys.*, 97:59, 1985. [Erratum: Commun. Math. Phys.98,433(1985)].

[33] Anna Hasenfratz. Improved gradient flow for step scaling function and scale setting. *PoS*, LATTICE2014:257, 2015.

[34] L. D. Faddeev and V. N. Popov. Feynman Diagrams for the Yang-Mills Field. *Phys. Lett.*, B25:29–30, 1967. [,325(1967)].

[35] Kenneth G. Wilson. Confinement of Quarks. *Phys. Rev.*, D10:2445–2459, 1974. [,319(1974)].

[36] Christof Gattringer and Christian B. Lang. Quantum chromodynamics on the lattice. *Lect. Notes Phys.*, 788:1–343, 2010.

[37] I. Montvay and G. Munster. *Quantum fields on a lattice*. Cambridge Monographs on Mathematical Physics. Cambridge University Press, 1997.

[38] H. J. Rothe. Lattice gauge theories: An Introduction. *World Sci. Lect. Notes Phys.*, 43:1–381, 1992. [World Sci. Lect. Notes Phys.82,1(2012)].

[39] Y. Iwasaki. Renormalization Group Analysis of Lattice Theories and Improved Lattice Action. II. Four-dimensional non-Abelian SU(N) gauge model. 1983.

[40] Taizo Muta. *Foundations of Quantum Chromodynamics: An Introduction to Perturbative Methods in Gauge Theories, (3rd ed.)*, volume 78 of *World scientific Lecture Notes in Physics*. World Scientific, Hackensack, N.J., 2010.

[41] K. Symanzik. Schrodinger Representation and Casimir Effect in Renormalizable Quantum Field Theory. *Nucl. Phys.*, B190:1–44, 1981.

[42] D. Friedan. A proof of the nielsen-ninomiya theorem. *Communications in Mathematical Physics*, 85(4):481–490, Dec 1982.

[43] Martin Luscher. Exact chiral symmetry on the lattice and the Ginsparg-Wilson relation. *Phys. Lett.*, B428:342–345, 1998.

[44] Martin Luscher, Stefan Sint, Rainer Sommer, and Peter Weisz. Chiral symmetry and O(a) improvement in lattice QCD. *Nucl. Phys.*, B478:365–400, 1996.

[45] B. Sheikholeslami and R. Wohlert. Improved Continuum Limit Lattice Action for QCD with Wilson Fermions. *Nucl. Phys.*, B259:572, 1985.

[46] John B. Kogut and Leonard Susskind. Hamiltonian Formulation of Wilson's Lattice Gauge Theories. *Phys. Rev.*, D11:395–408, 1975.

[47] David B. Kaplan. A Method for simulating chiral fermions on the lattice. *Phys. Lett.*, B288:342–347, 1992.

[48] Colin Morningstar. The Monte Carlo method in quantum field theory. In *21st Annual Hampton University Graduate Studies Program (HUGS 2006) Newport News, Virginia, June 5-23, 2006*, 2007.

[49] I. Montvay. Monte Carlo Methods in Quantum Field Theory. In *Taller de Altas Energias: Spring School on High Energy Physics (TAE 2007) Jaca, Spain, June 6-18, 2007*, 2007.

[50] Kurt Langfeld. Computational methods in quantum field theory. In *19th Heidelberg Physics Graduate Days Heidelberg, Germany, October 8-12, 2007*, 2007.

[51] A. D. Kennedy. Algorithms for dynamical fermions. 2006.

[52] Nicola Cabibbo and Enzo Marinari. A new method for updating su(n) matrices in computer simulations of gauge theories. *Physics Letters B*, 119(4):387 – 390, 1982.

[53] A.D. Kennedy and B.J. Pendleton. Improved heatbath method for monte carlo calculations in lattice gauge theories. *Physics Letters B*, 156(5):393 – 399, 1985.

[54] R. Petronzio and E. Vicari. An Overrelaxed Monte Carlo algorithm for SU(3) lattice gauge theories. *Phys. Lett.*, B248:159–162, 1990.

[55] R. Petronzio and E. Vicari. An Overheat bath algorithm for lattice gauge theories. *Phys. Lett.*, B254:444–448, 1991.

[56] Roberto Petronzio and Ettore Vicari. Overrelaxed operators in lattice gauge theories. *Phys. Lett.*, B245:581–584, 1990.

[57] Ulli Wolff. Monte Carlo errors with less errors. *Comput. Phys. Commun.*, 156:143–153, 2004. [Erratum: Comput. Phys. Commun.176,383(2007)].

[58] Stefan Schaefer, Rainer Sommer, and Francesco Virotta. Critical slowing down and error analysis in lattice QCD simulations. *Nucl. Phys.*, B845:93–119, 2011.

[59] Martin Luscher and Stefan Schaefer. Lattice QCD without topology barriers. *JHEP*, 07:036, 2011.

[60] Martin Lüscher. Step scaling and the Yang-Mills gradient flow. *JHEP*, 06:105, 2014.

[61] M. Albanese et al. Glueball Masses and String Tension in Lattice QCD. *Phys. Lett.*, B192:163–169, 1987.

[62] Colin Morningstar and Mike J. Peardon. Analytic smearing of SU(3) link variables in lattice QCD. *Phys. Rev.*, D69:054501, 2004.

[63] Anna Hasenfratz and Francesco Knechtli. Flavor symmetry and the static potential with hypercubic blocking. *Phys. Rev.*, D64:034504, 2001.

[64] B. Berg. Dislocations and Topological Background in the Lattice O(3) σ Model. *Phys. Lett.*, 104B:475–480, 1981.

[65] Jean Zinn-Justin. Renormalization and Stochastic Quantization. *Nucl. Phys.*, B275:135–159, 1986.

[66] Jean Zinn-Justin and Daniel Zwanziger. Ward Identities for the Stochastic Quantization of Gauge Fields. *Nucl. Phys.*, B295:297–331, 1988.

[67] William A. Bardeen, A. J. Buras, D. W. Duke, and T. Muta. Deep-inelastic scattering beyond the leading order in asymptotically free gauge theories. *Phys. Rev. D*, 18:3998–4017, Dec 1978.

[68] Robert V. Harlander and Tobias Neumann. The perturbative QCD gradient flow to three loops. *JHEP*, 06:161, 2016.

[69] A. Bazavov et al. Gradient flow and scale setting on MILC HISQ ensembles. *Phys. Rev.*, D93(9):094510, 2016.

[70] Patrick Fritzsch and Alberto Ramos. The gradient flow coupling in the Schrödinger Functional. *JHEP*, 10:008, 2013.

[71] Mattia Dalla Brida, Patrick Fritzsch, Tomasz Korzec, Alberto Ramos, Stefan Sint, and Rainer Sommer. Determination of the QCD Λ-parameter and the accuracy of perturbation theory at high energies. *Phys. Rev. Lett.*, 117(18):182001, 2016.

[72] Mattia Dalla Brida, Patrick Fritzsch, Tomasz Korzec, Alberto Ramos, Stefan Sint, and Rainer Sommer. A non-perturbative exploration of the high energy regime in $N_f = 3$ QCD. *Eur. Phys. J.*, C78(5):372, 2018.

[73] Mattia Dalla Brida and Martin Lüscher. SMD-based numerical stochastic perturbation theory. *Eur. Phys. J.*, C77(5):308, 2017.

[74] Mattia Dalla Brida and Martin Lüscher. The gradient flow coupling from numerical stochastic perturbation theory. *PoS*, LATTICE2016:332, 2016.

[75] S. Aoki et al. Nonperturbative O(a) improvement of the Wilson quark action with the RG-improved gauge action using the Schrodinger functional method. *Phys. Rev.*, D73:034501, 2006.

[76] T. Kaneko, S. Aoki, M. Della Morte, S. Hashimoto, R. Hoffmann, and R. Sommer. Non-perturbative improvement of the axial current with three dynamical flavors and the Iwasaki gauge action. *JHEP*, 04:092, 2007.

[77] Martin Luscher, Stefan Sint, Rainer Sommer, and Hartmut Wittig. Nonperturbative determination of the axial current normalization constant in O(a) improved lattice QCD. *Nucl. Phys.*, B491:344–364, 1997.

[78] Michele Della Morte, Roland Hoffmann, Francesco Knechtli, Rainer Sommer, and Ulli Wolff. Non-perturbative renormalization of the axial current with dynamical Wilson fermions. *JHEP*, 07:007, 2005.

[79] Hiroshi Suzuki. Energy–momentum tensor from the Yang–Mills gradient flow. *PTEP*, 2013:083B03, 2013. [Erratum: PTEP2015,079201(2015)].

[80] Sergio Caracciolo, Giuseppe Curci, Pietro Menotti, and Andrea Pelissetto. The Energy Momentum Tensor for Lattice Gauge Theories. *Annals Phys.*, 197:119, 1990.

[81] A. Patella, L. Del Debbio, and A. Rago. Poincaré symmetries and the Yang-Mills gradient flow. *PoS*, LATTICE2013:324, 2014.

[82] Etsuko Itou and Sinya Aoki. QCD Thermodynamics on the Lattice from the Gradient Flow. *PoS*, INPC2016:342, 2017.

[83] Masayuki Asakawa, Tetsuo Hatsuda, Etsuko Itou, Masakiyo Kitazawa, and Hiroshi Suzuki. Thermodynamics of SU(3) gauge theory from gradient flow on the lattice. *Phys. Rev.*, D90(1):011501, 2014. [Erratum: Phys. Rev.D92,no.5,059902(2015)].

[84] Claudio Bonati and Massimo D'Elia. Comparison of the gradient flow with cooling in $SU(3)$ pure gauge theory. *Phys. Rev.*, D89(10):105005, 2014.

[85] Héctor Mejía-Díaz, Wolfgang Bietenholz, Krzysztof Cichy, Philippe de Forcrand, Arthur Dromard, Urs Gerber, and Ilya Orson Sandoval. Topological Susceptibility under Gradient Flow. *EPJ Web Conf.*, 175:11024, 2018.

[86] Marco Cè, Cristian Consonni, Georg P. Engel, and Leonardo Giusti. Testing the Witten-Veneziano mechanism with the Yang-Mills gradient flow on the lattice. *PoS*, LATTICE2014:353, 2014.

[87] Marco Cè, Miguel García Vera, Leonardo Giusti, and Stefan Schaefer. The topological susceptibility in the large-N limit of SU(N) Yang–Mills theory. *Phys. Lett.*, B762:232–236, 2016.

[88] Christopher Monahan and Kostas Orginos. Locally-smeared operator product expansions. *PoS*, LATTICE2014:330, 2014.

[89] Martin Luscher, Rajamani Narayanan, Peter Weisz, and Ulli Wolff. The Schrodinger functional: A Renormalizable probe for nonAbelian gauge theories. *Nucl. Phys.*, B384:168–228, 1992.

[90] Stefan Sint and Rainer Sommer. The Running coupling from the QCD Schrodinger functional: A One loop analysis. *Nucl. Phys.*, B465:71–98, 1996.

[91] Stefan Sint. One loop renormalization of the QCD Schrodinger functional. *Nucl. Phys.*, B451:416–444, 1995.

[92] Stefan Sint. On the Schrodinger functional in QCD. *Nucl. Phys.*, B421:135–158, 1994.

[93] Stefan Sint and Pol Vilaseca. Lattice artefacts in the Schródinger Functional coupling for strongly interacting theories. *PoS*, LATTICE2012:031, 2012.

[94] Wolfram Research, Inc. Mathematica, Version 11.3. Champaign, IL, 2018.

[95] M. Pilar Hernandez. Lattice field theory fundamentals. In *Modern perspectives in lattice QCD: Quantum field theory and high performance computing. Proceedings, International School, 93rd Session, Les Houches, France, August 3-28, 2009*, pages 1–91, 2009.

[96] P. Hasenfratz and F. Niedermayer. Perfect lattice action for asymptotically free theories. *Nucl. Phys.*, B414:785–814, 1994.

[97] P. Weisz. Renormalization and lattice artifacts. In *Modern perspectives in lattice QCD: Quantum field theory and high performance computing. Proceedings, International School, 93rd Session, Les Houches, France, August 3-28, 2009*, pages 93–160, 2010.

[98] S. Capitani, M. Guagnelli, M. Luescher, S. Sint, R. Sommer, P. Weisz, and H. Wittig. Nonperturbative quark mass renormalization. *Nucl. Phys. Proc. Suppl.*, 63:153–158, 1998.

[99] Conrad Sanderson and Ryan Curtin. *Journal of Open Source Software*, Vol.1:26, 2016.